Characterizing Errors in RF Time of Flight Ranging Systems: A Simulation Approach

David Tung

Electrical Engineering and Computer Sciences
University of California at Berkeley

Technical Report No. UCB/EECS-2010-82
http://www.eecs.berkeley.edu/Pubs/TechRpts/2010/EECS-2010-82.html

May 18, 2010

Characterizing Errors in RF Time of Flight Ranging Systems: A Simulation Approach

David Tung

May 11, 2010

University of California, Berkeley
Department of Electrical Engineering and Computer Sciences
Berkeley, CA 94720-1770

Contents

Chapter 1

Introduction

The localization and tracking of objects is a very important area of research today, with a myriad of different applications. Some example applications are tracking vehicles for safety, tracking cellular phones for the purpose of quick responses to emergency 911 calls, tracking the location of inventory in a large warehouse, tracking the location of people and equipment in a hospital environment, etc. To further complicate matters, different applications have different requirements - different applications may need functionality in vastly different environments and may require different levels of accuracy.

As a result of these varied needs, many different systems for localization and tracking have been developed that utilize a wide range of different technologies. One of the most popular technologies for localization and tracking is the global position system, or GPS. A terrestrial GPS unit can measure the distance to several geosynchronous satellites and combine those distance measurements to estimate its location on earth. GPS has many positive qualities - it has wide coverage and high accuracy in wide-open environments, like rural areas or areas without many tall buildings. However, its accuracy is poor in indoor or urban environments with many tall buildings. As a result, several other technologies have emerged for localization and tracking - many of these are designed for smaller scales and in those urban and indoor environments where GPS accuracy degrades.

One type of technology performs localization by measuring the time of arrival (TOA) or time of flight (TOF). These are two different names for the same type of technology. If we have two units, we can get an estimate of the distance between the two units by measuring how long it takes an RF signal transmitted by one unit to arrive at the other unit and dividing this time by the speed of light. If we have three or more units with known positions, and if we can measure the distance between an object of interest to each of those three units, we can determine the location of the object of interest. A second type of technology performs localization by measuring the time difference of arrival (TDOA). This type of technology is similar to TOA/TOF technology; once again we have an object of interest and several units with known positions. The object of interest will send an RF signal to the other units, but instead of trying to measure the time of

flight, the other units simply note the difference of the arrival times among each of them and use this information to determine the location. A third type of technology uses angle of arrival (AOA) measurements; units with known locations measure the angle of arrival of a signal transmitted from the object of interest, and combine those measurements to determine the location of the object of interest. A fourth type of technology uses received signal strength (RSS) measurements; units with known locations measure the received signal strength of a signal transmitted from the object of interest and combine those measurements to determine the location of the object of interest. In our work, we look at time of flight ranging systems.

In the event that the time of flight range measurements are perfect, we can determine the position of the object of interest perfectly. However, this is generally not the case. Range estimation errors can arise from noise, multipath, and obstructions that block the line-of-sight path between the the two units performing a ranging operation. Errors in the range estimates can severely impact the accuracy of the location estimations. Therefore, any technology, techniques, or algorithms developed for localization and tracking need to be able to mitigate such errors. However, as building prototypes is costly and inefficient, it is important to be able to accurately simulate the effects of noise, multipath, and obstruction of the line-of-sight path on ranging, localization and tracking. In literature, algorithms have been proposed assuming different statistical models for the ranging errors. However, very little work has been done in terms of justifying the assumed models. There has been a lot of work done on how to simulate a wireless channel, but not much work has been done on translating that channel into a good model for the time of flight ranging errors.

The goal of my work is to bridge the gap and utilize accepted channel models to provide models for time of flight ranging errors under different scenarios and in different environments. These models will be useful to those who develop and design new techniques and algorithms for localization and tracking in that they will not be required to get into the details of actually simulating the physical channel.

Chapter 2

Motivation

In order to have a full appreciation for the work we present in this report, there first needs to be a greater understanding of the needs and issues in localization and tracking research. We begin this chapter by looking at prior research work in the area of developing algorithms for localization. Much of this prior work has a high-level approach to localization and tracking - the authors are interested in intelligent ways of filtering and combining range measurements in order to mitigate errors in the range measurements that come from noise, multipath, and non-line-of-sight conditions - they are less interested in how those measurements are actually obtained or the underlying physics of ranging operations. So, instead of simulating ranging operations, they adopt simplified statistical models for the estimation errors, often times without robust justifications or calculations to support their models. It is here that our work can be of great benefit - our work can provide a better model that is backed up by simulation data. After that, we will take a look at work that actually implemented time of flight ranging systems or tried to simulate the wireless channel and the ranging operation and address weaknesses that our work will address.

2.1 Statistical Models for Estimation Errors

The models used in prior literature are not consistent; there are many different kinds of models for time of flight ranging errors. We describe some of the models in this section. In general, these models do not deal with the time of flight, but rather the distance between our two units. This is reasonable since we are more interested in the distance, and the time of flight is merely the distance scaled by the speed of light. We denote the true distance between the two units as d, and we denote the distance estimate as $\hat{d}$. In general, the relationship between d and $\hat{d}$ is:

$$\hat{d} = d + e \tag{2.1}$$

where e is the estimation error and a random variable. We are interested in models for e.

Before looking at the models used in the literature, we will first take a high-level look at the different contributors to the time of flight ranging error. In a perfect situation, the RF signal at the receiver will just be a delayed version of the RF signal sent from the transmitter, and this delay will be exactly equal to the time of flight. However, the signal is garbled and corrupted by noise, multipath, and non-line-of-sight conditions. The noise refers to the additive noise from the environment - it may come from the thermal noise or from other RF devices. Multipath refers to the corruption that comes from delayed and attenuated copies of the signal that arise from the signal bouncing off of different objects in the environment before arriving at the receiver. Non-line-of-sight (NLOS) conditions arise when the direct (or line-of-sight) path between the transmitter and receiver is completely blocked by some obstruction. Whether or not there is a line-of-sight (LOS) path between the transmitter and receiver can change the distance estimate drastically. Thus, much of the literature considers separately the case when there is a LOS path and the case when there is not a LOS path. We denote the distance estimate when there is a LOS path as $\hat{d}_{LOS}$ and the distance estimate when the LOS path is obstructed as $\hat{d}_{NLOS}$. These two quantities are related to d:

$$\begin{aligned} \hat{d}_{LOS} &= d + e_{LOS} \\ \hat{d}_{NLOS} &= d + e_{NLOS} \end{aligned}$$

We want to consider the different models for the random variables e_{LOS} and e_{NLOS}.

Chan, et al. in [3] and Chen, et al. in [7] assume that the estimation error in the LOS and NLOS cases have the following form:

$$e_{LOS} = \epsilon \tag{2.2}$$

$$e_{NLOS} = \epsilon + \alpha \tag{2.3}$$

where ϵ is a Gaussian random variable, and α is a uniform random variable.

Zhang and Wong in [41] investigate the performance of localization and tracking when there is no LOS path at all; however, both the time of flight and the angle of arrival are known. In their simulations they assume that the estimation error under NLOS conditions has the following form:

$$e_{NLOS} = b + |\epsilon| \tag{2.4}$$

where ϵ is a Gaussian random variable. In their simulations, since the exact path that the signal took was known, b was a known offset that comes from the extra distance that the signal needed to travel.

Huerta, et al. in [22] assume the following form for the estimation error in the LOS and NLOS cases:

$$\begin{aligned} e_{LOS} &= \epsilon_{LOS} \\ e_{NLOS} &= \epsilon_{NLOS} \end{aligned}$$

In these definitions, ϵ_{LOS} is a Gaussian random variable, and ϵ_{NLOS} is a Rayleigh random variable.

2.2 Experimental Measurements of Estimation Errors

There has been work done that implements or simulates a time of flight ranging system and tries to characterize the estimation error. However, many of these examples of prior work have some weaknesses that our work will try to address.

Ciurana and Barcelo-Arroyo in [13] did not try to come up with a theoretical model for the estimation error; instead, they compiled a database of actual time of flight ranging measurements under different scenarios (when the LOS path is blocked, when the LOS path is partially blocked, and when the LOS path is unblocked) and took samples from this database. Although a database of measurements is useful, we have no idea how dependent the distribution of error is on the particular environment that the measurements were obtained from. A more theoretical model can help to address this problem.

Ciurana, et al. in [11] also took actual time of flight ranging measurements; however, they only considered the LOS scenario, and they found a Gaussian model to be the best fit for the estimation error, e_{LOS}. However, many of the problems with systems that utilize time of flight ranging come from the NLOS scenario - thus, it is imperative that we have a model for errors in the NLOS scenario.

Izquierdo, et al. in [23] took actual time of flight ranging measurements and fit the error to a Gaussian model. Unlike much of the other work, they did not differentiate between the LOS and the NLOS scenario. Their model was used by Ciurana, et al. in [12]. Our work differs from their work in that we will differentiate between the LOS and the NLOS scenario. The problem with combining the LOS and NLOS scenarios is that in any given environment, we really have no idea what fraction of the measurements are LOS and what fraction are NLOS. Thus, it is far more useful to consider separate models for the LOS scenario and the NLOS scenario.

Comsa, et al. in [14] tried to simulate ranging operations, as we do. Their work was focused on determining location, not just measuring ranges, and instead of using time of flight to estimate location they used time difference of arrival. For their simulation, they assumed that they had a number of reference sensors - they simulated the wireless channel between the mobile and one of sensors as AWGN, and they used the COST 207 model for wireless channels with 6 Rayleigh faded rays for the wireless channel between the mobile and the other sensors. The models that they used for their wireless channel are not as general as the models that we use. To assume that one of the channels will be AWGN is unrealistic; in addition to that, the COST 207 model assumes that the excess delays of the multipaths are deterministic; thus, it is not as useful a model for simulating time of flight ranging systems, since time of flight ranging errors are quite dependent on what the excess delays are.

Our work attempts to address the weaknesses of this prior work to provide useful models for the ranging error in both the LOS and NLOS scenarios.

Chapter 3

Simulating a Time of Flight Ranging System

In this chapter we discuss how we simulated a time of flight ranging system. We split our discussion into three sections. In the first section we discuss how we simulated the wireless channel. We begin from a physical picture of the wireless channel and move from that picture to a statistical model for the wireless channel. In the second section we discuss how, from our wireless channel simulation, we can simulate a time of flight ranging system. Finally, in the third section, we look at the parameter choices and design decisions that went into our specific simulation.

3.1 Simulating a Wireless Channel

3.1.1 Looking at the Physical Picture

The easiest way to get some intuition on how to simulate the wireless channel is to first look at a physical picture, in Figure 3.1. We have two units that we want to perform a ranging operation between - a base station and a mobile unit. Suppose that both units are stationary and separated by a distance of d meters. We will consider the case when the base station is sending a signal to the mobile. One path that the signal traverses to get to the mobile is LOS path between the base station and the mobile. The signal will reach the mobile after a delay $\tau_d = \frac{d}{c}$, where c is the speed of light, and with some attenuation (which we will denote by α). However, the signal can also arrive at the mobile via other paths by bouncing off of different reflectors in the environment. These other paths are what we call the multipath component. Our picture only depicts one-bounce paths, but these multipaths may include reflections off of several reflectors between the base station and the mobile. Consider the i^{th} path. The signal that travels via this path will arrive at the mobile with some delay larger than τ_d (since the shortest path between the base station and the mobile is the direct path). We will denote the delay in excess of τ_d by t_i. The signal that travels along this path

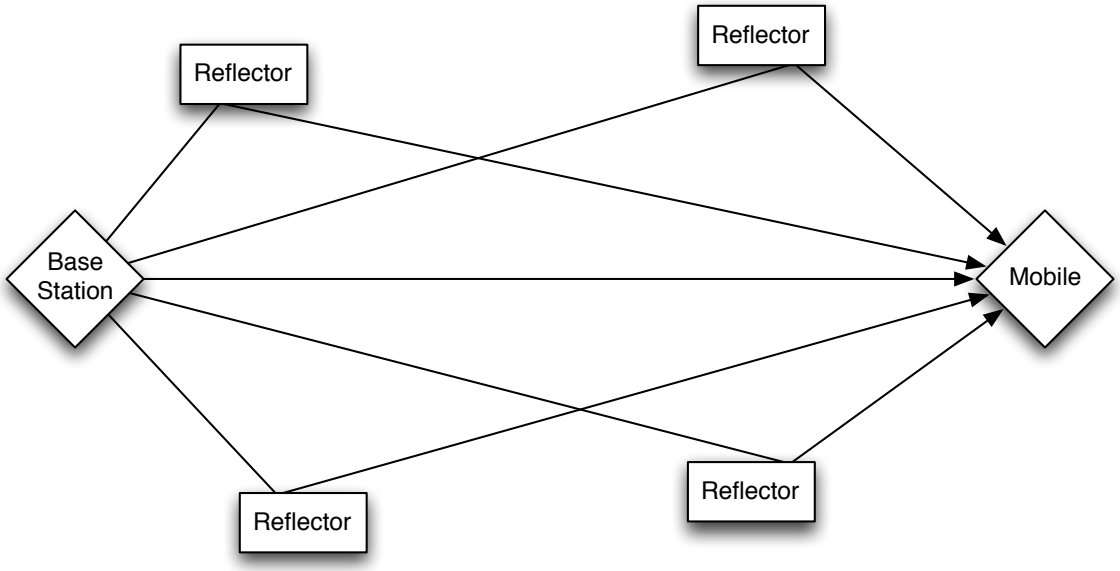

Figure 3.1: The general physical setup.

also experiences some attenuation, which we will denote by β_i. Suppose there are L such paths. The signal that we are sending from the base station at time t is $x(t)$. Then, from this picture, we can express the received signal at the mobile, $y(t)$, at time t as:

$$y(t) = \alpha x(t - \tau_d) + \sum_{i=1}^{L} \beta_i x(t - \tau_d - t_i) \tag{3.1}$$

where

$$\alpha, \beta_1, \ldots, \beta_L \in \mathbb{C}; \tau_d, t_1, \ldots, t_L > 0 \tag{3.2}$$

From the way that we express $y(t)$, we can see clearly that there is a contribution from the LOS path and a separate contribution from the multipaths. However, in addition to the signal from the LOS path and the multipaths, there will also be some contribution from noise at the mobile. So, our model becomes:

$$y(t) = \alpha x(t - \tau_d) + \sum_{i=1}^{L} \beta_i x(t - \tau_d - t_i) + n(t) \tag{3.3}$$

This is the general model, and similar models for the wireless channel are seen in [19] and [38]. We now move away from the physical picture and discuss reasonable statistical models for the parameters in the model.

3.1.2 Effect of Sampling

The number of multipaths, L, may be extremely large and highly dependent upon the environment. For example, in an indoor environment there are many walls and other objects for the signal to bounce off of. We would expect many multipaths and for them to all arrive within a short time interval. However, since we are dealing with real-world systems, we will not have access to the actual continuous time signal at the receiver; instead, we will have samples of the continuous time signal. Because we are sampling the received signal $y(t)$, we can actually use a simpler model for the received signal:

$$y(t) = ax(t - \tau_d) + \sum_{i=1}^{M} b_i x(t - \tau_d - \tau_i) + n(t) \tag{3.4}$$

This model looks very similar to our original model; however, we are considering M paths in this model, and we assert that M is much smaller than L. We have substituted a, b_i and τ_i for α, β_i, and t_i, but they still correspond to the attenuation of the LOS path, the attenuation of each multipath, and the excess delay of each multipath respectively.

To understand why we only have to consider M paths instead of L paths, we first return to the physical picture of our channel. There will be many copies of the signal that travel along different paths but arrive at the receiver with approximately the same excess delay τ_i. For some intuition behind this, we look at Figure 3.2; this is a zoomed in picture of what happens at one of the reflectors. There are many reflections off of this one reflector; each of the reflected paths off of this reflector will have a different attenuation, but they will have roughly the same arrival time at the receiver. Now, if we were looking at the actual continuous time signal $y(t)$ at the receiver, then it would be best accurate to model $y(t)$ by considering all of these paths with their individual attenuations β_i and individual excess delays t_i. However, we are sampling our received signal $y(t)$; in general, the sampling interval is much larger than the inter-arrival times in these clusters of paths, and we will not be able to tell that there are many different paths. Instead, the copies of the signal traveling along these paths will all appear to arrive at the same time; since we are summing them together at the receiver, we can treat the contribution of all the paths in the cluster as a single copy of the transmitted signal with excess delay τ_i and attenuation b_i, which is the sum of all of the attenuations β_i of paths in the cluster. In our picture we treated all of the paths that bounced off of the same reflector as belonging to the same cluster, but in general we treat all paths that have roughly the same delay as belonging to the same cluster.

So, because we are taking samples, and since the sampling interval is so much larger than the inter-arrival times of the different paths, we can split all of the reflected paths into M different clusters; we can treat the contribution of each of these clusters as a single copy of the transmitted signal with attenuation b_i and excess delay τ_i. In addition to that, we can combine all of the reflected paths that arrive closely in time with the LOS path to the first term; thus, the first term then corresponds to the cluster of paths that arrive with delay τ_d, and its attenuation a is the

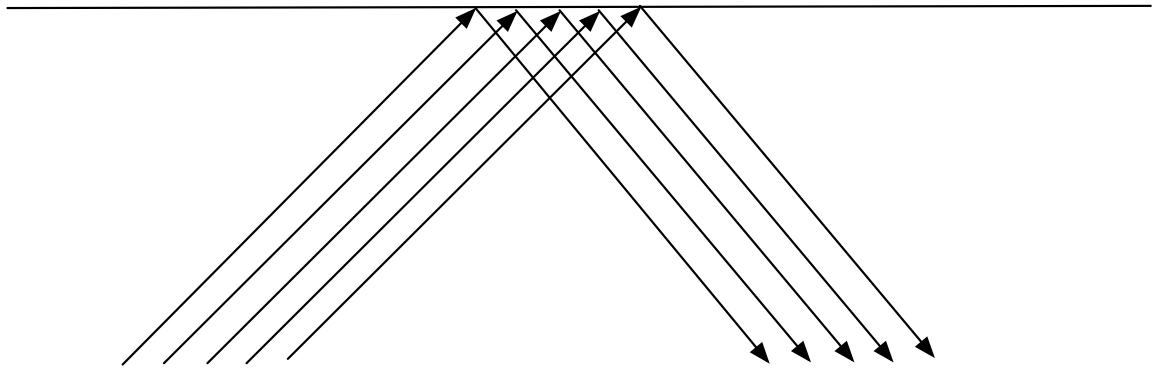

Figure 3.2: Zooming in to see to get a better picture of what happens at the reflectors. The rays are parallel because we are assuming that the source is in the far field.

sum of α and all of the β_i's that correspond to the reflected paths. Modeling $y(t)$ in this way will have implications on how we model the attenuation coefficients $a, b_1, \ldots, b_M$ and the excess delays $\tau_1, \ldots, \tau_M$.

3.1.3 Modeling the Channel Attenuation

We need to model the attenuation coefficients $a, b_1, \ldots, b_M$. We will begin by considering the coefficients that correspond to the multipaths, the b_i's. A common practice is to model these coefficients as i.i.d circular symmetric Gaussian random variables; that is, $b_i \sim CN(0,1)$. This notation means that $b_i = B_R + iB_I$, where $B_R, B_I \sim N(0, 1/2)$ and are i.i.d. This model is known as Rayleigh fading because in this model $|b_i|$ has a Rayleigh distribution.

In order to see why this model is reasonable, remember that each of the b_i's is the sum of many random variables: the β_i's that belong to the i^{th} cluster. By the central limit theorem, we know that the attenuation coefficient b_i should be Gaussian.

Now, we consider how to model the coefficient that corresponds to the LOS path, a. The common practice is to model a as the sum of a dominant component and a circular symmetric Gaussian random variable. That is, we have:

$$a = \sqrt{\kappa} e^{i\theta} + CN(0,1) \tag{3.5}$$

The first term in this sum corresponds to attenuation of the actual LOS path and the second term corresponds to the sum of the attenuations of the multipaths whose lengths are so close to the length of the LOS path that they arrive at roughly the same time. The parameter κ is a fixed

value called the Rician factor denoting how much power is in the direct path, and θ is a uniform random variable on the range $[0, 2\pi)$, and it denotes the phase of the direct path. We model the contribution from the multipath as a circular symmetric Gaussian random variable for the same reasons that we described above. This model is known as Rician fading because $|a|$ has a Rician distribution.

3.1.4 Modeling the Delays and the Number of Multipath Components

Before discussing how to model the excess delays, the τ_i's, and the number of multipath components, M, we first need to define some more characteristics of our wireless channels and our measurement system.

The first thing we need to consider is the delay spread of the channel. The delay spread is the difference between the arrival time of the longest path and the arrival time of the shortest path that the signal takes from the transmitter to the receiver. It depends heavily upon the physical configuration of the environment. A more useful characteristic is the RMS delay spread. The RMS delay spread tells us how long the interval is in which most of the reflected signals that contain a significant amount of energy arrive. We denote the RMS delay spread by τ_{RMS}. Thus, we assume that all significant copies of the signal will arrive at our receiver between time τ_d and time $\tau_d+\tau_{RMS}$.

The second thing we need to consider is the bandwidth available for the ranging operation, since in practice there is limited bandwidth allotted. The bandwidth affects the transmitted signal $x(t)$ and the sampling rate of our measurement system. As we saw above, the sampling rate has a big effect on how many multipaths M we need to simulate. If our sampling rate is high, then even if the time of arrival between two copies of the signal is small, we may be able to distinguish one from the other. However, if the sampling rate is low, then we will not be able to tell that there are two copies. The bandwidth of the transmitted signal also has an effect. Signals that have high bandwidth tend to be more localized in time. Thus, if our signal has higher bandwidth then it is easier to identify two separate copies of the signal that arrive close together in time. However, if our signal has lower bandwidth, it is more likely that we will see two copies of the same signal as just one copy. We denote the bandwidth of our signal by W and the sampling interval of our measurement system by T_{sample}. We sample at the Nyquist frequency, and our bandwidth W is the total bandwidth; thus $T_{sample} = \frac{1}{W}$.

So, we see that if W is large, then we should be able to resolve more distinct paths. Thus, the larger W is, the larger M should be. Also, if τ_{RMS} is larger, there is a larger interval where reflections with significant energy can arrive, and we would expect to see more reflections. Thus, the larger τ_{RMS} is, the larger M should be. So, from these parameters, we define M to be:

$$M = \left\lceil \frac{\tau_{RMS}}{T_{sample}} \right\rceil \tag{3.6}$$

This is similar to what is done in [35].

We model the excess delays, the τ_i's, as i.i.d. uniform random variables on the interval $[0, \tau_{RMS}]$. The excess delays of these clusters is uniform because we do not assume anything a priori about the reflectors in the environment. Since we are clustering paths that have roughly the same delay, we would not expect clusters to clump together in any part of the interval $[0, \tau_{RMS}]$.

3.1.5 Modeling the Noise

The additive noise that we are modeling is thermal noise, and thus can be reasonably modeled as Gaussian. Also, there is logically no predilection for a certain phase. So at any time t, the noise $n(t)$ is a circular symmetric Gaussian random variable, with power N_0. We denote $n(t) \sim CN(0, N_0)$. For the purpose of our simulations, we will have N_0 be a parameter that depends on the SNR.

3.1.6 Dealing with Movement

Up to this point we have only looked at the picture where both the base station and the mobile are stationary and the environment is static. In general, this is not going to be the case - and thus the different parameters of our model become time-varying. So, our model for $y(t)$ becomes:

$$y(t) = a(t)x(t - \tau_d(t)) + \sum_{i=1}^{M} b_i(t)x(t - \tau_d(t) - \tau_i(t)) + n(t) \tag{3.7}$$

However, we are considering things moving much slower than the speed of light, and so there will not be significant short-term time variation in the length of the signal paths. Therefore, we can treat $\tau_d(t)$ and the $\tau_i(t)$'s as constants over the course of a single ranging operation. However, we still need to consider how $a(t)$ and the $b_i(t)$'s vary over time.

Many models have been proposed to determine how $a(t)$ and the $b_i(t)$'s change and how they are correlated over time. We assume that $a(t)$ and $b_i(t)$ are uncorrelated with each other, that the LOS component of $a(t)$ is constant, and that the multipath component of $a(t)$ and all of the $b_i(t)$'s are independently and identically distributed. We have independence since we assume that the amplitudes and phases of each individual path are independent, as in [37]. A common model for determining this correlation over time is Clarke's model, which is described in [18] and [37]. The situation described in Clarke's model involves a stationary base station and moving mobile unit surrounded by a ring of scatterers. The model also assumes an isotropic antenna gain pattern. We need to know how $b_i(t)$ is correlated over time.

The base station is not moving but the mobile is moving at a velocity of v m/s. Let f_c be the carrier frequency of our signal. Then, the magnitude of the maximum Doppler shift we would see is $f_d = \frac{vf_c}{c}$, where c is the speed of light. This quantity tells us how wide a frequency band our signal gets spread out over as a result of the fact that our mobile is moving. Clarke's model tells us that if our maximum Doppler shift is f_d, then the normalized autocorrelation function of $b_i(t)$ is a zeroth-order Bessel function of the first kind:

$$R(\tau) = J_0(2\pi f_d \tau) \tag{3.8}$$

The corresponding power spectral density is:

$$S(f) = \begin{cases} \frac{1}{\pi f_d \sqrt{1-(f/f_d)^2}} & |f| \leq f_d \\ 0 & \text{otherwise} \end{cases} \tag{3.9}$$

Plots of $R(\tau)$ and $S(f)$ when $f_d = 100$ Hz are shown in Figure 3.3

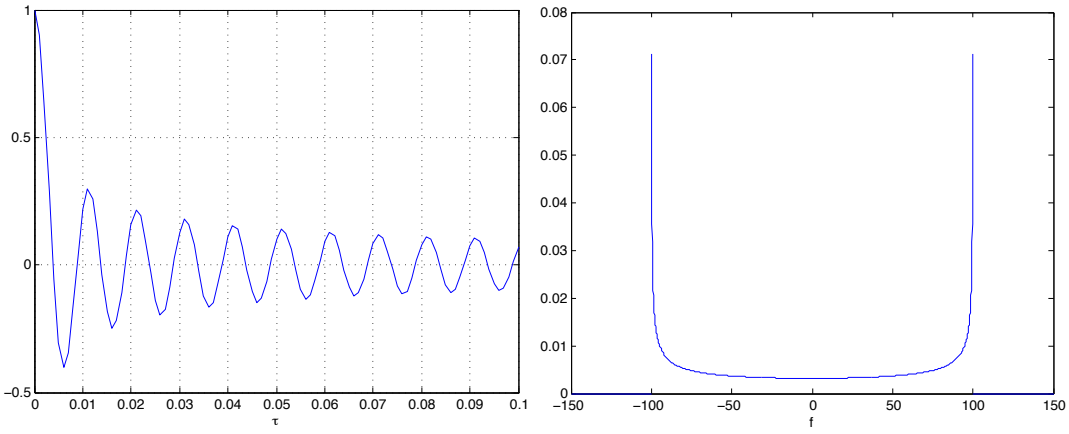

Figure 3.3: Autocorrelation function and power spectral density of Rayleigh fading in Clarke's model.

Given f_d, there are several methods for generating instances of $b_i(t)$ that have the desired autocorrelation properties. One well-known method is Jakes' method, which uses a sum-of-sinusoids approach and is described in [24]. Young and Beaulieu propose a method in [40] which takes the IDFT of appropriately weighted Gaussian random variates to generate samples of $b_i(t)$. Baddour and Beaulieu propose a different method in [1] which uses an autoregressive modeling approach to generate an IIR filter for Gaussian random variates - the resulting output are samples of $b_i(t)$. We have implemented the approach used in [40], and the resulting output for a one second long interval of $b_i(t)$ with $f_d = 100$ Hz is shown in Figure 3.4.

3.1.7 Summary

We end this section with a quick summary of our model and the relevant parameters before we move on to discussing how we simulated a time of flight ranging system. We started with a physical picture and ended up with the following relationship between our transmitted signal $x(t)$ and our received signal $y(t)$:

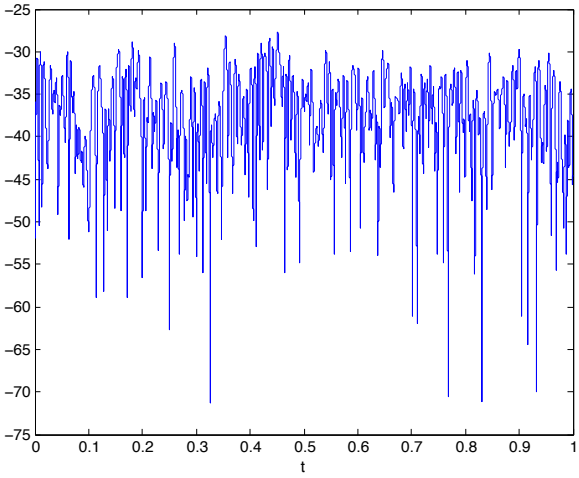

Figure 3.4: dB plot of the magnitude of a one second sample of $b_i(t)$ with $f_d = 100$ Hz.

$$y(t) = a(t)x(t - \tau_d) + \sum_{i=1}^{M} b_i(t)x(t - \tau_d - \tau_i) + n(t) \tag{3.10}$$

The relevant parameters that we need to know before simulating are the distance between the mobile and base station (d), the RMS delay spread (τ_{RMS}), the sampling interval (T_{sample}), the Rician factor (κ), the SNR, the speed of the mobile (v), and the carrier frequency (f_c). The relation between the parameters in our equation and these parameters is summarized in Table 3.1.

	Dependent on
M	$\left\lceil \frac{\tau_{RMS}}{T_{sample}} \right\rceil$
$a(t)$	Depends on κ, v, and f_c
$b_i(t)$	Depends on v and f_c
τ_d	$\frac{d}{c}$
τ_i	$\sim Unif[0, \tau_{RMS}]$
$n(t)$	$\sim CN(0, N_0)$ where $N_0 = \frac{1}{SNR}$

Table 3.1: Dependency of equation parameters on environment parameters.

3.2 Simulating a Time of Flight Ranging System

Now that we have a suitable model for the wireless channel we can move on to how we would simulate a time of flight ranging system. First, we review the basic idea behind time of flight ranging systems. We have two devices that we want to measure the range between - the base station and the mobile. We assume the base station initiates the ranging operation. The base station will send some kind of known signal to the mobile. Ideally, the mobile will receive the transmitted signal delayed by the amount of time it took the signal to travel between the base station and the mobile. However, in general the received signal will be corrupted by noise, contributions from multipath reflections, and there may not be an LOS path. From this received signal, the mobile attempts to intelligently determine the delay and deduce the time that it took the signal to travel from the base station to itself, and thus deduce the distance between the base station and the mobile. This is the basic idea behind time of flight ranging systems.

In general there are many different ways that real-world time of flight ranging systems are realized - there are often differences in the architecture or infrastructure that are used for the system. One type of system uses Wi-Fi packets to do ranging; this type of system is implemented by Ciurana, et al. in [10], Golden and Bateman [19], and Hoene and William in [21]; it was also simulated by Llombart, et al. in [26]. In these systems, the base station sends a packet to the mobile and waits to receive an acknowledgment. It measures the time between when it transmitted its packet to when it receives the acknowledgment - this time is equal two times the time of flight plus the processing time at the base station and at the mobile. The processing time can be measured, and thus an estimate of the time of flight can be obtained. Other systems are similar, but they may send a custom signal, such as the motes implemented by Lanzisera in [25].

In simulating a time of flight ranging system, there are two main components. The first is the simulation of the wireless channel. Given relevant parameters like the ones described in the previous section and an input signal $x(t)$, we need to program a simulator to accurately simulate the channel and give us reasonable instances of $y(t)$. Our simulator is simply an implementation of the wireless channel model that we described in the previous section, and thus we will not discuss it further in this section. The second component is the estimator, which estimates the time of flight τ_d from $y(t)$. We now describe how we implemented our estimator. Our goal is not to engineer the best possible estimator given the model, but rather to simulate the most commonly used estimator so that we can see how the error is distributed. Although many real-world systems are designed to measure the round trip time instead of the one-way time of flight in order to get around time synchronization issues between the base station and the mobile, we will make the simplifying assumption that the base station and mobile are perfectly synchronized in time. Thus, we only have to simulate the channel in one direction, from the base station to the mobile, and the estimator at the mobile.

3.2.1 Overview of Estimator

In Figure 3.5, we see an overview of our estimator. We assume that the base station has transmitted a single pulse at time 0. Our estimator takes in samples of the received signal, $y(t)$. It then upsamples these samples in order to improve the time resolution beyond T_{sample}, as is done in [25]. Since we know that our received signal $y(t)$ is the superposition of copies of the transmitted signal at different delays, we need some way to try and resolve the delays of the different copies. We do this by passing these samples through a matched filter, correlating them with a template signal, which is our transmitted signal $x(t)$. The peaks in the correlated signal correspond to different copies of the transmitted signal. We are only interested in the magnitude and location in time of the peaks, so we take the magnitude of the correlated signal. We assume that the earliest copy of the transmitted signal must be from the line of sight path, and thus we want to find the location in time of the first peak and treat that as the estimate of the delay. However, since there is noise, there may be earlier peaks as a result of the noise. Therefore, we instead want to find the location in time of the first peak above a certain threshold, and use that as the time of flight estimate.

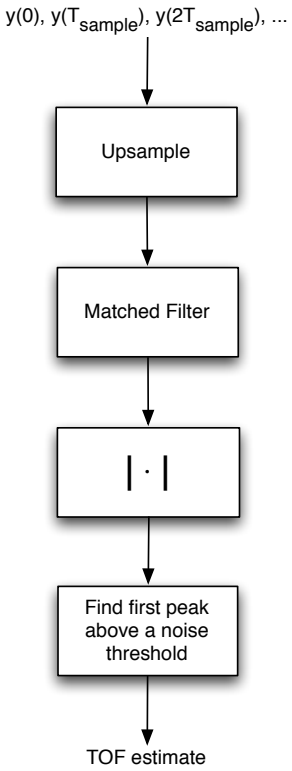

Figure 3.5: Overview of our estimator.

3.2.2 The Matched Filter

We use a matched filter to determine the specific time of arrival - this same approach is used by Golden and Bateman in [19] and Lanzisera in [25].

Let the samples of the output after upsampling be denoted by $y(0), y(T), y(2T), \ldots, y(nT)$. Define $y(kT) = 0$ for k outside of the range 0 to n. Our transmitted signal, $x(t)$ is a causal and finite duration signal. Let $x(0), x(T), \ldots, x(mT)$ be the nonzero samples of $x(t)$, with $x(kT) = 0$ for k outside the range 0 to m. We can assume that $m < n$. Then we define the output of the matched filter to be $z(0), z(T), \ldots$, where:

$$z(kT) = \sum_{j=1}^{m} x(jT)y((k+j)T) \tag{3.11}$$

The matched filter is best understood through an example. Let $x(t)$ be our transmitted signal; suppose that in our received signal $y(t)$ we see two copies of $x(t)$ - one that traveled along the LOS path and arrived in 100 ns and another copy that arrived 400 ns after the first, with half the energy. A plot of $x(t)$ and $y(t)$ are shown in figure 3.6.

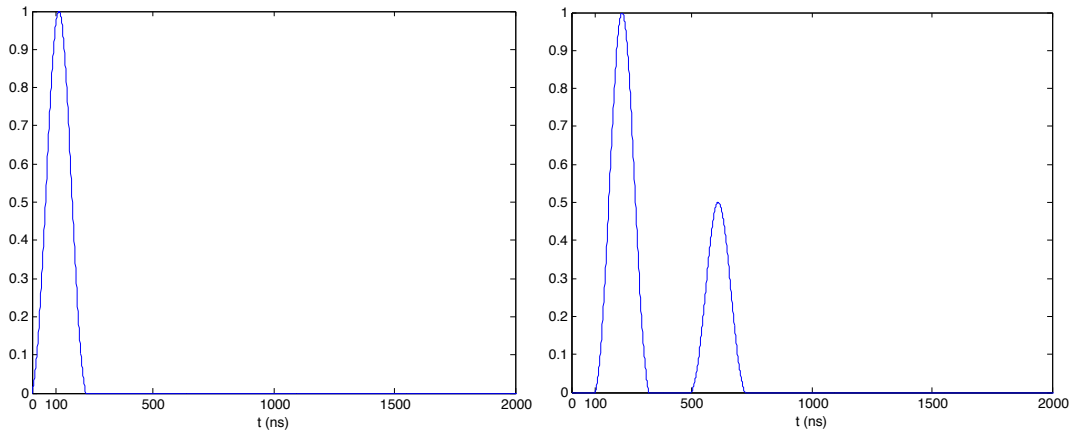

Figure 3.6: Plot of $x(t)$, our transmitted signal, and $y(t)$, the received signal.

We then run the received signal $y(t)$ through our matched filter. The output of the matched filter, $z(t)$, is shown in figure 3.7. We can see from this figure that there is a peak at 100 ns and a peak at 500 ns, which correspond to the arrival times of the two copies of $x(t)$.

3.2.3 Determining the Noise Threshold

The choice of a noise threshold is an important choice - if the noise threshold is too high, then we run the risk of ignoring peaks that correspond to real copies of the transmitted signal. However,

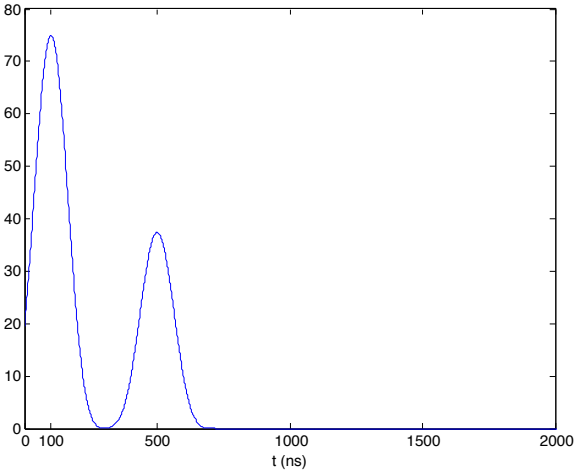

Figure 3.7: Plot of $z(t)$, the output of the matched filter.

if the noise threshold is too low, then we run the risk of falsely identifying peaks that are due to noise as ones that come from copies of the transmitted signal. The choice for the noise threshold is determined by many things - the transmitted signal (which is in turn dependent on the bandwidth), the sampling rate (which is also dependent on the bandwidth), the upsampling factor, and the SNR. Instead of trying to come up with an analytical form for the optimal noise threshold, we determined a threshold empirically through simulations; we chose our threshold to minimize the chance of falsely identifying peaks that were the result of noise as from copies of the signal. Thus, our noise thresholds are quite conservative. For a given bandwidth, upsampling factor, and SNR, we would run one thousand simulations where no signal was transmitted - thus at the receiver you would only see noise. We would get samples at the receiver, upsample them, and then run them through the matched filter and identify the largest peak. We found the largest peak over all one thousand simulations. In order to have better guarantee that we would not falsely identify peaks, we multiplied the value of this peak by 1.1 and set that to be our noise threshold.

3.3 Parameter Choices and Design Decisions for our Simulator

In this section we want to summarize the specific parameter choices and design decisions we made for our simulator.

3.3.1 General Assumptions

As mentioned above, one assumption that we made was that our base station and mobile are perfectly synchronized in time. This is generally not the case in real world systems, and it can be a serious problem since even discrepancies on the order of nanoseconds can substantially affect the accuracy of our estimates. Many real world systems get around this by measuring the round trip time it takes for a signal to travel from the base station to the mobile and then back to the base station instead of the one way time of flight. This gets around the problem of time synchronization because all of the meaningful time measurements will happening on the same device.

A second assumption we made was that we would always sample exactly at the Nyquist frequency, and we also assumed that all of our filters are ideal. One result of this is that for different bandwidths the samples will have different resolutions in time. Thus, we always pick the upsampling factor U such that the time between samples after upsampling is $\frac{5}{9} * 10^{-10} \approx 0.556$ ns. This value was chosen because the bandwidth values that we were interested in were 3 MHz, 6 MHz, and 18 MHz, and we wanted to have nice values for U.

A third assumption we made was that a ranging operation would take at most 10 μs - that is, we assumed that at the mobile we would receive the signal from the base station within 10 μs. This is a reasonable assumption since a delay of 10 μs corresponds to a separation distance of 3 kilometers.

3.3.2 Bandwidth

Our choices for the bandwidth values to simulate were based on the spectrum that has been allocated for location and monitoring services. We chose three different spectrums of bandwidth to look at: 3 MHz of spectrum in the 200 MHz frequency band, 6 MHz of spectrum in the 900 MHz band, and 18 MHz of spectrum in the 900 MHz band.

3.3.3 Effect of Movement

As we discussed previously, when we introduce movement it causes the gains for the different paths to vary over time. How fast the gains vary is determined by the maximum Doppler shift $f_d = \frac{vf_c}{c}$. However, since we are only looking at 10 μs long time intervals, it turns out that the channel gains remain roughly constant for the values of v and f_c that we are interested in. Thus, mobility has no effect on the simulating of the ranging operation. Therefore, we decide to model the channel gains as constant over the 10 μs interval that a ranging operation takes.

3.3.4 Transmitted Signal

We decided to make the transmitted signal $x(t)$ a shifted and truncated raised cosine - it is a good choice because the raised cosine is a bandlimited signal that also dies quickly in the time domain.

The raised cosine $g(t)$ is:

$$g(t) = \left(\frac{\sin(\pi t/T)}{\pi t/T}\right)\left(\frac{\cos(\alpha\pi t/T)}{1-(2\alpha t/T)^2}\right) \tag{3.12}$$

It's frequency response $G(f)$ is:

$$G(f) = \begin{cases} T & |f| \leq \frac{1-\alpha}{2T} \\ T\cos^2\left[\frac{\pi T}{2\alpha}\left(|f| - \frac{1-\alpha}{2T}\right)\right] & \frac{1-\alpha}{2T} \leq |f| \leq \frac{1+\alpha}{2T} \\ 0 & \frac{1+\alpha}{2T} < |f| \end{cases} \tag{3.13}$$

T and α are parameters of the raised cosine; α is called the excess bandwidth parameter and can take values from 0 to 1. For higher values of α, $g(t)$ dies faster in the time domain while becoming more spread out in the frequency domain. We want $g(t)$ to die quickly in the time domain so that we can approximate it as a finite duration signal. Therefore, we choose $\alpha = 1$, which means that $G(f)$ is zero outside the range $\pm\frac{1}{T}$. If we are limited to a bandwidth of W, this means that we want $\frac{1}{T} = \frac{W}{2}$. So we set $T = \frac{2}{W}$. We plot an example of $g(t)$ and $G(f)$ in Figure 3.8 for $W = 18$ MHz.

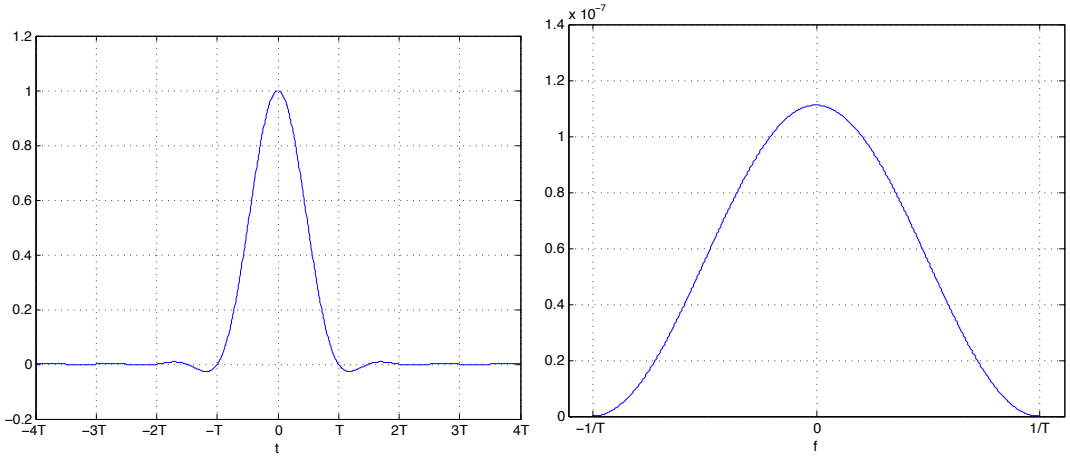

Figure 3.8: Time domain and frequency domain representation of a raised cosine function with $W = 18$ MHz.

In practice, we need $x(t)$ to be both finite and causal. Therefore, we have:

$$x(t) = \begin{cases} g(t-T) & 0 \leq t \leq 2T \\ 0 & \text{otherwise} \end{cases} \tag{3.14}$$

We plot $x(t)$ for $W = 18$ MHz in Figure 3.9.

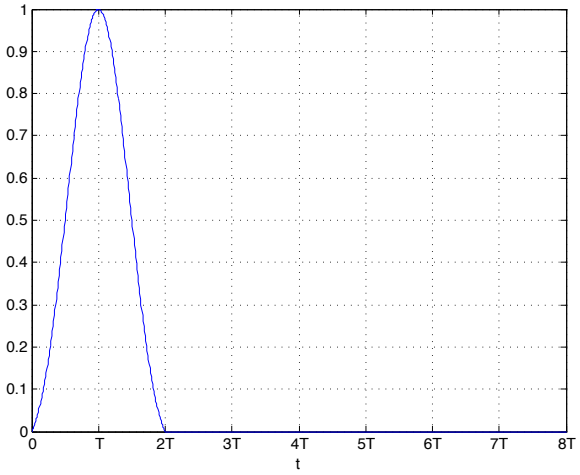

Figure 3.9: Plot of the transmitted signal, $x(t)$, a shifted and truncated raised cosine pulse with $W = 18$ MHz.

3.3.5 RMS Delay Spread

The values for the RMS delay spread are chosen based on some of the experimental results in the literature. Our goal was to find suitable values for different environments that we were interested in simulating. However, it turns out that there is a lot of disagreement between different measurement campaigns for the RMS delay spread, even though they are operating in similar environments. We have summarized these findings in Table 3.2.

It is clear that there each environment that these values vary over a huge range. Some factors that contribute to this variance are the actual layout of the environment and the carrier frequency, f_c, because of different absorption properties at different frequencies. To simplify our simulations, instead of allowing our RMS delay spreads to vary over such a huge range, we decided to pick a representative value for each environment. For the outdoor urban environment, we decided to use $5\,\mu$s; for the highway environment we decided to use $1\,\mu$s; for the indoor environment we decided to use $0.1\,\mu$s.

Environment	RMS Delay Spread	Notes	Reference
Outdoor Urban	$< 1.4\,\mu$s	In "big urban" environment	[35]
	$< 1.3\,\mu$s	In "small urban" environment	[35]
	$> 2\,\mu$s	Happens in half the cases	[32]
	$< 15\,\mu$s	Worst case scenario	[32]
	$< 3\,\mu$s	In "small urban" environment	[39]
	$0.03 - 0.06\,\mu$s	Research park environment	[30]
	$0.1 - 0.16\,\mu$s	Research park environment	[27]
	$0.09 - 0.38\,\mu$s		[33]
	$0.22 - 6\,\mu$s	90% of values fall in this range	[9]
	$< 2.7\,\mu$s	Worst case scenario in Hamburg	[34]
	$< 5.4\,\mu$s	Worst case scenario in Stuttgart	[34]
	$< 4.0\,\mu$s	Worst case scenario in Dusseldorf	[34]
	$< 8.3\,\mu$s	Worst case scenario in Frankfurt	[34]
	$< 19.6\,\mu$s	Worst case scenario in Kronberg	[34]
Highway	$< 0.45\,\mu$s		[8]
	$< 0.5\,\mu$s		[31]
	$< 1.8\,\mu$s	High traffic	[35]
	$< 1.2\,\mu$s	Low traffic	[35]
Indoor	$0.01 - 0.1\,\mu$s		[29]
	$0.02 - 0.04\,\mu$s		[20]
	$0.03 - 0.13\,\mu$s		[16]
	$< 0.05\,\mu$s		[2]
	$< 0.1\,\mu$s		[4]
	$< 0.1\,\mu$s		[5]
	$< 0.1\,\mu$s		[6]
	$< 0.05\,\mu$s		[17]

Table 3.2: Summary of RMS delay spread values reported in the literature.

3.3.6 Rician κ-factor

We wanted to consider several different scenarios in our simulations - a scenario when the LOS path is strong, a scenario when the LOS path is weak, and a scenario when there is no LOS path. Davis and Linnartz did work on measuring the strength of the LOS path in [15] - they reported that the Rician κ-factor typically fell in the range from 5 to 11. Thus, we set $\kappa = 10$ in our strong LOS scenario and set $\kappa = 5$ in our weak LOS scenario.

3.3.7 SNR

We decide to look at several different values for the SNR, which we define as the ratio of the power in the gain of one of the reflected paths to the noise. Recall that we are modeling the gain of each reflected path as a $CN(0, 1)$ random variable. Thus, we model the noise $n(t)$ as a $CN(0, 1/SNR)$ random variable.

The values of SNR that we simulate are $0, 3, 5, 10, 15$, and 20 dB. However, we are primarily interested in the large SNR regime. Much of the literature on measuring RMS delay spread reports high SNR values, and the power of thermal noise is assumed to be quite low. The typical practice to distinguish between multipath and noise in the literature is to pick some threshold and then consider everything below this threshold noise and everything above this threshold multipath. These thresholds are usually in reference to the power of the strongest path. For example, Sen and Matolak in [35] pick a threshold of 25 dB below the strongest path. Paier, et al. in [31] pick a threshold of 60 dB below the strongest path. Cheng, et al. in [8] pick a threshold of 15 dB below the strongest path. These are large thresholds, and thus we considered it appropriate to focus on the large values of SNR in our analysis.

3.3.8 Summary

We end this chapter by summarizing our parameter choices as well as their effect on the other parameters of our channel model. Recall that our model for the wireless channel is:

$$y(t) = ax(t - \tau_d) + \sum_{i=1}^{M} b_i x(t - \tau_d - \tau_i) + n(t) \tag{3.15}$$

Note that we no longer have the channel gains varying over time as per our discussion above. Thus, we no longer need to worry about the effect of the mobile velocity v or the carrier frequency f_c on our model. Therefore, we simply model each of the reflected path gains as:

$$b_i \sim CN(0, 1) \tag{3.16}$$

In the event that there is a LOS path, we model the gain as:

$$a = \sqrt{\kappa} e^{i\theta} + CN(0, 1) \tag{3.17}$$

The Rician factor κ is either 10 or 5, depending on whether we are considering a scenario where the LOS path is strong or weak.

We look at 6 different values for the SNR: $0, 3, 5, 10, 15$, and 20 dB. The effect of the SNR on our simulation is that they determine the power of the noise. Our noise $n(t) \sim CN(0, 1/SNR)$.

We look at three different values for the bandwidth, W: $3, 6$, and 18 MHz. We look at three different values for the RMS delay spread, τ_{RMS}, that correspond to our three different environments of interest: $5\,\mu$s (outdoor), $1\,\mu$s (highway), and $0.1\,\mu$s (indoor). These two parameters together determine the rest of our model parameters. Their effect is summarized in tables 3.3 and 3.4.

W	T_{sample}	U
3 MHz	$\approx 0.056\,\mu$s	600
6 MHz	$\approx 0.167\,\mu$s	300
18 MHz	$\approx 0.333\,\mu$s	100

Table 3.3: Values of sampling interval T_{sample} and upsampling factor U for our possible choices of bandwidth W.

	3 MHz	6 MHz	18 MHz
$5\,\mu$s (outdoor)	15	30	90
$1\,\mu$s (highway)	3	6	18
$0.1\,\mu$s (indoor)	1	1	2

Table 3.4: Number of reflected paths M for our possible choices of bandwidth W and RMS delay spread τ_{RMS}.

Chapter 4

Simulation Results

In this chapter, we look at the results from our simulations. We begin by describing how we collected data from our simulator. We then look at several tools that were useful for fitting the collected data to different models. Next, we take a look at the actual data and we fit those different sets of data to models and evaluate how good the fits are. Finally, we end with a discussion where we summarize our findings on what models are actually useful models for the actual data.

4.1 Data Collection

We implemented all of our simulations in MATLAB. The model for the wireless channel and the estimator were implemented as we described in chapter 3. We set the mobile and the base station to be 500 meters apart. There were several parameters that we varied: the scenario (whether or not we had a LOS path and the strength of that LOS path), the RMS delay spread (the environment), the bandwidth, and the SNR. We considered three different scenarios (a strong LOS scenario, a weak LOS scenario, and an NLOS scenario), three different values for the RMS delay spread (0.1, 1, and 5 μs), three different values for the bandwidth (3, 6, and 18 MHz), and six different values for the SNR (0, 3, 5, 10, 15, and 20 dB). This amounts to 162 different possible combinations of parameters. For each of these combinations of parameters, we first calculated the noise threshold. Then, we simulated 1000 ranging operations and recorded the time of the first peak above the noise threshold. In the event that there was no peak above the noise threshold, we recorded that the ranging operation failed on that attempt. This happens more often at lower SNR - this result makes sense because it is more likely for the actual signal to get lost in the noise at low SNR.

After recording all of the times, we multiplied them by the speed of light and subtracted off the true distance between the mobile and base station (500 meters) to yield measurements of the error between the measurements and the true distance. Recalling the language of chapter 2, d is our true distance, $\hat{d}$ is our distance estimate, and e is the estimation error. They have the following

relationship:

$$e = \hat{d} - d \tag{4.1}$$

We want a model for the estimation error, e.

4.2 Tools for Model Fitting

There were two types of tools that we needed for model fitting - we needed tools to find the best fits for the theoretical models to the data and we needed tools to evaluate how good these fits were. For fitting the models, we used maximum likelihood estimation to estimate the parameters of the different models. For evaluating the models, we used two tools: we used QQ-plots to give us a way to visually evaluate how good the models were, and we used K-L divergence as a metric of how far the theoretical model deviated from the data as a way to compare different models.

4.2.1 Different Models and MLE Fitting

We looked at nine different theoretical distributions to model the error measurements: normal, exponential, Rayleigh, gamma, Cauchy, skewed normal, exponential power, Weibull, and the Student's t. Of these nine distributions, four of them cannot take on negative values - the exponential, Rayleigh, gamma, and Weibull. However, some of our error measurements are negative, so in order to accommodate for this we added an extra location parameter to each of these distributions to indicate how much the distribution needed to be shifted.

Each of these distributions is a parametric distribution. We used maximum-likelihood estimation to find the parameters that result in the best fit for the data. Suppose $\overline{e}$ is the vector of our errors, and θ is some set of parameters for our theoretical distribution. Let $p(\overline{e}|\theta)$ be the PDF of our theoretical distribution with parameters θ. Then the maximum-likelihood estimate for the parameters is:

$$\theta_{MLE} = \arg\max_{\theta} p(\overline{e}\,|\,\theta) \tag{4.2}$$

There are some built in functions in MATLAB that do maximum-likelihood estimation of parameters for certain distributions, like `normfit`. For the rest of the distributions, we use the built-in function `mle`.

Normal Distribution

The normal distribution has two parameters: a location parameter μ and a scale parameter $\sigma > 0$. It's PDF is:

$$f(x) = \frac{1}{\sqrt{2\pi\sigma^2}} e^{-\frac{(x-\mu)^2}{2\sigma^2}} \tag{4.3}$$

A plot of the PDF of the normal random variable for different parameters is in Figure 4.1

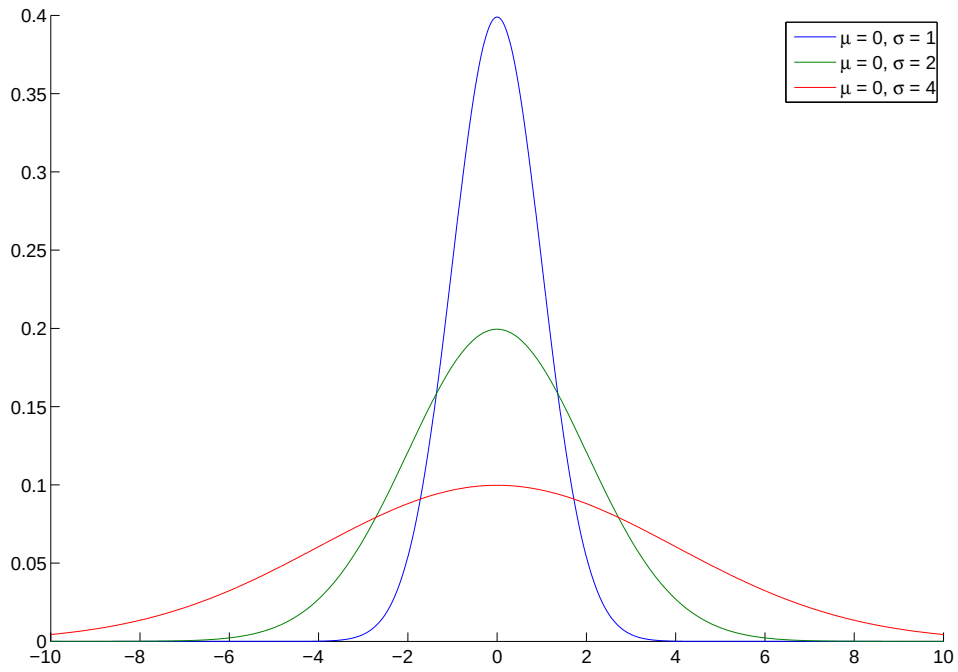

Figure 4.1: Plot of the PDF of a normal random variable for various parameters.

Exponential Distribution

The exponential distribution normally has one parameter, a scale parameter $\lambda > 0$. We add an additional parameter, a location parameter x_0 that indicates how far left along the x-axis we need to shift it. It's PDF is:

$$f(x) = \lambda e^{-\lambda(x+x_0)} \tag{4.4}$$

A plot of the PDF of the exponential random variable for different parameters is in Figure 4.2

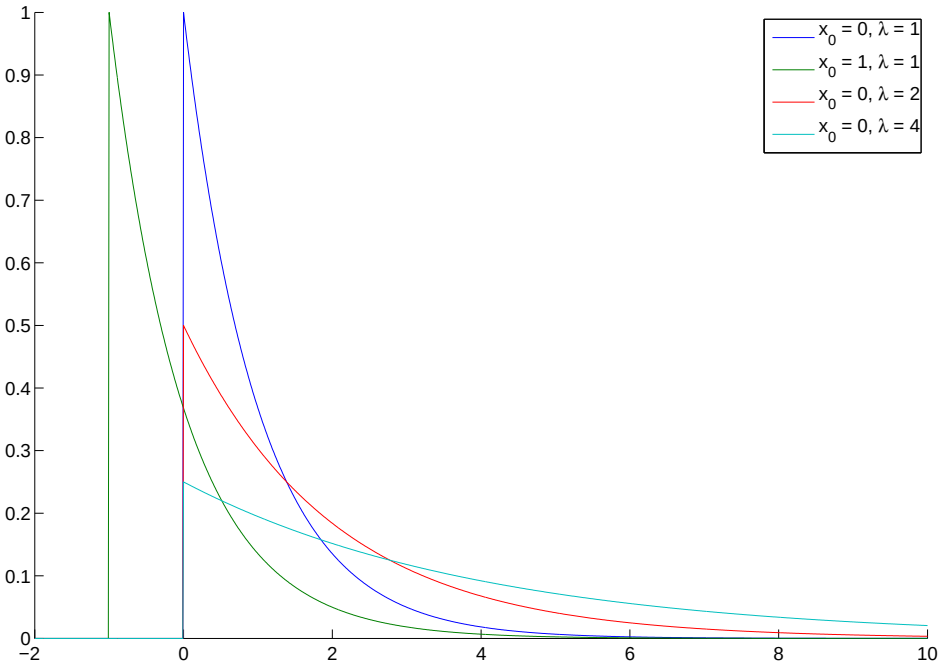

Figure 4.2: Plot of the PDF of a exponential random variable for various parameters.

Rayleigh Distribution

The Rayleigh distribution normally has one parameter, a scale parameter $\sigma > 0$. We add an additional parameter, a location parameter x_0 that indicates how far left along the x-axis we need to shift it. It's PDF is:

$$f(x) = \frac{x + x_0}{\sigma^2} e^{-\frac{(x+x_0)^2}{2\sigma^2}} \tag{4.5}$$

A plot of the PDF of the Rayleigh random variable for different parameters is in Figure 4.3

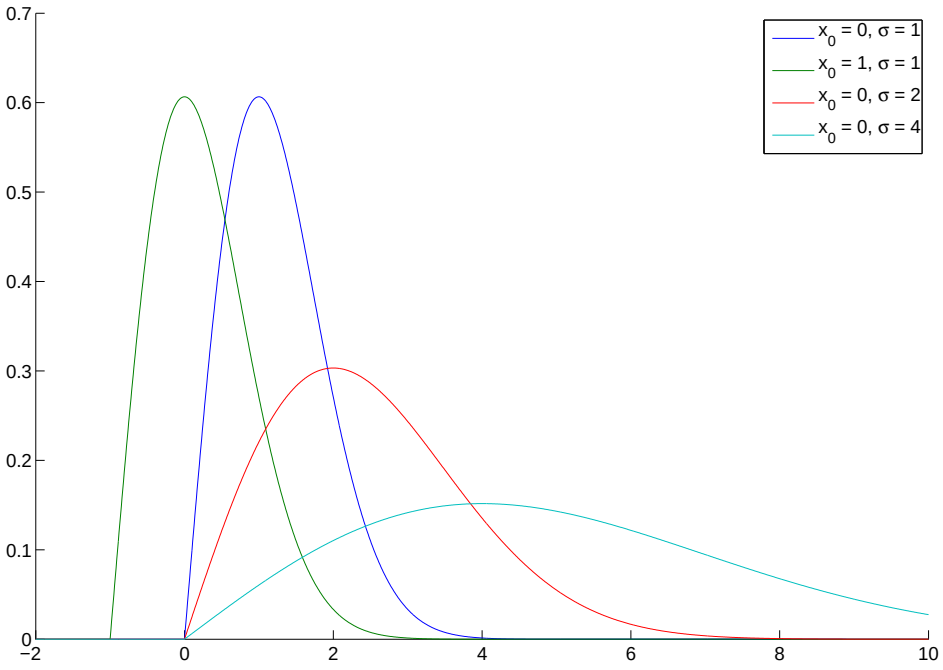

Figure 4.3: Plot of the PDF of a Rayleigh random variable for various parameters.

Gamma Distribution

The gamma distribution normally has two parameters, a shape parameter $k > 0$ and a scale parameter $\theta > 0$. We add an additional parameter, a location parameter x_0 that indicates how far left along the x-axis we need to shift it. It's PDF is:

$$f(x) = (x + x_0)^{k-1} \frac{e^{-(x+x_0)/\theta}}{\Gamma(k)\theta^k} \tag{4.6}$$

where $\Gamma(x)$ is the gamma function. If k is an integer, then it coincides with the distribution of a sum of k i.i.d./ exponential random variables. A plot of the PDF of the gamma random variable for different parameters is in Figure 4.4

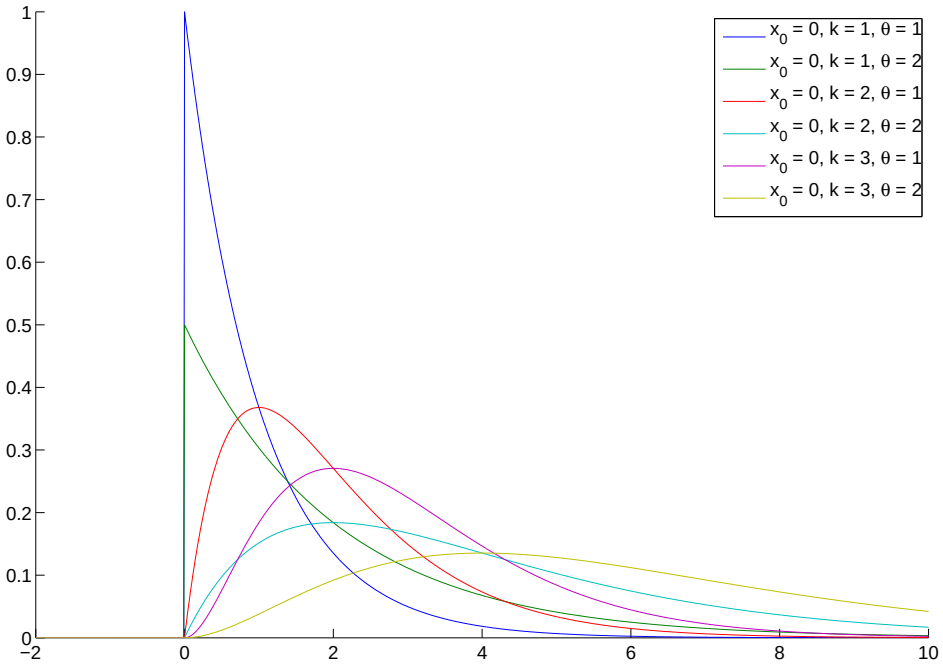

Figure 4.4: Plot of the PDF of a gamma random variable for various parameters.

Cauchy Distribution

The Cauchy distribution has two parameters: a location parameter x_0 and a scale parameter $\gamma > 0$. It's PDF is:

$$f(x) = \frac{1}{\pi\gamma\left[1 + \left(\frac{x-x_0}{\gamma}\right)^2\right]} \tag{4.7}$$

It has heavier tails than the normal distribution. A plot of the PDF of the Cauchy random variable for different parameters is in Figure 4.5

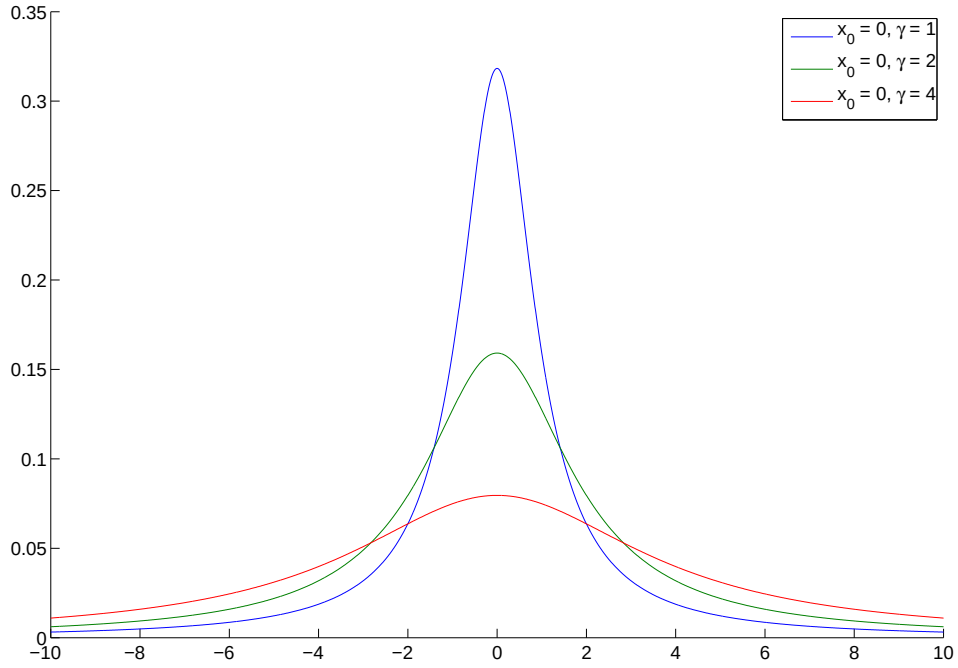

Figure 4.5: Plot of the PDF of a Cauchy random variable for various parameters.

Skewed Normal Distribution

The skewed normal distribution has three parameters: a location parameter ϵ, a scale parameter $\omega > 0$, and a shape parameter α. It's PDF is:

$$f(x) = \left(\frac{2}{\omega}\right) \phi\left(\frac{x-\epsilon}{\omega}\right) \Phi\left(\alpha\left(\frac{x-\epsilon}{\omega}\right)\right) \tag{4.8}$$

where $\phi(x)$ is the PDF of the standard normal random variable and $\Phi(x)$ is the CDF of the standard normal random variable. The distribution is left skewed when $\alpha < 0$ and right skewed when $\alpha > 0$. A plot of the PDF of the skewed normal random variable for different parameters is in Figure 4.6

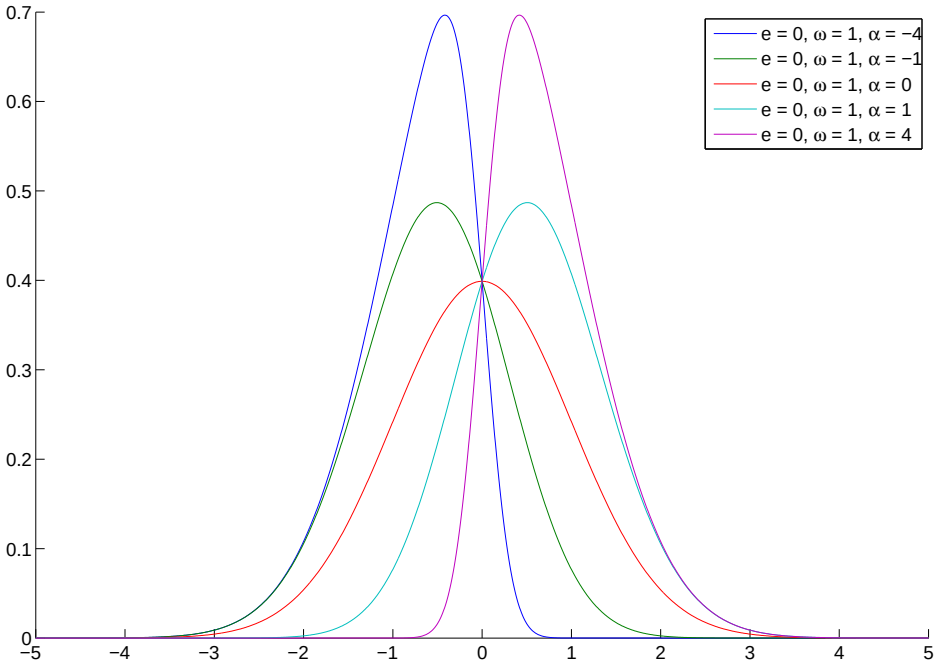

Figure 4.6: Plot of the PDF of a skewed normal random variable for various parameters.

Exponential Power Distribution

The exponential power distribution has three parameters: a location parameter μ, a scale parameter $\alpha > 0$, and a shape parameter $\beta > 0$. It's PDF is:

$$\frac{\beta}{2\alpha\Gamma(1/\beta)} e^{-(|x-\mu|/\alpha)^{\beta}} \tag{4.9}$$

where $\Gamma(x)$ is the gamma function. The exponential power distribution is a part of the generalized family of normal distributions with its extra shape parameter. When $\beta = 2$ it coincides with a normal distribution and when $\beta = 1$ it coincides with a Laplace distribution. As $\beta approaches \infty$, it approaches the uniform distribution. A plot of the PDF of the exponential power random variable for different parameters is in Figure 4.7

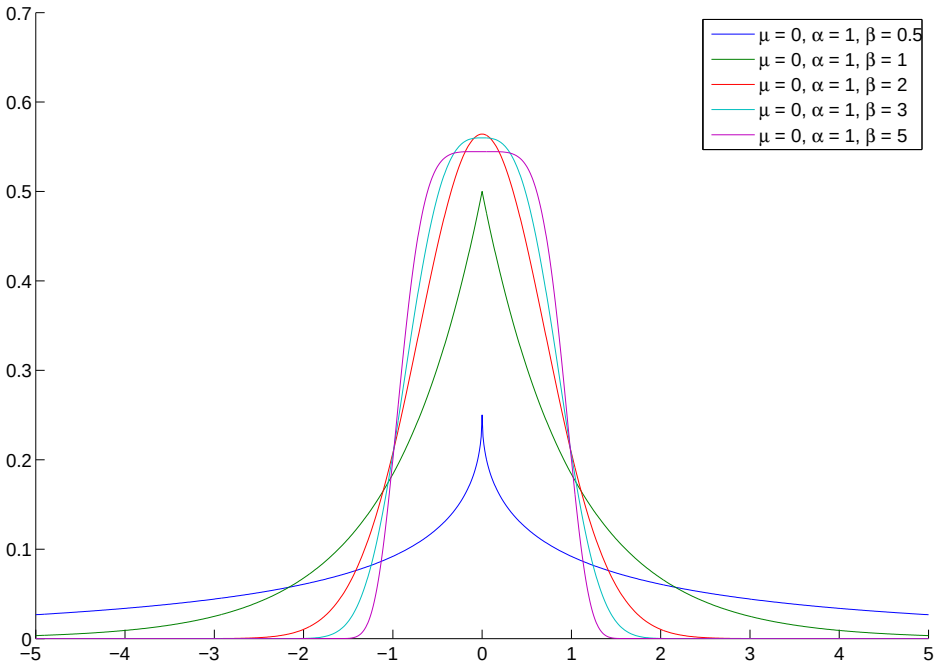

Figure 4.7: Plot of the PDF of a exponential power random variable for various parameters.

Weibull Distribution

The Weibull distribution normally has two parameters: a shape parameter $k > 0$ and a scale parameter $\lambda > 0$. We add an additional parameter, a location parameter x_0 that indicates how far left along the x-axis we need to shift it. It's PDF is:

$$f(x) = \begin{cases} \frac{k}{\lambda}\left(\frac{x+x_0}{\lambda}\right)^{k-1} e^{-((x+x_0)/\lambda)^k} & x + x_0 \geq 0 \\ 0 & x + x_0 < 0 \end{cases} \tag{4.10}$$

When $k = 1$, it coincides with an exponential distribution, and when $k = 2$ it coincides with a Rayleigh distribution. A plot of the PDF of the Weibull random variable for different parameters is in Figure 4.8

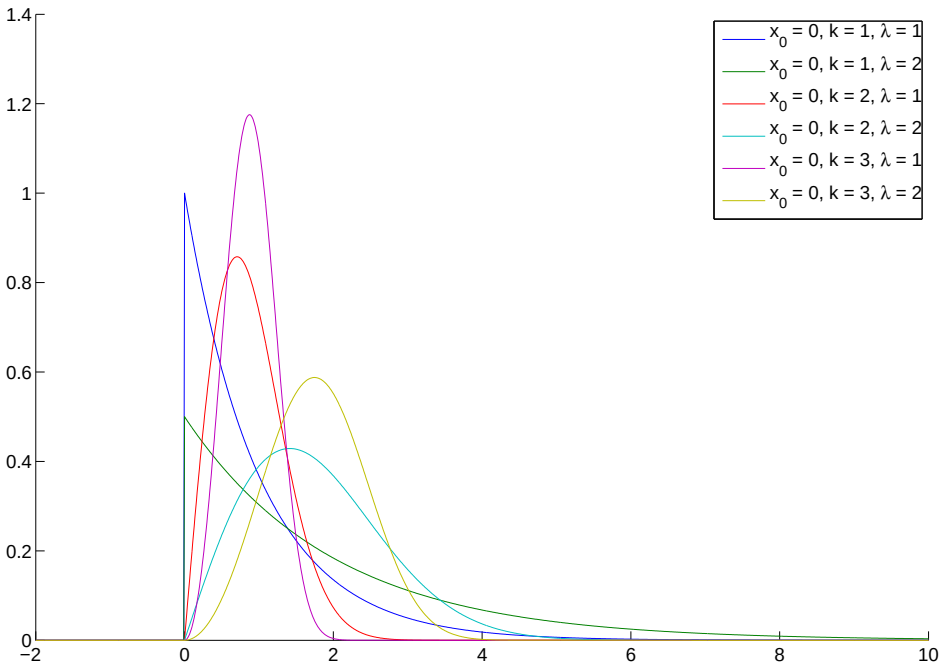

Figure 4.8: Plot of the PDF of a Weibull random variable for various parameters.

Student's t-distribution

The Student's t-distribution has three parameters: a location parameter μ, a scale parameter $\sigma > 0$, and a degree of freedoms parameter $\nu > 0$. It's PDF is:

$$f(x) = \frac{\Gamma\left(\frac{\nu+1}{2}\right)}{\sigma\sqrt{\nu\pi}\Gamma\left(\frac{\nu}{2}\right)}\left[\frac{\nu + \left(\frac{x-\mu}{\sigma}\right)^2}{\nu}\right]^{-\left(\frac{\nu+1}{2}\right)} \tag{4.11}$$

where $\Gamma(x)$ is the Gamma function. The Student's t-distribution is often often used in statistics to model data that is more prone to outliers as it has heavier tails than the normal distribution. When $\nu = 1$, it coincides with a Cauchy distribution. As ν approaches ∞, the Student's t-distribution approaches a normal distribution. A plot of the PDF of the Student's t-random variable for different parameters is in Figure 4.9

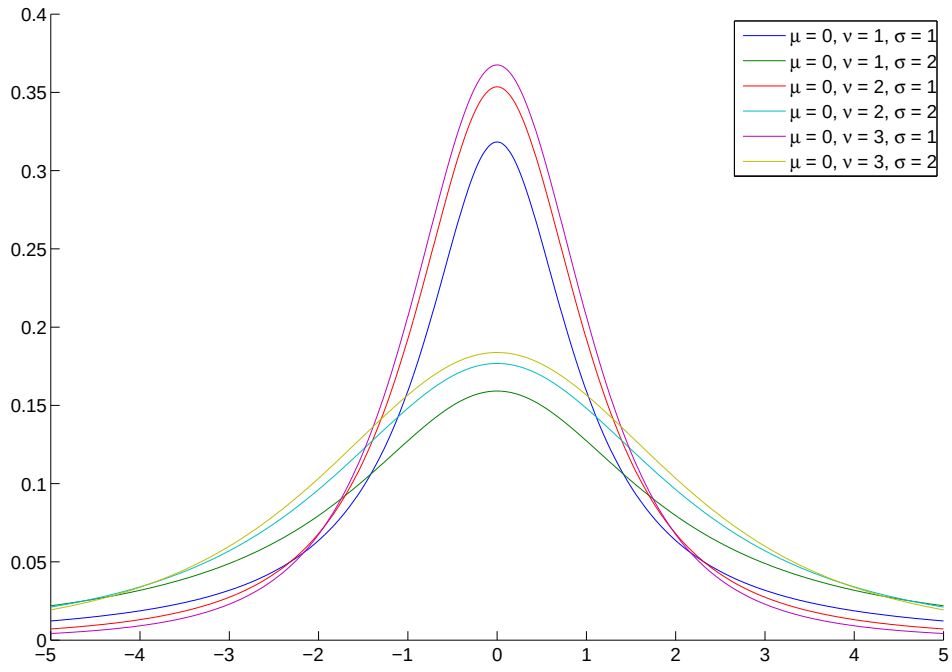

Figure 4.9: Plot of the PDF of a Student's t-random variable for various parameters.

4.2.2 QQ-Plots

A QQ-plot is a graphical method for comparing two probability distributions with each other. It plots the quantiles of one distribution versus the quantiles of the other distribution. If the points of the QQ-plot lie on the line $x = y$, then it is likely that these two distributions are the same distribution. If the points lie on a line, but not on the line $x = y$, then it is likely that the two distributions are similar, but they differ by a scale or location factor.

We use the built in function `qqplot(X,Y)` in MATLAB. This function takes in two data sets, X and Y, and plots the quantiles of X versus the quantiles of Y. Since we are interested in comparing the actual data to some theoretical distribution, we set X to be a vector of our actual error measurements, and we set Y to be a large number of samples from our theoretical distribution.

The usage of a QQ-plot is best illustrated through an example. Suppose that we have three data sets. X and Y are both collections of 1000 samples of a standard normal random variable. Z is a collection of 1000 samples of an exponential random variable with location parameter 0 and scale parameter 2. To make the plots easy to read, we have chosen to plot every fifth percentile. In Figure 4.10 we have the QQ-plot of X versus Y. Every blue point corresponds to a fifth percentile of X and Y. The red line is the line that is the best fit for the blue points, and the black line is the line $y = x$.

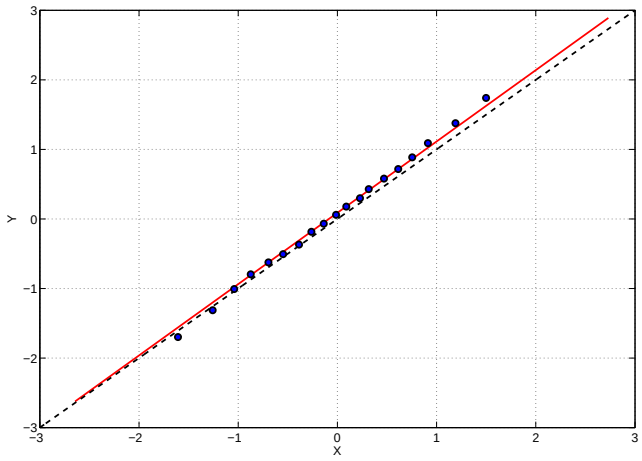

Figure 4.10: QQ-plot of X versus Y.

We start our interpretation by looking at the blue points. We see that the leftmost blue point has an x-value of -1.6 and a y-value of -1.7. This means that 5% of the values in X are in the interval $(-\infty, -1.6]$, and 5% of the values in Y are in the interval $(-\infty, -1.7]$. The second blue point has an x-value of -1.2 and a y-value of -1.3. This means that 5% of the values in X are

in the interval $(-1.6, -1.2]$, and 5% of the values in Y are in the interval $(-1.7, -1.3]$, and so on. However, it is more useful to look at the red and black lines. We see that the blue points do appear to follow the red line well, and that the red line is very close to the black line. This means that X and Y were likely drawn from the same distribution, which is what we would expect.

In Figure 4.11 we have the QQ-plot of X versus Z. In this plot, we see that the blue points do not follow the red line very well. On top of that the red line is not very close to the black line. This means that X and Z were likely not drawn from the same distribution, which is what we would expect.

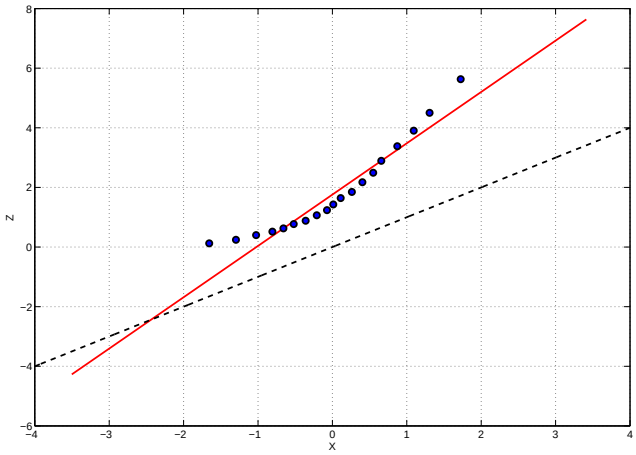

Figure 4.11: QQ-plot of X versus Z.

4.2.3 K-L Divergence

We used Kulback-Leibler divergence as a metric for determining which of our fitted distributions are the better fits to the actual data. Given two probability mass functions, $p(x)$ and $q(x)$, the K-L divergence is defined as:

$$D(p||q) = \sum_x p(x) \log \frac{p(x)}{q(x)} \tag{4.12}$$

We use the convention that $0 \log \frac{0}{q} = 0$, for all q, and that $p \log \frac{p}{0} = \infty$ for $p \neq 0$. The K-L divergence is not a true distance because it is not symmetric. However, it is useful as a tool to compare how similar two distributions are.

Suppose that $p(x)$ is the actual distribution that our data is drawn from, and let $q_1(x)$ and $q_2(x)$ be two possible fits to the actual data. We say that if $D(p||q_1) < D(p||q_2)$, then q_1 is probably a better fit to the actual data than q_2.

There are several issues that we need to work through. The first issue is that we do not have the actual distribution $p(x)$ - although, we do have the data. The second issue is that this equation for the K-L divergence is for discrete data, whereas in general we would expect the data to be continuous. There is a form of the K-L divergence for continuous distributions that replaces the summation with integrals. However, instead of choosing this route (which would require us to estimation the density of $p(x)$ from the observed data), we decided to stick to the formula for the K-L divergence for discrete data. We do this through binning.

4.3 Looking at the Data

In Figures 4.12 - 4.20 we plotted the empirical CDF of the error for all successful ranging operations. Each figure focuses on a single scenario (LOS, weak LOS, or NLOS) in a single environment (outdoor, highway, or indoor) and compares the effect of SNR and bandwidth on the distribution of the error. The accompanying tables in Tables 4.1 - 4.9 also focus on a single scenario in a single environment and gives a summary of the number of failed ranging operations for different values of SNR and bandwidth.

On the whole, the data behaves as we would expect it to behave. Lower SNR causes the magnitude of the ranging error to increase, and it also results in a greater number of failed ranging operations. The error gets worse from the LOS to the weak LOS scenario, and it gets worse still when we go to the NLOS scenario. Decreased RMS delay spread also decreases the error, which makes sense because the interval of time in which we can see strong reflections is decreased. However, decreased RMS delay spread also increases the chances that we will miss the signal entirely, and thus it also results in a greater number of failed ranging operations.

The only discrepancy between what we see and what we expect is with regards to bandwidth. We would expect greater error as bandwidth decreases - however, the plots seem to say that the the error gets worse as bandwidth increases, especially at low SNR and in the LOS and weak LOS scenarios. However, this discrepancy can be explained by noting that at lower bandwidth there is a better chance for ranging operations to fail. A large proportion of the failed ranging operations are likely cases when the LOS path was weak and we would have likely characterized a reflection as the LOS signal, thus resulting in a large error. When the bandwidth is large, we were able to detect this reflection; however, when the bandwidth is small, we missed it and ended up characterizing the ranging operation as a failure. Thus, it appears that decreased bandwidth results in less error, when it is not actually the case.

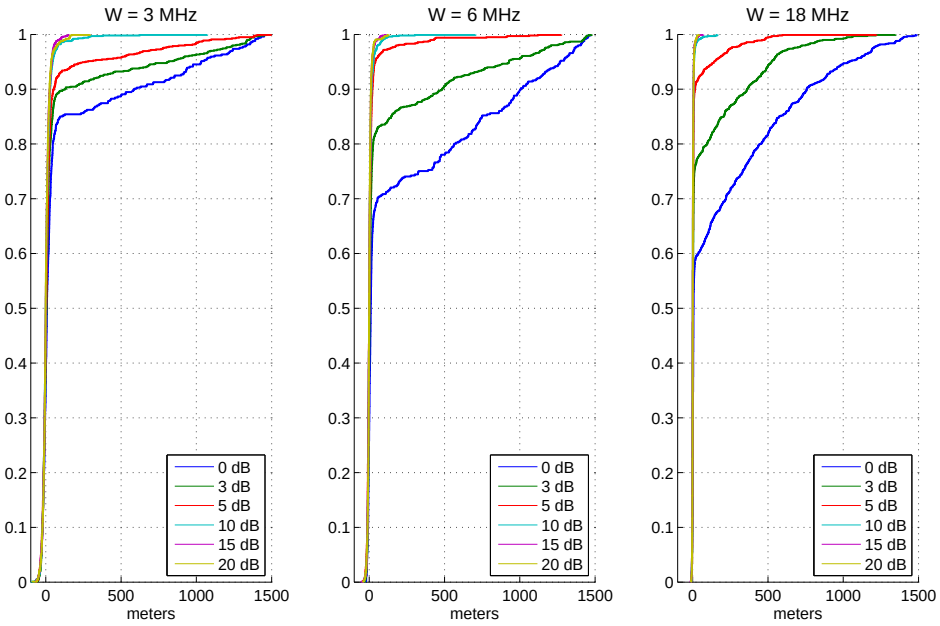

Figure 4.12: Comparison of the empirical CDF of the error of all successful ranging operations under the LOS scenario and in the outdoor environment for different values of SNR and bandwidth.

	3 MHz	**6 MHz**	**18 MHz**
0 dB	506	499	67
3 dB	99	83	1
5 dB	12	0	0
10 dB	0	0	0
15 dB	0	0	0
20 dB	0	0	0

Table 4.1: Number of failed ranging operations out of 1000 under the LOS scenario and in the outdoor environment for different values of SNR and bandwidth.

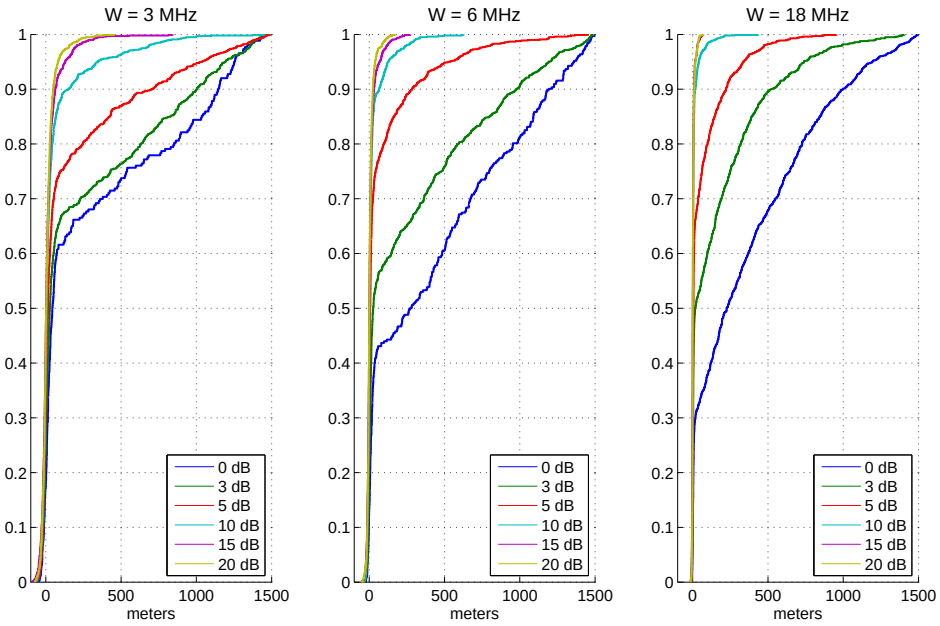

Figure 4.13: Comparison of the empirical CDF of the error of all successful ranging operations under the weak LOS scenario and in the outdoor environment for different values of SNR and bandwidth.

	3 MHz	**6 MHz**	**18 MHz**
0 dB	737	668	88
3 dB	229	149	2
5 dB	43	0	0
10 dB	3	0	0
15 dB	0	0	0
20 dB	0	0	0

Table 4.2: Number of failed ranging operations out of 1000 under the weak LOS scenario and in the outdoor environment for different values of SNR and bandwidth.

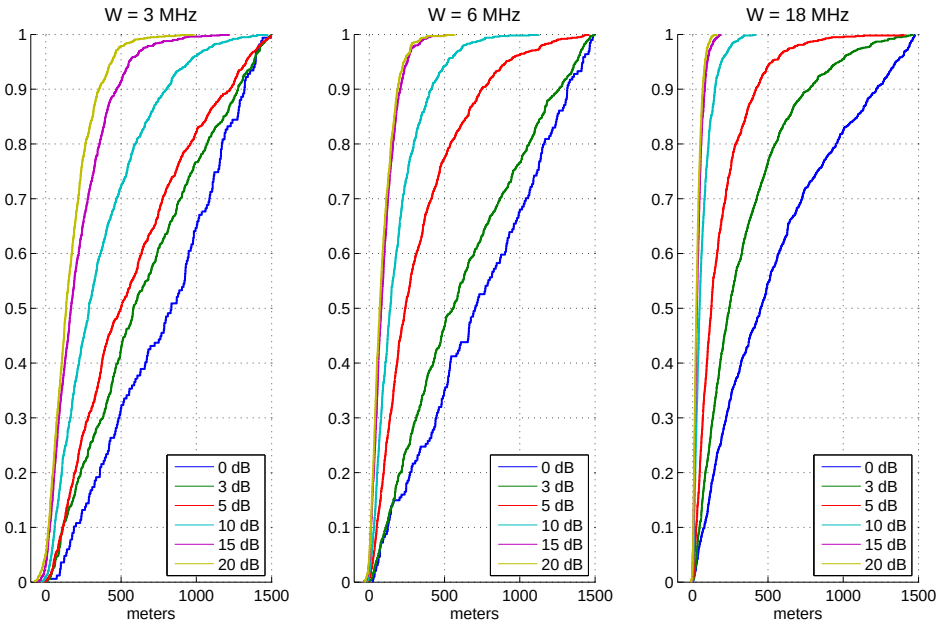

Figure 4.14: Comparison of the empirical CDF of the error of all successful ranging operations under the NLOS scenario and in the outdoor environment for different values of SNR and bandwidth.

	3 MHz	**6 MHz**	**18 MHz**
0 dB	833	806	158
3 dB	451	285	9
5 dB	171	7	0
10 dB	12	0	0
15 dB	0	0	0
20 dB	0	0	0

Table 4.3: Number of failed ranging operations out of 1000 under the NLOS scenario and in the outdoor environment for different values of SNR and bandwidth.

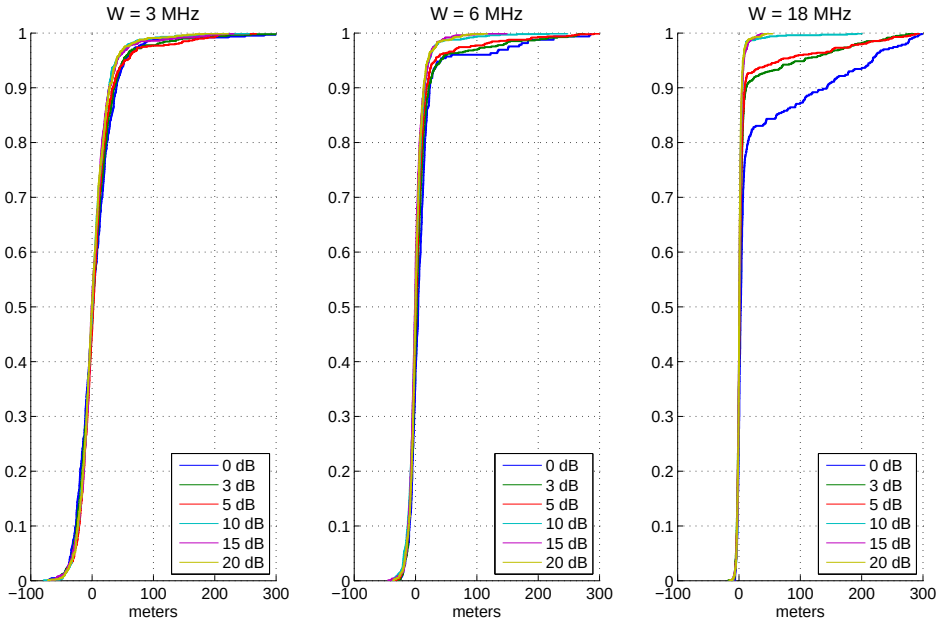

Figure 4.15: Comparison of the empirical CDF of the error of all successful ranging operations under the LOS scenario and in the highway environment for different values of SNR and bandwidth.

	3 MHz	**6 MHz**	**18 MHz**
0 dB	380	673	528
3 dB	103	179	47
5 dB	129	24	30
10 dB	2	1	1
15 dB	0	0	0
20 dB	0	0	0

Table 4.4: Number of failed ranging operations out of 1000 under the LOS scenario and in the highway environment for different values of SNR and bandwidth.

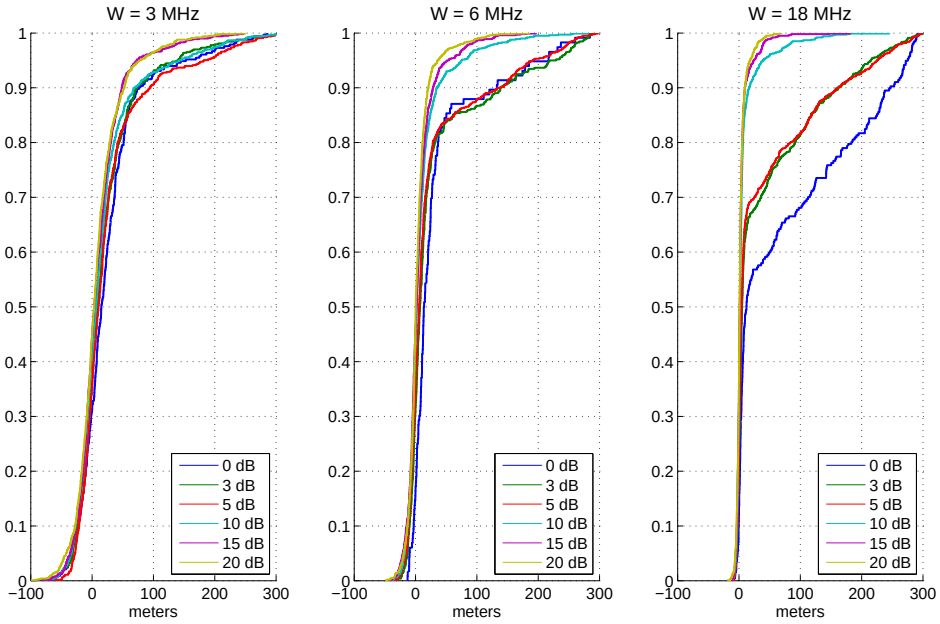

Figure 4.16: Comparison of the empirical CDF of the error of all successful ranging operations under the weak LOS scenario and in the highway environment for different values of SNR and bandwidth.

	3 MHz	**6 MHz**	**18 MHz**
0 dB	668	884	743
3 dB	366	480	96
5 dB	351	168	68
10 dB	29	11	0
15 dB	1	0	0
20 dB	1	0	0

Table 4.5: Number of failed ranging operations out of 1000 under the weak LOS scenario and in the highway environment for different values of SNR and bandwidth.

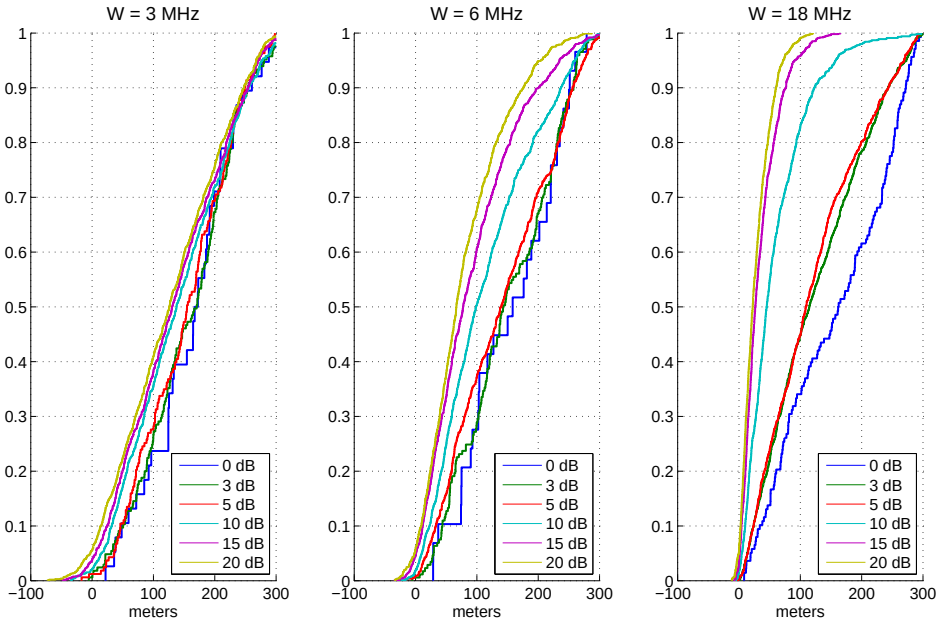

Figure 4.17: Comparison of the empirical CDF of the error of all successful ranging operations under the NLOS scenario and in the highway environment for different values of SNR and bandwidth.

	3 MHz	**6 MHz**	**18 MHz**
0 dB	962	971	862
3 dB	835	827	242
5 dB	837	457	216
10 dB	284	90	1
15 dB	72	4	0
20 dB	14	0	0

Table 4.6: Number of failed ranging operations out of 1000 under the NLOS scenario and in the highway environment for different values of SNR and bandwidth.

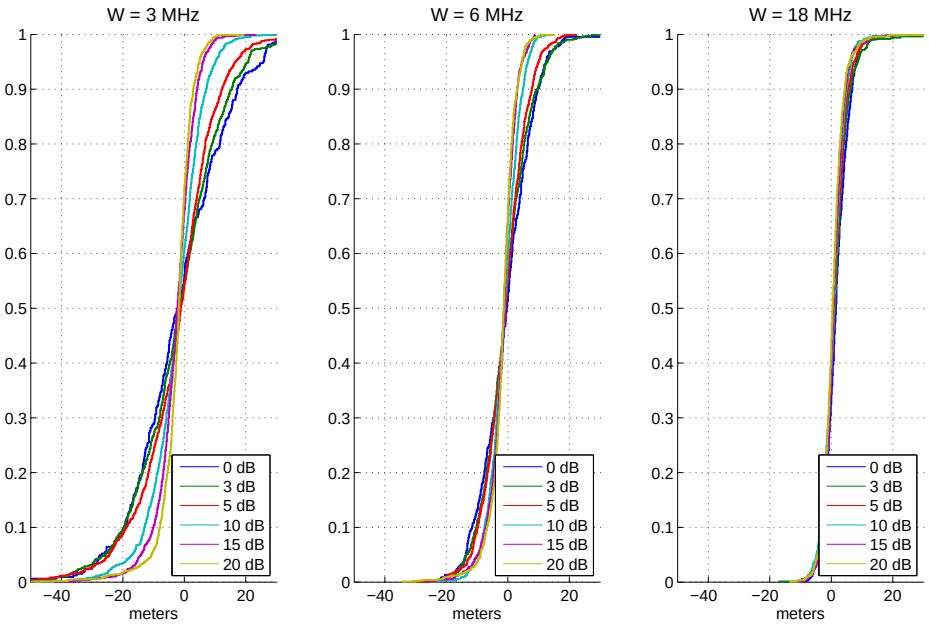

Figure 4.18: Comparison of the empirical CDF of the error of all successful ranging operations under the LOS scenario and in the indoor environment for different values of SNR and bandwidth.

	3 MHz	**6 MHz**	**18 MHz**
0 dB	674	546	526
3 dB	204	177	146
5 dB	66	99	62
10 dB	10	15	8
15 dB	2	3	0
20 dB	0	0	0

Table 4.7: Number of failed ranging operations out of 1000 under the LOS scenario and in the indoor environment for different values of SNR and bandwidth.

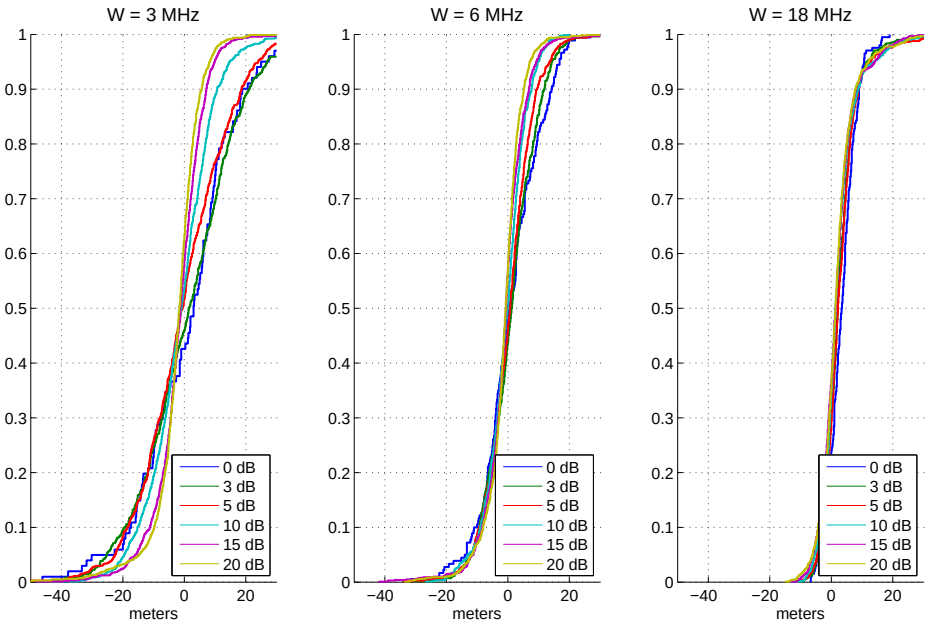

Figure 4.19: Comparison of the empirical CDF of the error of all successful ranging operations under the weak LOS scenario and in the indoor environment for different values of SNR and bandwidth.

	3 MHz	**6 MHz**	**18 MHz**
0 dB	899	820	796
3 dB	509	444	387
5 dB	295	303	260
10 dB	68	78	39
15 dB	20	11	4
20 dB	8	2	1

Table 4.8: Number of failed ranging operations out of 1000 under the weak LOS scenario and in the indoor environment for different values of SNR and bandwidth.

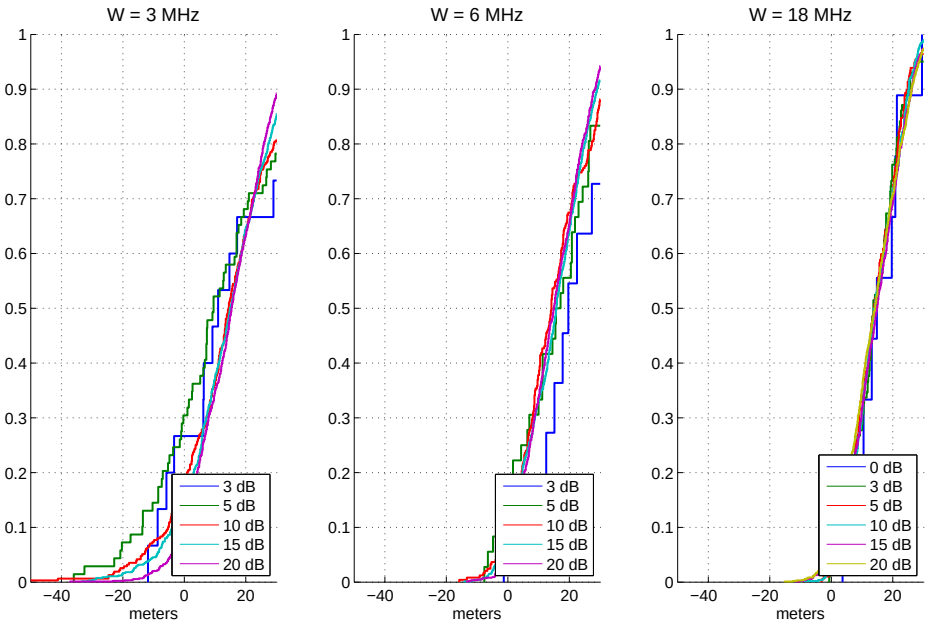

Figure 4.20: Comparison of the empirical CDF of the error of all successful ranging operations under the NLOS scenario and in the indoor environment for different values of SNR and bandwidth.

	3 MHz	**6 MHz**	**18 MHz**
0 dB	1000	1000	991
3 dB	985	989	899
5 dB	931	964	803
10 dB	688	754	476
15 dB	338	272	132
20 dB	115	132	60

Table 4.9: Number of failed ranging operations out of 1000 under the NLOS scenario and in the indoor environment for different values of SNR and bandwidth.

4.4 Model Fitting

In Figures 4.21 - 4.38 we have plotted nine different sets of data, the PDF of the fitted distributions, and QQ-plots to help evaluate which distributions are the best fit. Each figure focuses on a single scenario in a single environment, and we choose to look at the data that is associated with an SNR of 20 dB and a bandwidth of 18 MHz. There PDF plots look at a histogram of the errors and overlays a plot of the PDF of the best fit for each of our nine distributions. In the QQ-plots we look at every five percentiles. So, for example, the x-value of the leftmost point on each QQ-plot corresponds to the 5^{th} percentile of the actual data while the y-value of the leftmost point corresponds to the 5^{th} percentile of the fitted distribution. The second point corresponds to the 10^{th} percentile, and so on. We also plot the line that is the best fit to the points in red, and the line $y = x$ in black.

The accompanying tables in Tables 4.10 - 4.18 also focus on a single scenario in a single environment. In these tables, we give the KL-divergence between the actual data and the fitted model for all nine candidate distributions. For each distribution, we consider 9 sets of data: we have three choices for the bandwidth and we decide to restrict ourselves to three choices for the SNR - $10, 15$, and 20 dB. We decided to restrict ourselves to the three highest values for the SNR in light of our discussion in Chapter 3, and also because at lower SNR there are a lot fewer points to fit a model to because there are more failed ranging operations. For each set of data, we fit the distribution to it and record the KL-divergence between the data and the fitted distribution.

By looking at the QQ-plots, we get a good idea for what distributions would be good fits for different scenarios and environments. In the QQ-plots, we look for points that follow the line $y = x$. In many of the plots we see that the points follow a line, but it is not $y = x$, which tells us that the theoretical distribution is either more spread out or less spread out than the actual data. It is the distributions where the QQ-plots follow the line $y = x$ that we can consider as good fit. We see that in the LOS and weak LOS scenarios that the Cauchy, the exponential power, and the Student's t-distribution tend to provide good fits. In the NLOS scenario, we see that the normal, gamma, skew normal, exponential power, Weibull, and the Student's t-distribution tend to provide good fits. In addition to these, we see that the Rayleigh distribution also provides a good fit in the NLOS scenario in the outdoor and highway environments. However, when there are errors that are much smaller than the bulk of errors, as in the NLOS scenario in the indoor environment, it provides a much poorer fit since the bulk of the density in our shifted Rayleigh distribution is concentrated around the smallest value.

We get a similar picture by looking at the table of KL-divergence values. For the LOS and weak LOS scenarios, we see that the exponential power and Student's t-distributions are good choices in every environment. The Cauchy distribution is also a good choice in the outdoor and highway environment, but we see that in the indoor environment it is actually worse than the normal, gamma, skew normal, and Weibull distributions. For the NLOS scenario in the outdoor and highway environments, we see that the Rayleigh, gamma, skew normal, and Weibull distributions are good fits. For the NLOS scenario in the indoor environment, we see that the normal, gamma,

skew normal, exponential power, Weibull, and Student's t-distributions are good fits.

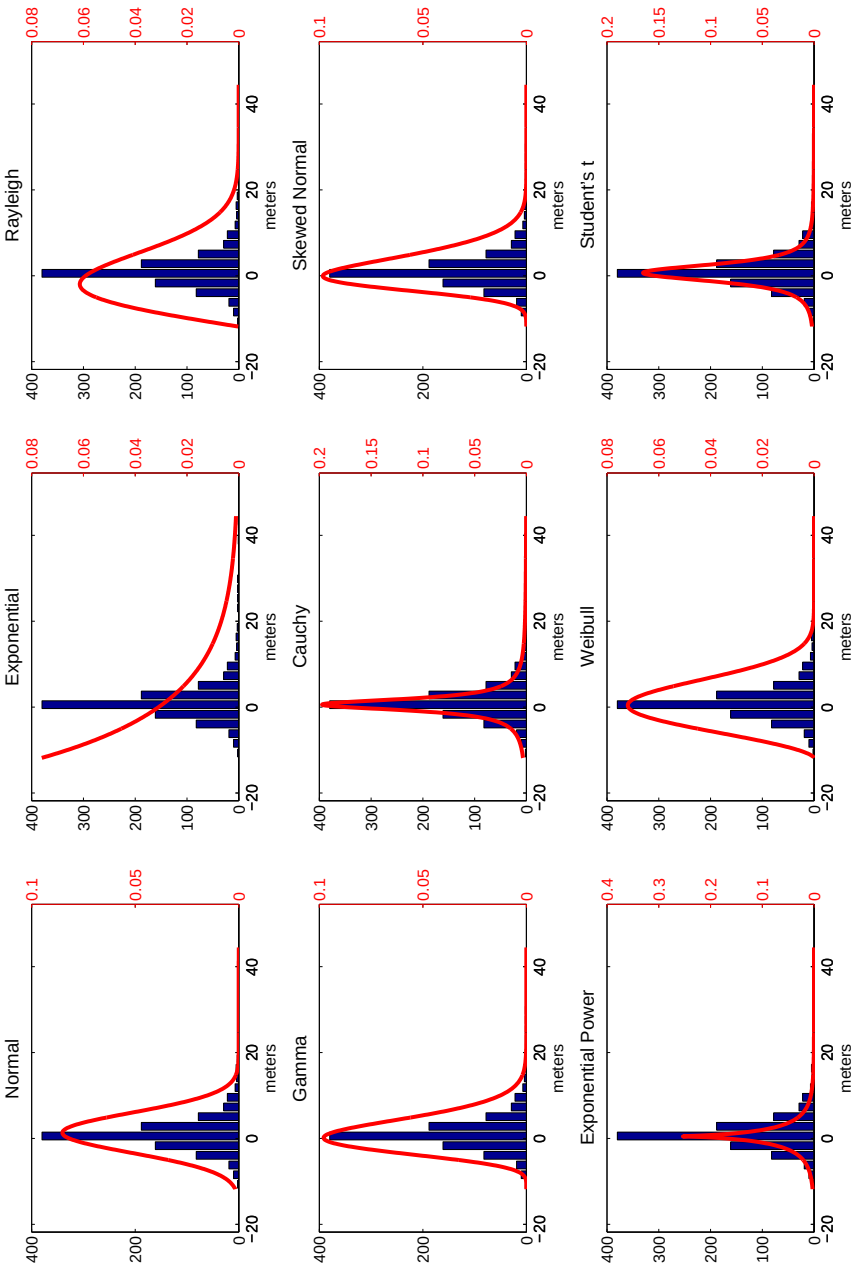

Figure 4.21: Histogram of the error of all successful ranging operations under the LOS scenario and in the outdoor environment and the PDF of the fitted distribution for nine different types of distributions.

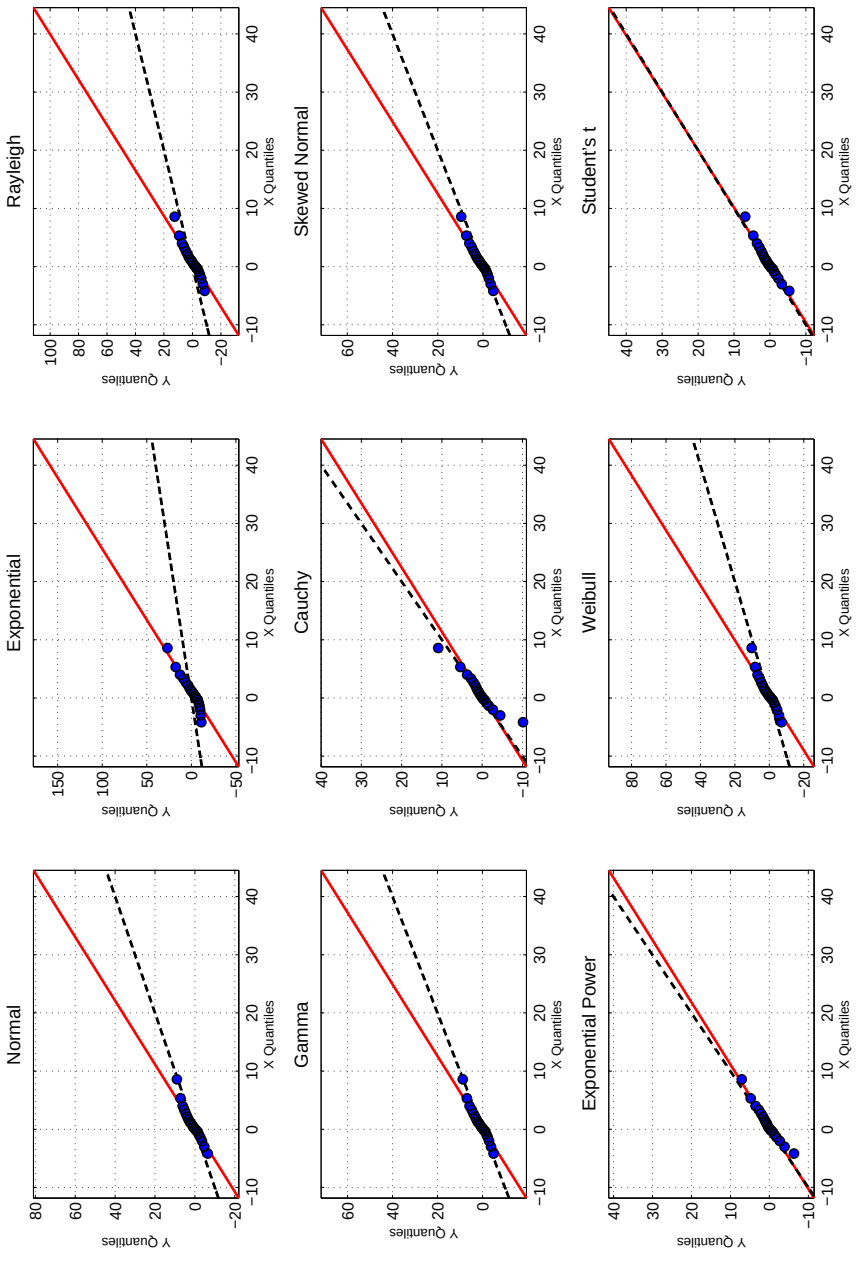

Figure 4.22: QQ plot of the quantiles of the error of all successful ranging operations under the LOS scenario and in the outdoor environment versus the fitted distribution for nine different types of distributions.

	Normal	Exponential	Rayleigh
3 MHz, 10 dB	0.8909	1.3249	0.7336
3 MHz, 15 dB	0.1924	1.2002	0.4438
3 MHz, 20 dB	0.4224	1.5552	0.7376
6 MHz, 10 dB	0.7464	0.5528	0.5682
6 MHz, 15 dB	0.3151	1.7145	0.8500
6 MHz, 20 dB	0.4950	1.4322	0.6703
18 MHz, 10 dB	1.2225	0.7981	0.9302
18 MHz, 15 dB	0.5271	1.4531	0.6851
18 MHz, 20 dB	0.4044	1.2923	0.5477
Mean	0.5796	1.2582	0.6852

	Gamma	Cauchy	Skew Normal
3 MHz, 10 dB	0.3480	0.0876	0.5329
3 MHz, 15 dB	0.1375	0.1262	0.1337
3 MHz, 20 dB	0.2350	0.1193	0.2489
6 MHz, 10 dB	0.2438	0.0121	0.5113
6 MHz, 15 dB	0.1973	0.1294	0.1929
6 MHz, 20 dB	0.2865	0.0988	0.3212
18 MHz, 10 dB	0.4181	0.0289	0.7849
18 MHz, 15 dB	0.2736	0.0896	0.3141
18 MHz, 20 dB	0.2202	0.1083	0.2408
Mean	0.2622	0.0889	0.3645

	Exponential Power	Weibull	Student's t
3 MHz, 10 dB	0.0856	0.7334	0.0345
3 MHz, 15 dB	0.0399	0.2409	0.0280
3 MHz, 20 dB	0.0681	0.5157	0.0474
6 MHz, 10 dB	0.0408	0.3900	0.0173
6 MHz, 15 dB	0.0587	0.4639	0.0363
6 MHz, 20 dB	0.0596	0.5438	0.0343
18 MHz, 10 dB	0.0667	0.6323	0.0289
18 MHz, 15 dB	0.0551	0.5745	0.0312
18 MHz, 20 dB	0.0599	0.4263	0.0475
Mean	0.0594	0.5023	0.0339

Table 4.10: Table of KL-divergence values between the error of all successful ranging operations under the LOS scenario and in the outdoor environment and the fitted distributions for nine different types of distributions for different values of SNR and bandwidth.

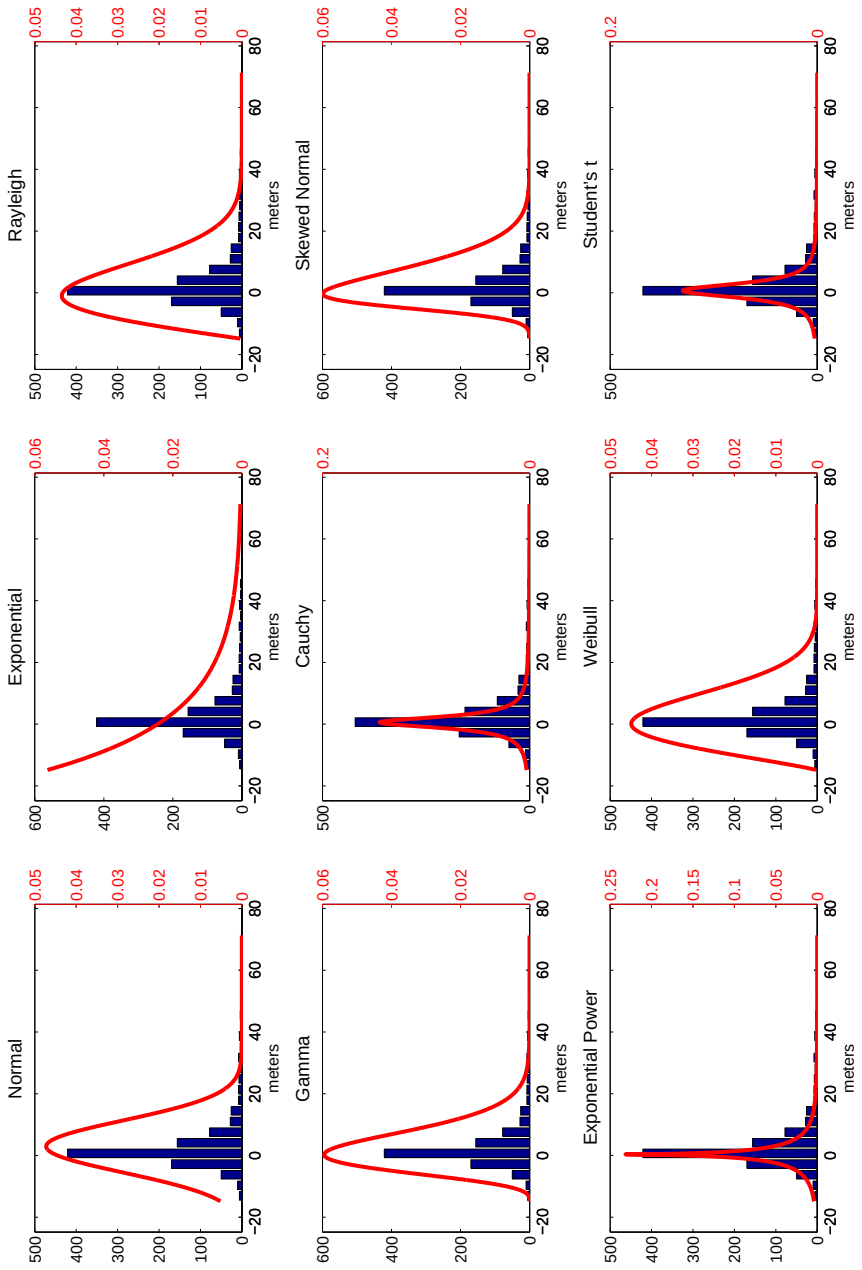

Figure 4.23: Histogram of the error of all successful ranging operations under the weak LOS scenario and in the outdoor environment and the PDF of the fitted distribution for nine different types of distributions.

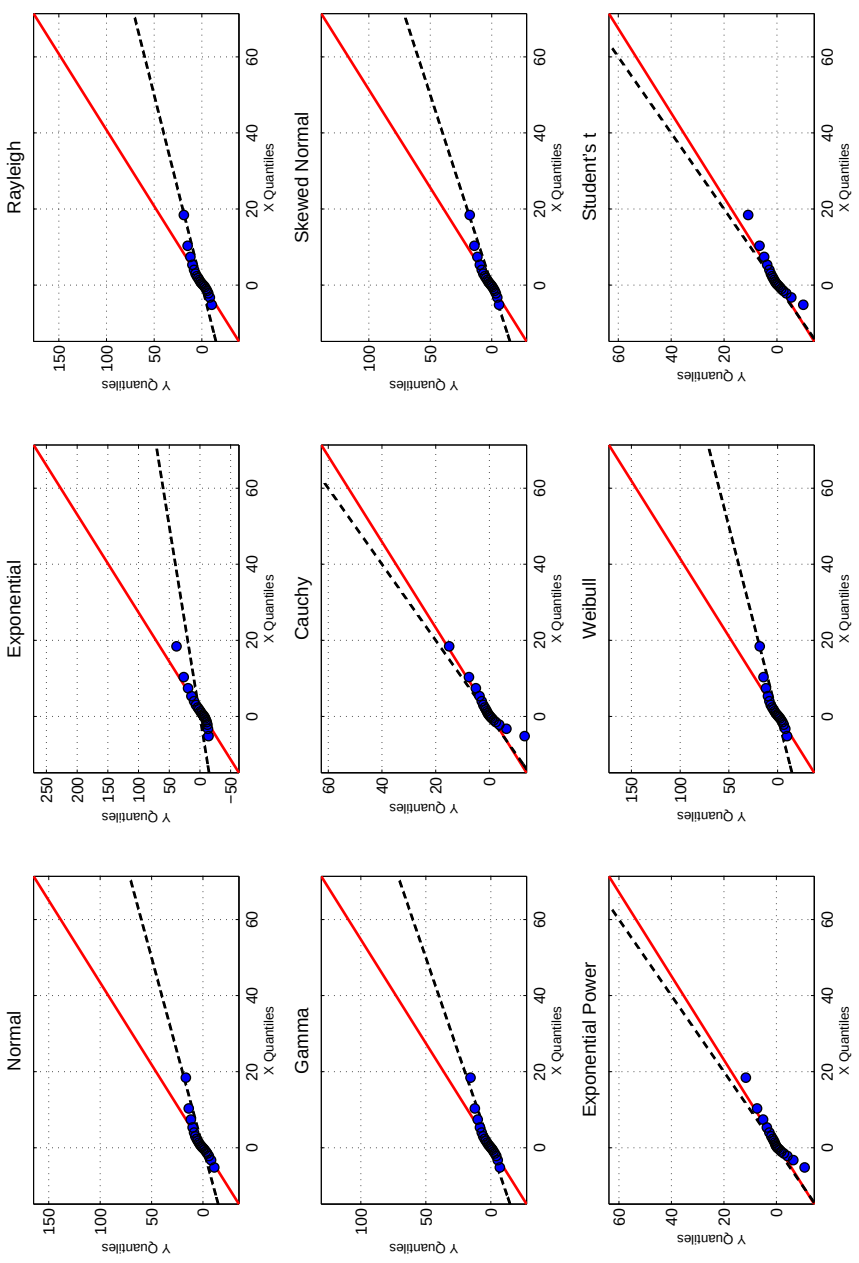

Figure 4.24: QQ plot of the quantiles of the error of all successful ranging operations under the weak LOS scenario and in the outdoor environment versus the fitted distribution for nine different types of distributions.

	Normal	Exponential	Rayleigh
3 MHz, 10 dB	1.5354	0.8404	1.2423
3 MHz, 15 dB	0.7773	1.0934	0.5756
3 MHz, 20 dB	0.5645	0.8141	0.3754
6 MHz, 10 dB	1.2631	0.6723	1.0140
6 MHz, 15 dB	0.7678	1.0532	0.5637
6 MHz, 20 dB	0.5115	1.2871	0.5777
18 MHz, 10 dB	0.6839	0.1521	0.7937
18 MHz, 15 dB	0.6819	1.1197	0.5473
18 MHz, 20 dB	0.6445	1.1225	0.5396
Mean	0.8255	0.9061	0.6921

	Gamma	Cauchy	Skew Normal
3 MHz, 10 dB	0.7073	0.1421	0.9851
3 MHz, 15 dB	0.3170	0.1057	0.3824
3 MHz, 20 dB	0.2142	0.1027	0.2832
6 MHz, 10 dB	0.5432	0.1075	0.8191
6 MHz, 15 dB	0.3469	0.1144	0.3913
6 MHz, 20 dB	0.2687	0.1163	0.2788
18 MHz, 10 dB	0.3887	0.0550	0.9041
18 MHz, 15 dB	0.3180	0.1210	0.3493
18 MHz, 20 dB	0.3376	0.1169	0.3544
Mean	0.3824	0.1091	0.5275

	Exponential Power	Weibull	Student's t
3 MHz, 10 dB	0.2180	0.7979	0.1392
3 MHz, 15 dB	0.1137	0.5755	0.0879
3 MHz, 20 dB	0.0981	0.3715	0.0559
6 MHz, 10 dB	0.1273	0.6229	0.1125
6 MHz, 15 dB	0.1228	0.5631	0.0988
6 MHz, 20 dB	0.0952	0.4915	0.0694
18 MHz, 10 dB	0.0682	0.2712	0.0626
18 MHz, 15 dB	0.1164	0.5386	0.0896
18 MHz, 20 dB	0.1132	0.5290	0.0984
Mean	0.1192	0.5290	0.0905

Table 4.11: Table of KL-divergence values between the error of all successful ranging operations under the weak LOS scenario and in the outdoor environment and the fitted distributions for nine different types of distributions for different values of SNR and bandwidth.

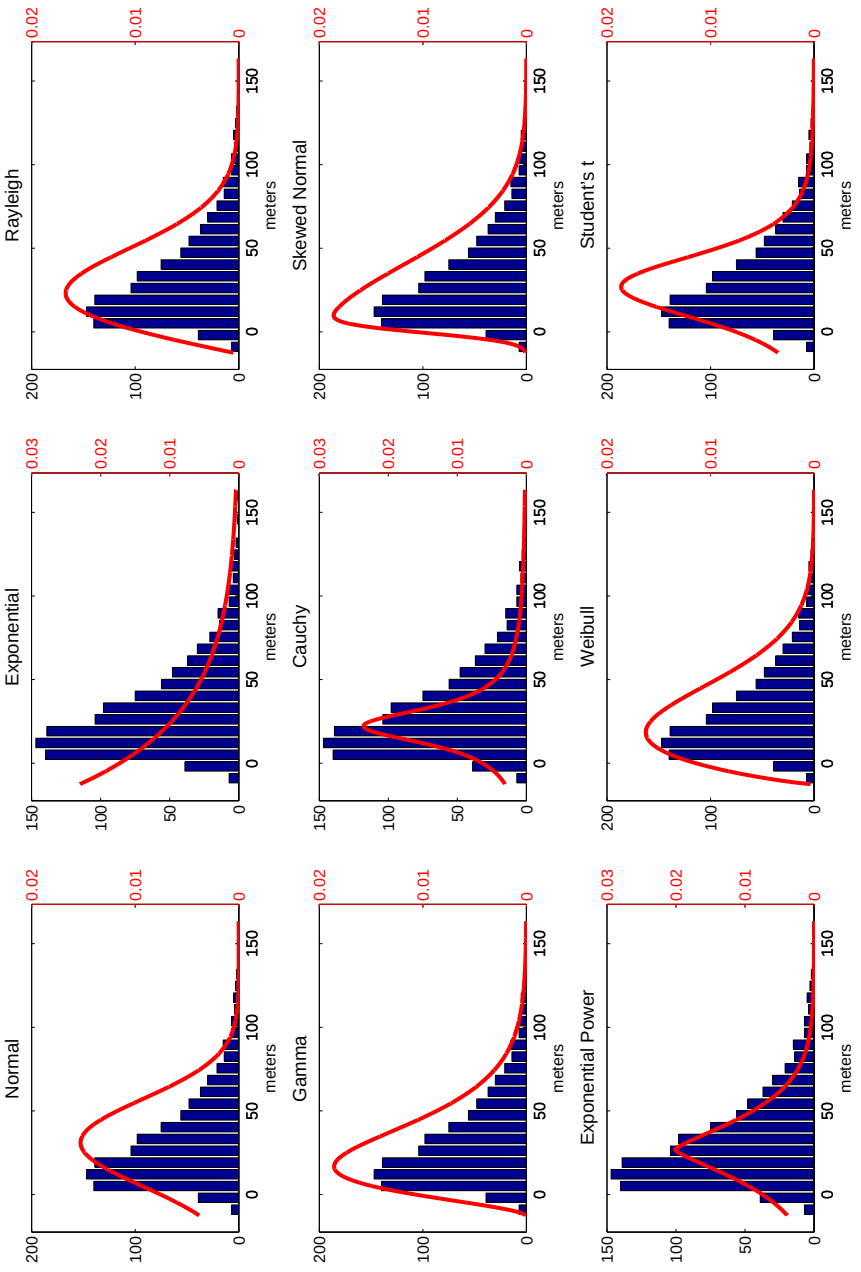

Figure 4.25: Histogram of the error of all successful ranging operations under the NLOS scenario and in the outdoor environment and the PDF of the fitted distribution for nine different types of distributions.

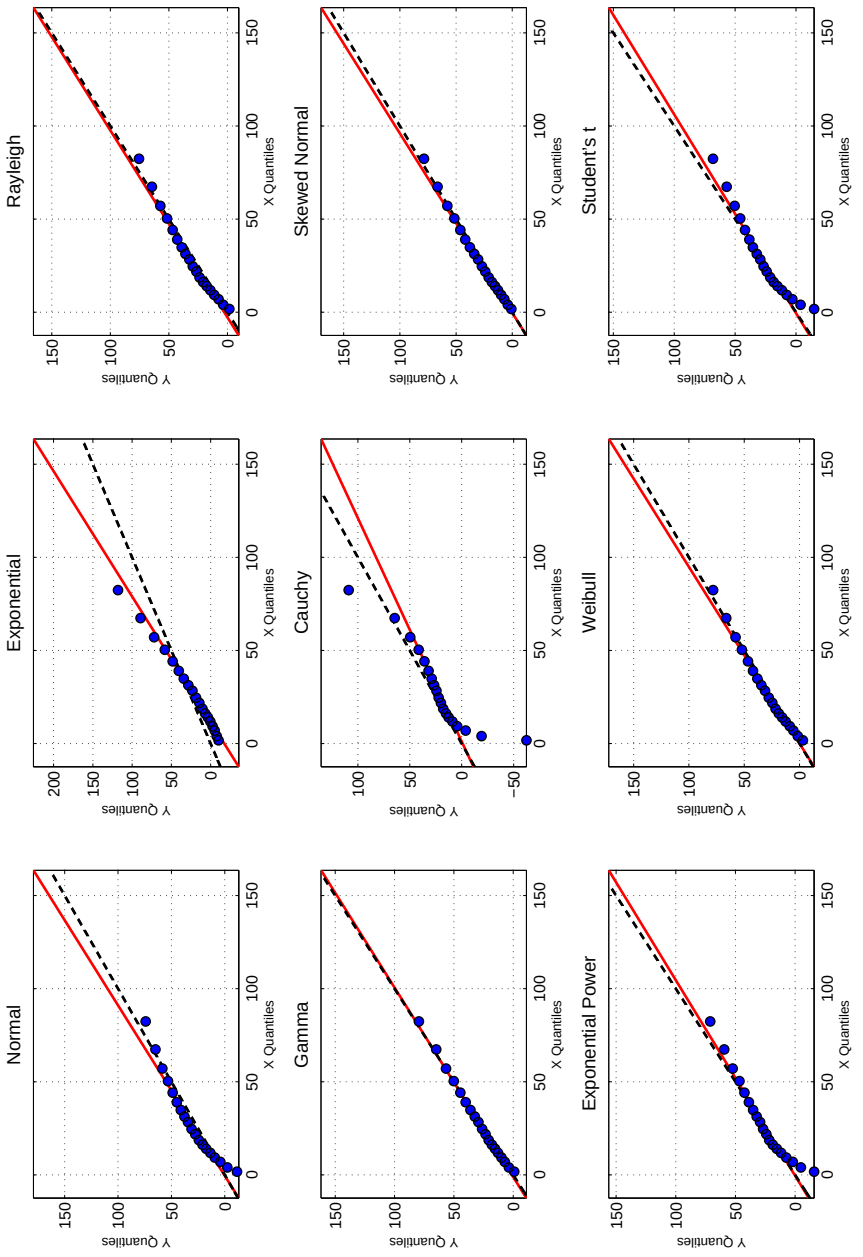

Figure 4.26: QQ plot of the quantiles of the error of all successful ranging operations under the NLOS scenario and in the outdoor environment versus the fitted distribution for nine different types of distributions.

	Normal	Exponential	Rayleigh
3 MHz, 10 dB	0.2499	0.1509	0.1190
3 MHz, 15 dB	0.2755	0.2494	0.1272
3 MHz, 20 dB	0.1928	0.3742	0.0685
6 MHz, 10 dB	0.2484	0.0844	0.1370
6 MHz, 15 dB	0.2053	0.3621	0.0705
6 MHz, 20 dB	0.2461	0.3261	0.0954
18 MHz, 10 dB	0.2888	0.0614	0.1884
18 MHz, 15 dB	0.2810	0.2684	0.1165
18 MHz, 20 dB	0.2476	0.3898	0.0917
Mean	0.2484	0.2518	0.1127

	Gamma	Cauchy	Skew Normal
3 MHz, 10 dB	0.0343	0.3929	0.0231
3 MHz, 15 dB	0.0414	0.3658	0.0416
3 MHz, 20 dB	0.0289	0.2931	0.0333
6 MHz, 10 dB	0.0151	0.2240	0.0491
6 MHz, 15 dB	0.0240	0.3304	0.0263
6 MHz, 20 dB	0.0343	0.3421	0.0352
18 MHz, 10 dB	0.0300	0.1946	0.0969
18 MHz, 15 dB	0.0259	0.3278	0.0331
18 MHz, 20 dB	0.0320	0.3437	0.0237
Mean	0.0295	0.3127	0.0402

	Exponential Power	Weibull	Student's t
3 MHz, 10 dB	0.2450	0.0389	0.2360
3 MHz, 15 dB	0.2439	0.0644	0.2202
3 MHz, 20 dB	0.1616	0.0569	0.1423
6 MHz, 10 dB	0.1647	0.0240	0.1547
6 MHz, 15 dB	0.1875	0.0539	0.1648
6 MHz, 20 dB	0.2132	0.0661	0.1895
18 MHz, 10 dB	0.1500	0.0366	0.1539
18 MHz, 15 dB	0.2252	0.0577	0.2023
18 MHz, 20 dB	0.2188	0.0743	0.1993
Mean	0.2011	0.0525	0.1848

Table 4.12: Table of KL-divergence values between the error of all successful ranging operations under the NLOS scenario and in the outdoor environment and the fitted distributions for nine different types of distributions for different values of SNR and bandwidth.

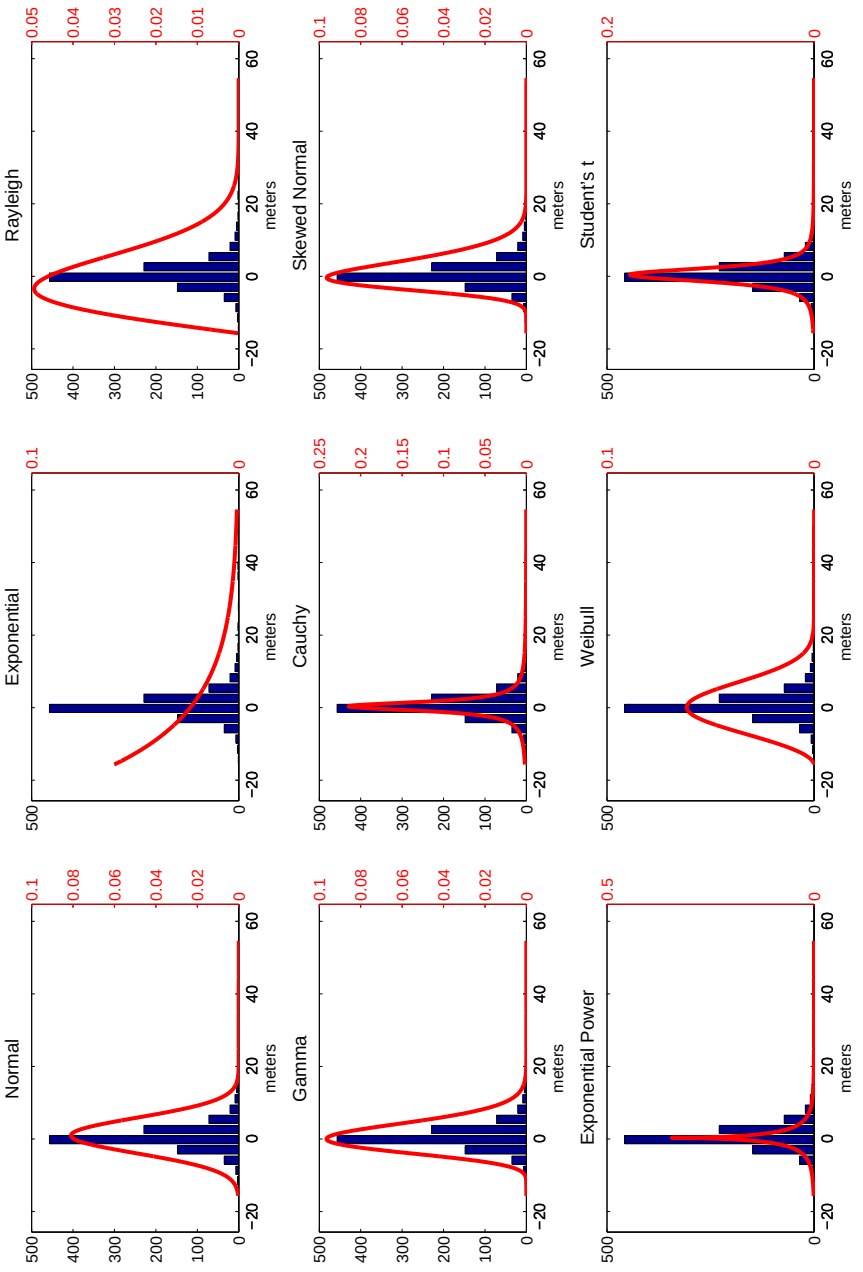

Figure 4.27: Histogram of the error of all successful ranging operations under the LOS scenario and in the highway environment and the PDF of the fitted distribution for nine different types of distributions.

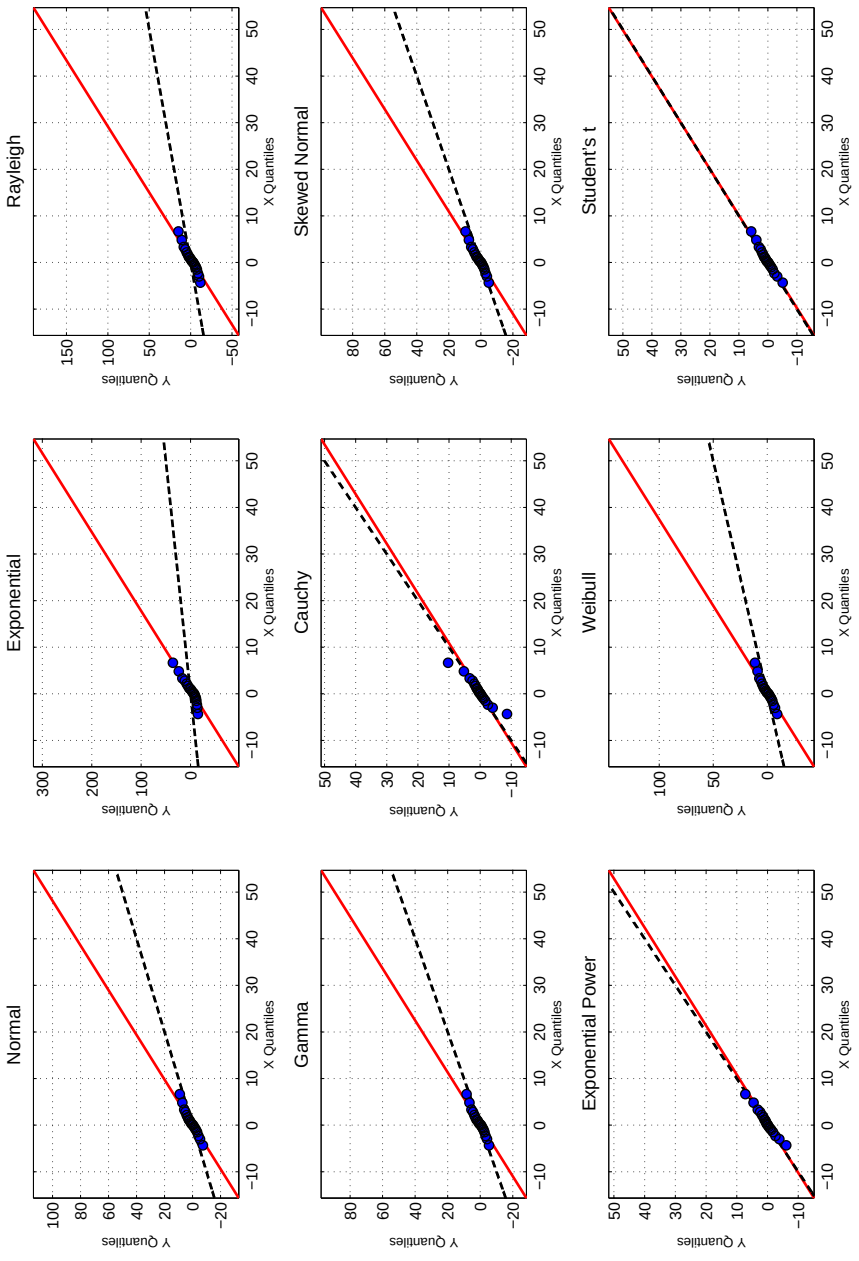

Figure 4.28: QQ plot of the quantiles of the error of all successful ranging operations under the LOS scenario and in the highway environment versus the fitted distribution for nine different types of distributions.

	Normal	Exponential	Rayleigh
3 MHz, 10 dB	0.2797	1.2928	0.5122
3 MHz, 15 dB	0.3882	1.1134	0.4336
3 MHz, 20 dB	0.2379	1.1753	0.4224
6 MHz, 10 dB	0.5948	1.1771	0.5397
6 MHz, 15 dB	0.3481	1.4584	0.6523
6 MHz, 20 dB	0.3501	1.2372	0.5002
18 MHz, 10 dB	1.5821	1.1855	1.2044
18 MHz, 15 dB	0.4523	1.3453	0.6015
18 MHz, 20 dB	0.5910	1.7196	0.8979
Mean	0.5360	1.3005	0.6405

	Gamma	Cauchy	Skew Normal
3 MHz, 10 dB	0.1285	0.1607	0.1474
3 MHz, 15 dB	0.1931	0.1262	0.2217
3 MHz, 20 dB	0.1055	0.1568	0.1174
6 MHz, 10 dB	0.2630	0.1092	0.3537
6 MHz, 15 dB	0.2073	0.1095	0.2092
6 MHz, 20 dB	0.1957	0.1076	0.2112
18 MHz, 10 dB	0.5890	0.0686	1.0154
18 MHz, 15 dB	0.2475	0.1038	0.2657
18 MHz, 20 dB	0.3329	0.0927	0.3597
Mean	0.2514	0.1150	0.3224

	Exponential Power	Weibull	Student's t
3 MHz, 10 dB	0.0664	0.3352	0.0365
3 MHz, 15 dB	0.0791	0.3706	0.0366
3 MHz, 20 dB	0.0618	0.2688	0.0371
6 MHz, 10 dB	0.0716	0.5229	0.0302
6 MHz, 15 dB	0.0518	0.4378	0.0388
6 MHz, 20 dB	0.0507	0.3766	0.0294
18 MHz, 10 dB	0.1194	0.9411	0.0488
18 MHz, 15 dB	0.0683	0.4765	0.0459
18 MHz, 20 dB	0.0609	0.7024	0.0339
Mean	0.0700	0.4924	0.0375

Table 4.13: Table of KL-divergence values between the error of all successful ranging operations under the LOS scenario and in the highway environment and the fitted distributions for nine different types of distributions for different values of SNR and bandwidth.

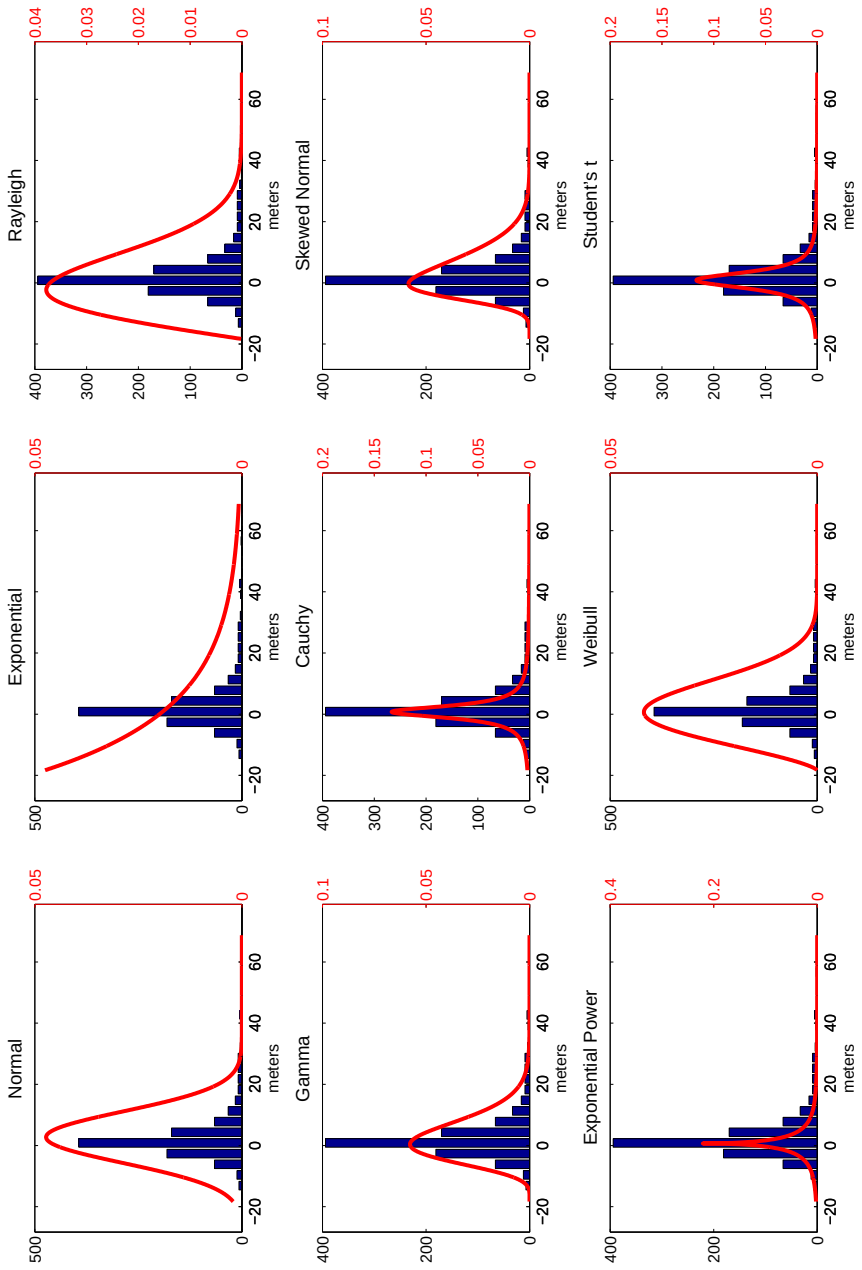

Figure 4.29: Histogram of the error of all successful ranging operations under the weak LOS scenario and in the highway environment and the PDF of the fitted distribution for nine different types of distributions.

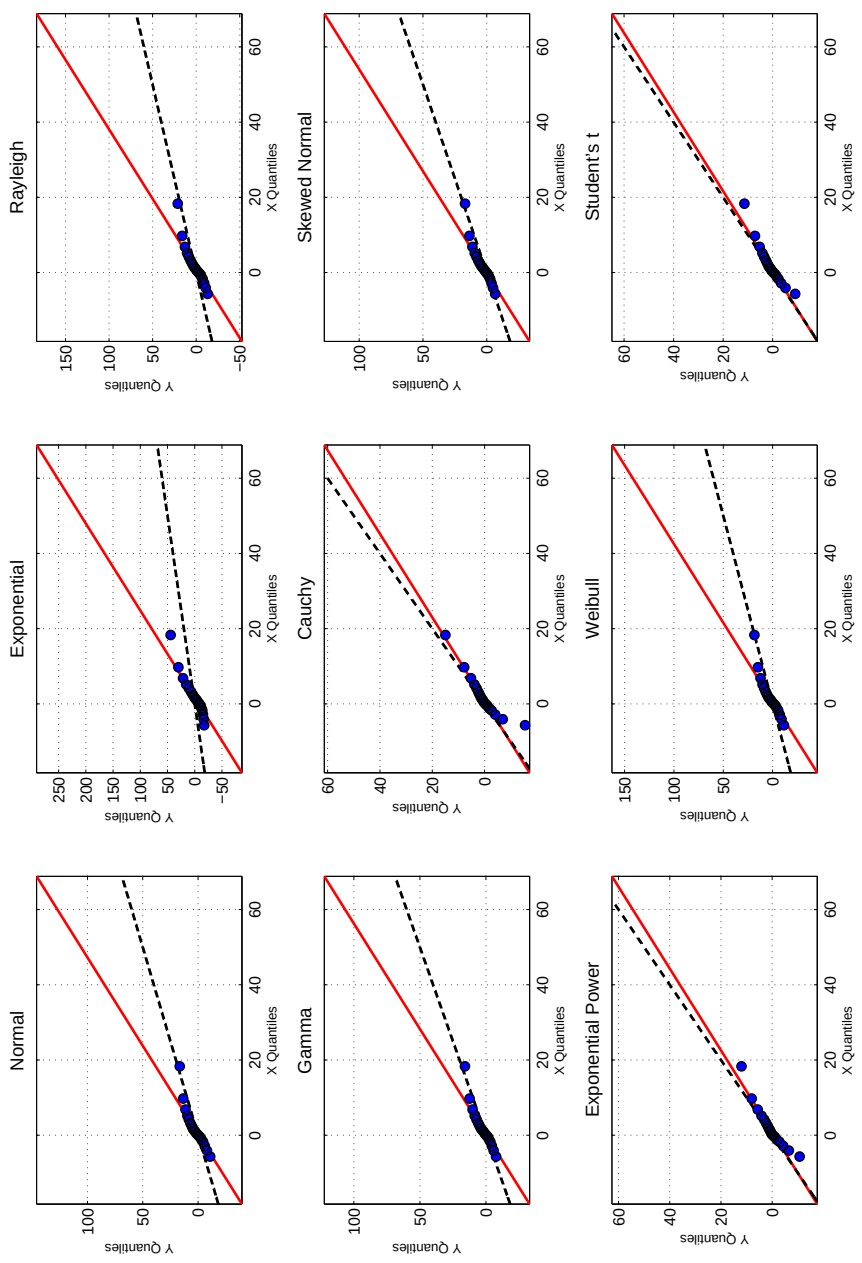

Figure 4.30: QQ plot of the quantiles of the error of all successful ranging operations under the weak LOS scenario and in the highway environment versus the fitted distribution for nine different types of distributions.

	Normal	Exponential	Rayleigh
3 MHz, 10 dB	0.5422	0.6780	0.3394
3 MHz, 15 dB	0.3154	0.9349	0.3113
3 MHz, 20 dB	0.2520	1.1947	0.4421
6 MHz, 10 dB	0.7950	0.7080	0.5139
6 MHz, 15 dB	0.5209	0.8264	0.3535
6 MHz, 20 dB	0.4900	1.1924	0.5126
18 MHz, 10 dB	1.1166	0.5424	0.9379
18 MHz, 15 dB	0.9574	0.7260	0.6768
18 MHz, 20 dB	0.5902	1.3125	0.6181
Mean	0.6200	0.9017	0.5228

	Gamma	Cauchy	Skew Normal
3 MHz, 10 dB	0.2002	0.1722	0.2432
3 MHz, 15 dB	0.1366	0.1601	0.1524
3 MHz, 20 dB	0.1398	0.1308	0.1352
6 MHz, 10 dB	0.2801	0.1376	0.3756
6 MHz, 15 dB	0.2144	0.1324	0.2545
6 MHz, 20 dB	0.2572	0.0938	0.4900
18 MHz, 10 dB	0.4791	0.0591	0.8188
18 MHz, 15 dB	0.3502	0.0642	0.5169
18 MHz, 20 dB	0.3148	0.1118	0.3234
Mean	0.2636	0.1180	0.3678

	Exponential Power	Weibull	Student's t
3 MHz, 10 dB	0.1659	0.3213	0.1309
3 MHz, 15 dB	0.1054	0.2678	0.0691
3 MHz, 20 dB	0.0599	0.2749	0.0493
6 MHz, 10 dB	0.1596	0.4313	0.1165
6 MHz, 15 dB	0.1234	0.3532	0.0864
6 MHz, 20 dB	0.0721	0.4562	0.0419
18 MHz, 10 dB	0.0952	0.5278	0.0729
18 MHz, 15 dB	0.1064	0.5152	0.0665
18 MHz, 20 dB	0.0961	0.5503	0.0809
Mean	0.1093	0.4109	0.0794

Table 4.14: Table of KL-divergence values between the error of all successful ranging operations under the weak LOS scenario and in the highway environment and the fitted distributions for nine different types of distributions for different values of SNR and bandwidth.

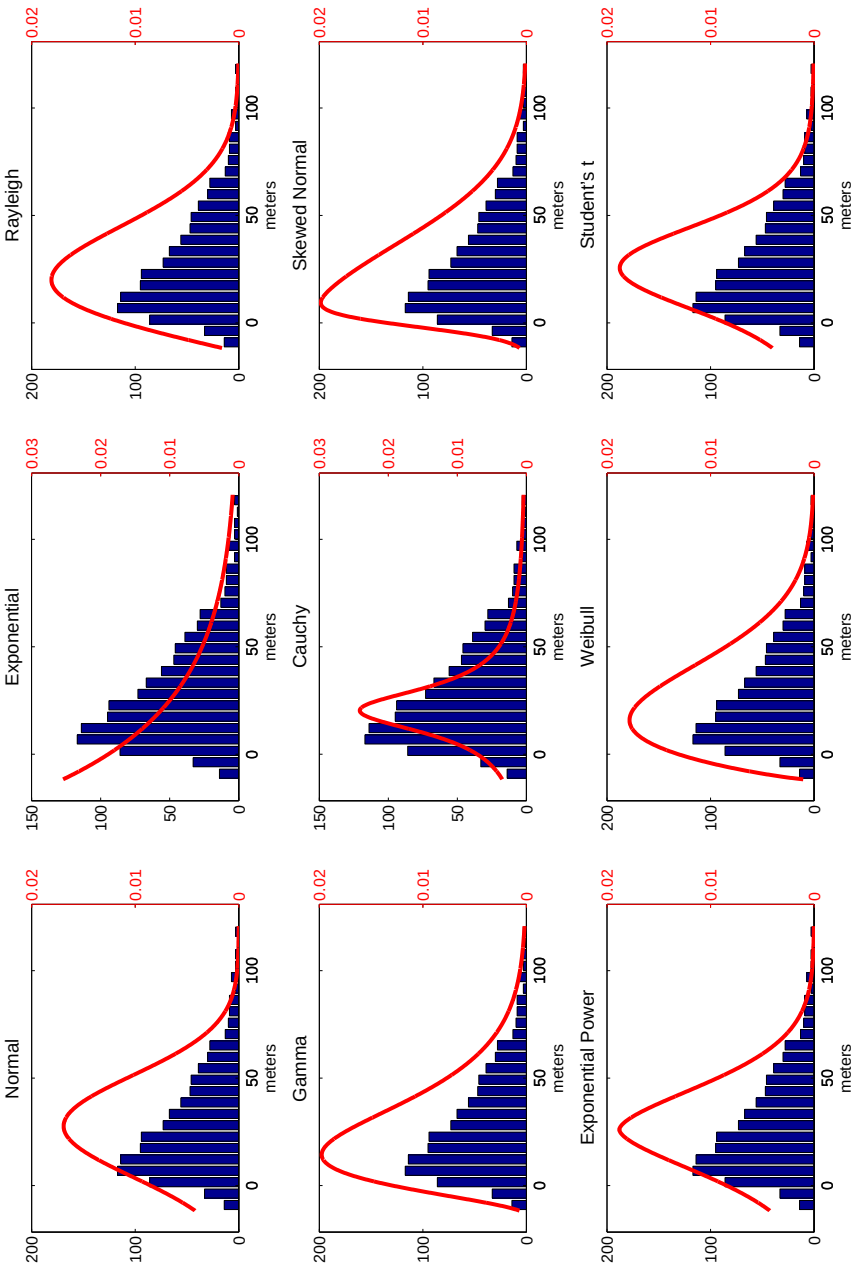

Figure 4.31: Histogram of the error of all successful ranging operations under the NLOS scenario and in the highway environment and the PDF of the fitted distribution for nine different types of distributions.

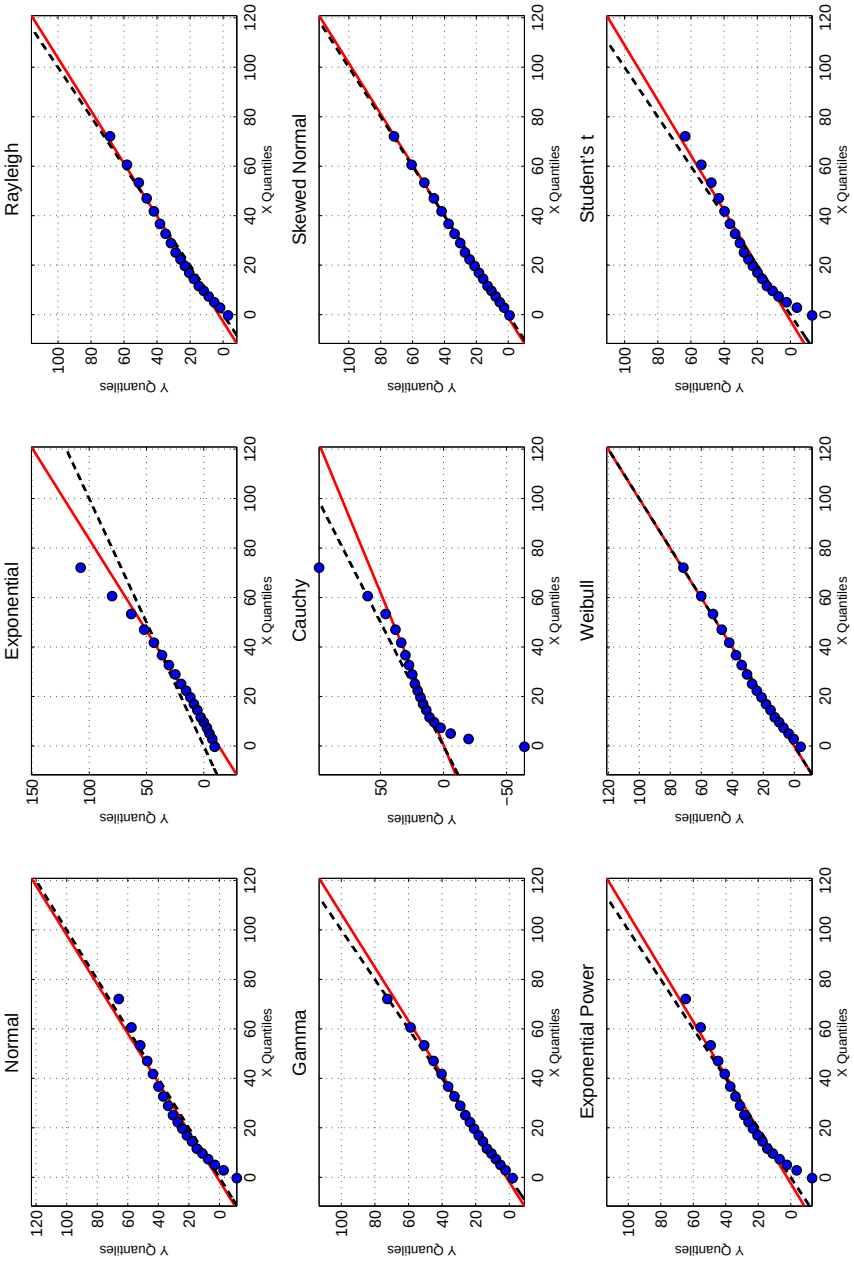

Figure 4.32: QQ plot of the quantiles of the error of all successful ranging operations under the NLOS scenario and in the highway environment versus the fitted distribution for nine different types of distributions.

	Normal	Exponential	Rayleigh
3 MHz, 10 dB	0.0865	0.5573	0.0831
3 MHz, 15 dB	0.0991	0.5904	0.0952
3 MHz, 20 dB	0.0779	0.6910	0.1128
6 MHz, 10 dB	0.1684	0.3610	0.0742
6 MHz, 15 dB	0.1629	0.3644	0.0458
6 MHz, 20 dB	0.1322	0.3722	0.0355
18 MHz, 10 dB	0.2736	0.1240	0.1461
18 MHz, 15 dB	0.2530	0.2068	0.1056
18 MHz, 20 dB	0.1749	0.3172	0.0513
Mean	0.1587	0.3983	0.0833

	Gamma	Cauchy	Skew Normal
3 MHz, 10 dB	0.0826	0.4433	0.0859
3 MHz, 15 dB	0.0940	0.4498	0.0985
3 MHz, 20 dB	0.0764	0.4450	0.0779
6 MHz, 10 dB	0.0763	0.4562	0.0586
6 MHz, 15 dB	0.0294	0.3817	0.0171
6 MHz, 20 dB	0.0270	0.3251	0.0205
18 MHz, 10 dB	0.0284	0.2604	0.0546
18 MHz, 15 dB	0.0228	0.3208	0.0287
18 MHz, 20 dB	0.0191	0.3316	0.0126
Mean	0.0506	0.3793	0.0505

	Exponential Power	Weibull	Student's t
3 MHz, 10 dB	0.0197	0.0623	0.0882
3 MHz, 15 dB	0.0230	0.0725	0.1008
3 MHz, 20 dB	0.0134	0.0560	0.0798
6 MHz, 10 dB	0.0924	0.0665	0.1697
6 MHz, 15 dB	0.1623	0.0385	0.1628
6 MHz, 20 dB	0.1324	0.0319	0.1313
18 MHz, 10 dB	0.1907	0.0397	0.1777
18 MHz, 15 dB	0.2136	0.0398	0.1976
18 MHz, 20 dB	0.1675	0.0345	0.1549
Mean	0.1128	0.0491	0.1403

Table 4.15: Table of KL-divergence values between the error of all successful ranging operations under the NLOS scenario and in the highway environment and the fitted distributions for nine different types of distributions for different values of SNR and bandwidth.

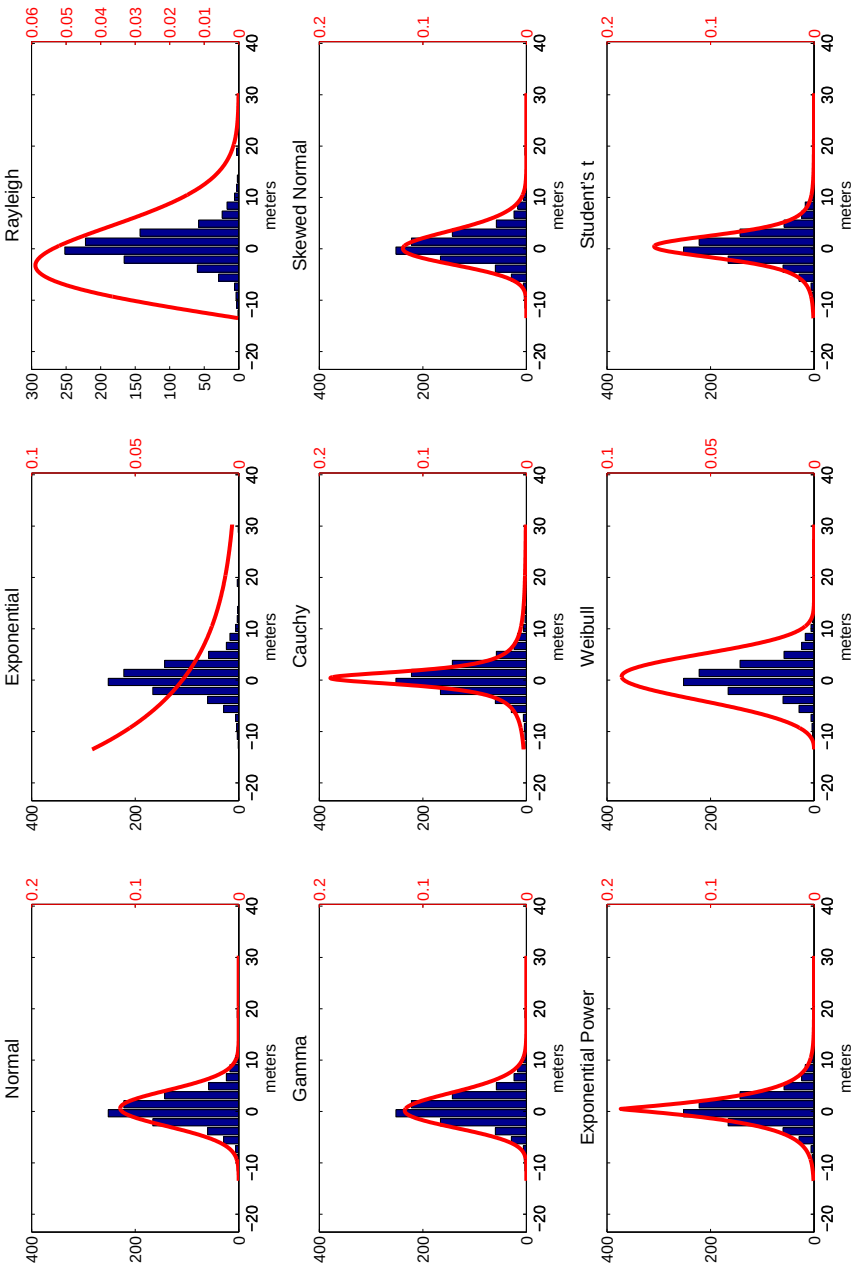

Figure 4.33: Histogram of the error of all successful ranging operations under the LOS scenario and in the indoor environment and the PDF of the fitted distribution for nine different types of distributions.

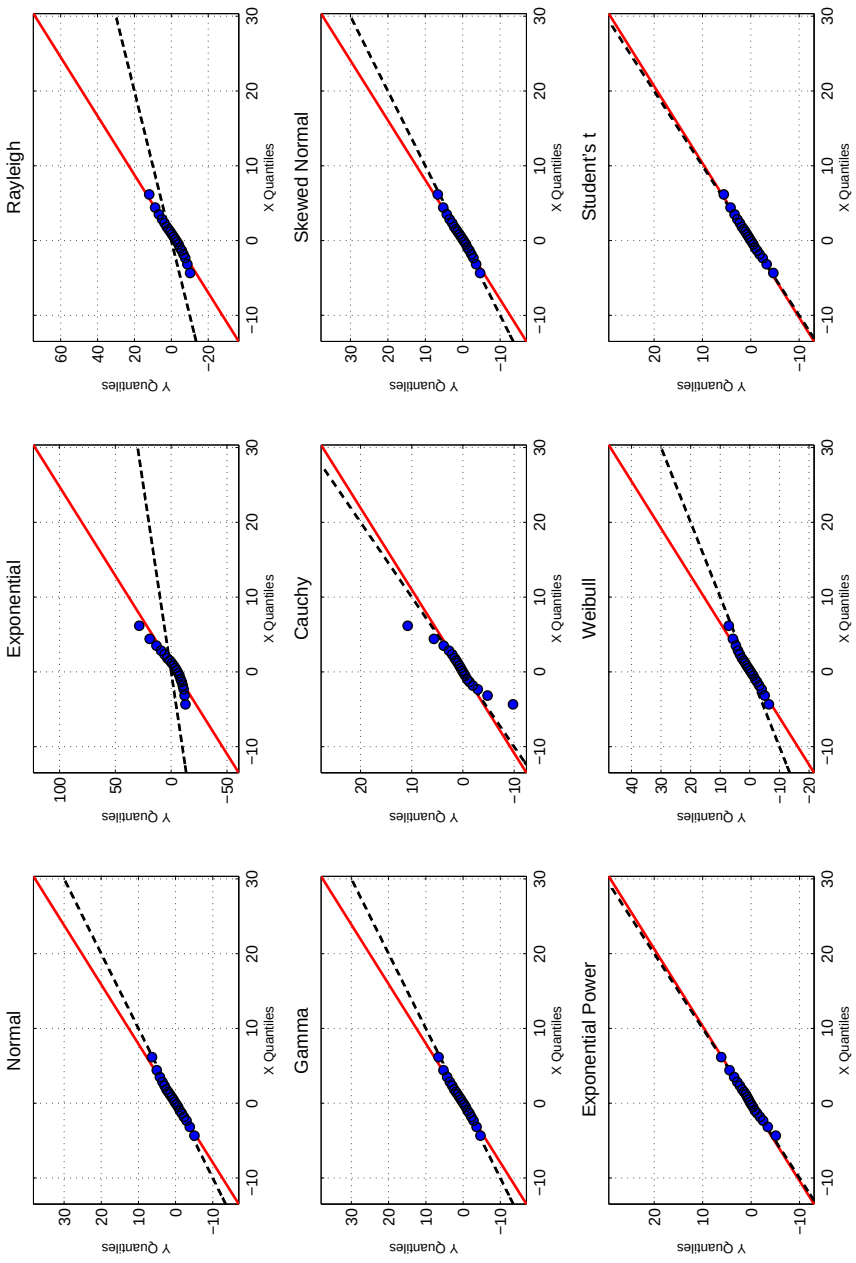

Figure 4.34: QQ plot of the quantiles of the error of all successful ranging operations under the LOS scenario and in the indoor environment versus the fitted distribution for nine different types of distributions.

	Normal	Exponential	Rayleigh
3 MHz, 10 dB	0.0823	1.8792	0.9705
3 MHz, 15 dB	0.1183	2.1945	1.2580
3 MHz, 20 dB	0.3172	2.8481	1.8853
6 MHz, 10 dB	0.0333	1.6700	0.7787
6 MHz, 15 dB	0.1365	1.9527	1.0547
6 MHz, 20 dB	0.2113	2.4528	1.5058
18 MHz, 10 dB	0.0801	1.2285	0.4324
18 MHz, 15 dB	0.1063	1.2816	0.4741
18 MHz, 20 dB	0.1263	1.5394	0.6793
Mean	0.1346	1.8941	1.0043

	Gamma	Cauchy	Skew Normal
3 MHz, 10 dB	0.0839	0.1819	0.0823
3 MHz, 15 dB	0.1204	0.1656	0.1183
3 MHz, 20 dB	0.3206	0.1263	0.3172
6 MHz, 10 dB	0.0344	0.2303	0.0333
6 MHz, 15 dB	0.1386	0.1606	0.1365
6 MHz, 20 dB	0.2141	0.1328	0.2113
18 MHz, 10 dB	0.0582	0.1935	0.0603
18 MHz, 15 dB	0.0770	0.1712	0.0741
18 MHz, 20 dB	0.0913	0.1618	0.0882
Mean	0.1265	0.1693	0.1246

	Exponential Power	Weibull	Student's t
3 MHz, 10 dB	0.0376	0.0819	0.0266
3 MHz, 15 dB	0.0408	0.0799	0.0253
3 MHz, 20 dB	0.0601	0.1693	0.0464
6 MHz, 10 dB	0.0246	0.0274	0.0213
6 MHz, 15 dB	0.0564	0.0839	0.0476
6 MHz, 20 dB	0.0457	0.1225	0.0354
18 MHz, 10 dB	0.0286	0.1370	0.0204
18 MHz, 15 dB	0.0351	0.1636	0.0232
18 MHz, 20 dB	0.0342	0.2309	0.0206
Mean	0.0404	0.1218	0.0297

Table 4.16: Table of KL-divergence values between the error of all successful ranging operations under the LOS scenario and in the indoor environment and the fitted distributions for nine different types of distributions for different values of SNR and bandwidth.

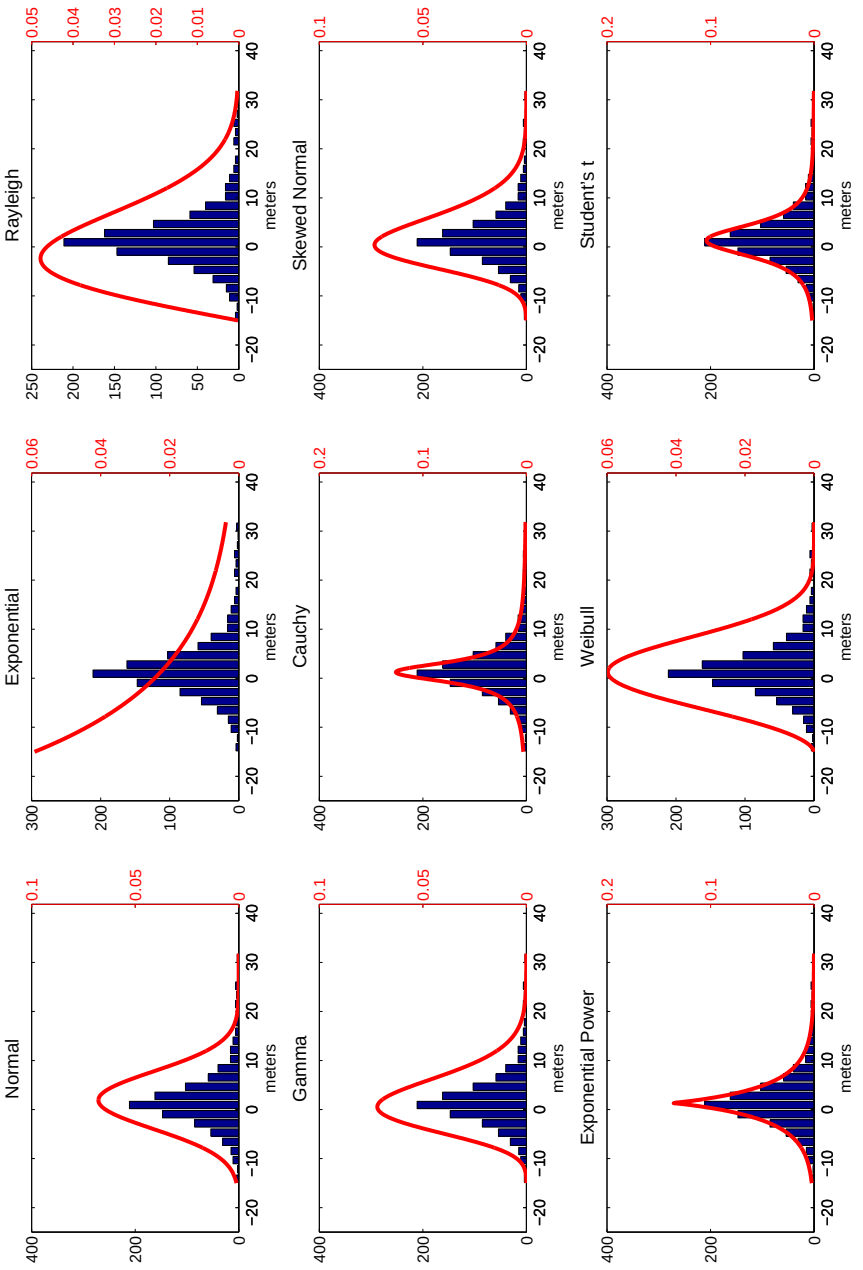

Figure 4.35: Histogram of the error of all successful ranging operations under the weak LOS scenario and in the indoor environment and the PDF of the fitted distribution for nine different types of distributions.

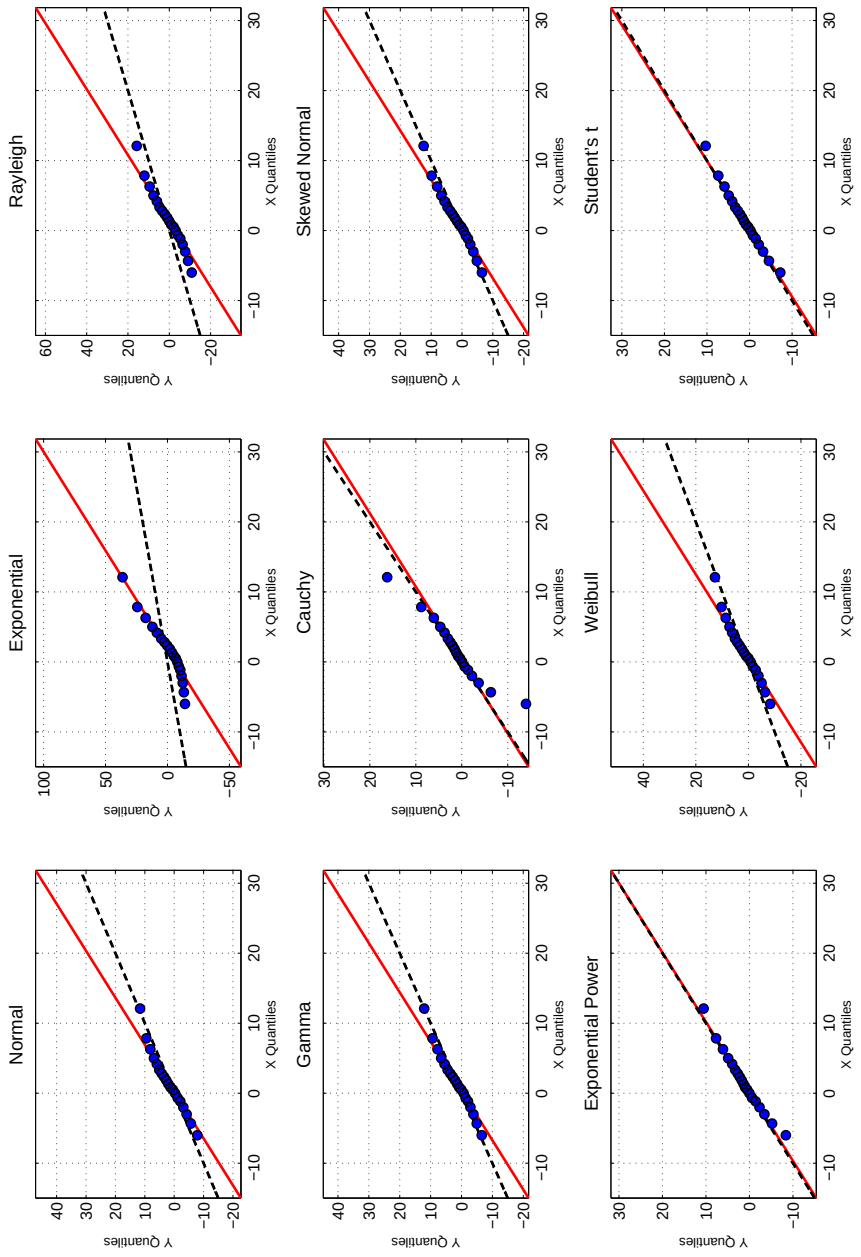

Figure 4.36: QQ plot of the quantiles of the error of all successful ranging operations under the weak LOS scenario and in the indoor environment versus the fitted distribution for nine different types of distributions.

	Normal	Exponential	Rayleigh
3 MHz, 10 dB	0.0336	1.4035	0.5538
3 MHz, 15 dB	0.1021	1.9865	1.0658
3 MHz, 20 dB	0.2654	2.2384	1.3181
6 MHz, 10 dB	0.0495	1.3797	0.5460
6 MHz, 15 dB	0.1751	2.0938	1.1761
6 MHz, 20 dB	0.1802	1.9660	1.0647
18 MHz, 10 dB	0.2438	1.0425	0.3404
18 MHz, 15 dB	0.2020	0.9972	0.2996
18 MHz, 20 dB	0.2105	1.1263	0.3951
Mean	0.1625	1.5816	0.7511

	Gamma	Cauchy	Skew Normal
3 MHz, 10 dB	0.0337	0.2133	0.0336
3 MHz, 15 dB	0.1034	0.1619	0.1021
3 MHz, 20 dB	0.2668	0.1090	0.2654
6 MHz, 10 dB	0.0506	0.2083	0.0495
6 MHz, 15 dB	0.1756	0.1228	0.1751
6 MHz, 20 dB	0.1812	0.1143	0.1802
18 MHz, 10 dB	0.1131	0.1578	0.1162
18 MHz, 15 dB	0.1048	0.1860	0.1053
18 MHz, 20 dB	0.1441	0.1235	0.1403
Mean	0.1304	0.1552	0.1297

	Exponential Power	Weibull	Student's t
3 MHz, 10 dB	0.0199	0.0494	0.0182
3 MHz, 15 dB	0.0331	0.1179	0.0270
3 MHz, 20 dB	0.0506	0.4445	0.0281
6 MHz, 10 dB	0.0300	0.0432	0.0311
6 MHz, 15 dB	0.0320	0.3269	0.0276
6 MHz, 20 dB	0.0334	0.2778	0.0254
18 MHz, 10 dB	0.0817	0.2370	0.0670
18 MHz, 15 dB	0.0870	0.1917	0.0733
18 MHz, 20 dB	0.0463	0.2423	0.0409
Mean	0.0460	0.2145	0.0376

Table 4.17: Table of KL-divergence values between the error of all successful ranging operations under the weak LOS scenario and in the indoor environment and the fitted distributions for nine different types of distributions for different values of SNR and bandwidth.

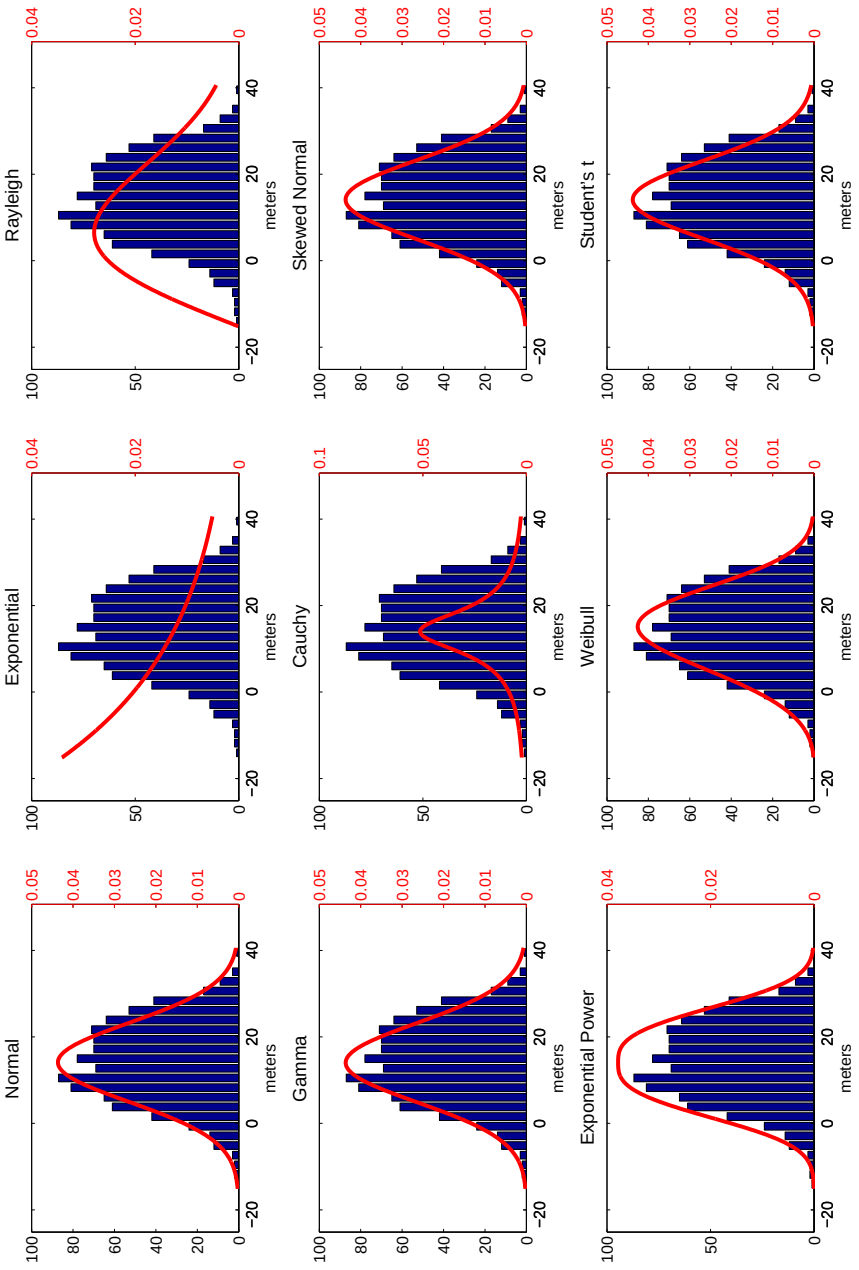

Figure 4.37: Histogram of the error of all successful ranging operations under the NLOS scenario and in the indoor environment and the PDF of the fitted distribution for nine different types of distributions.

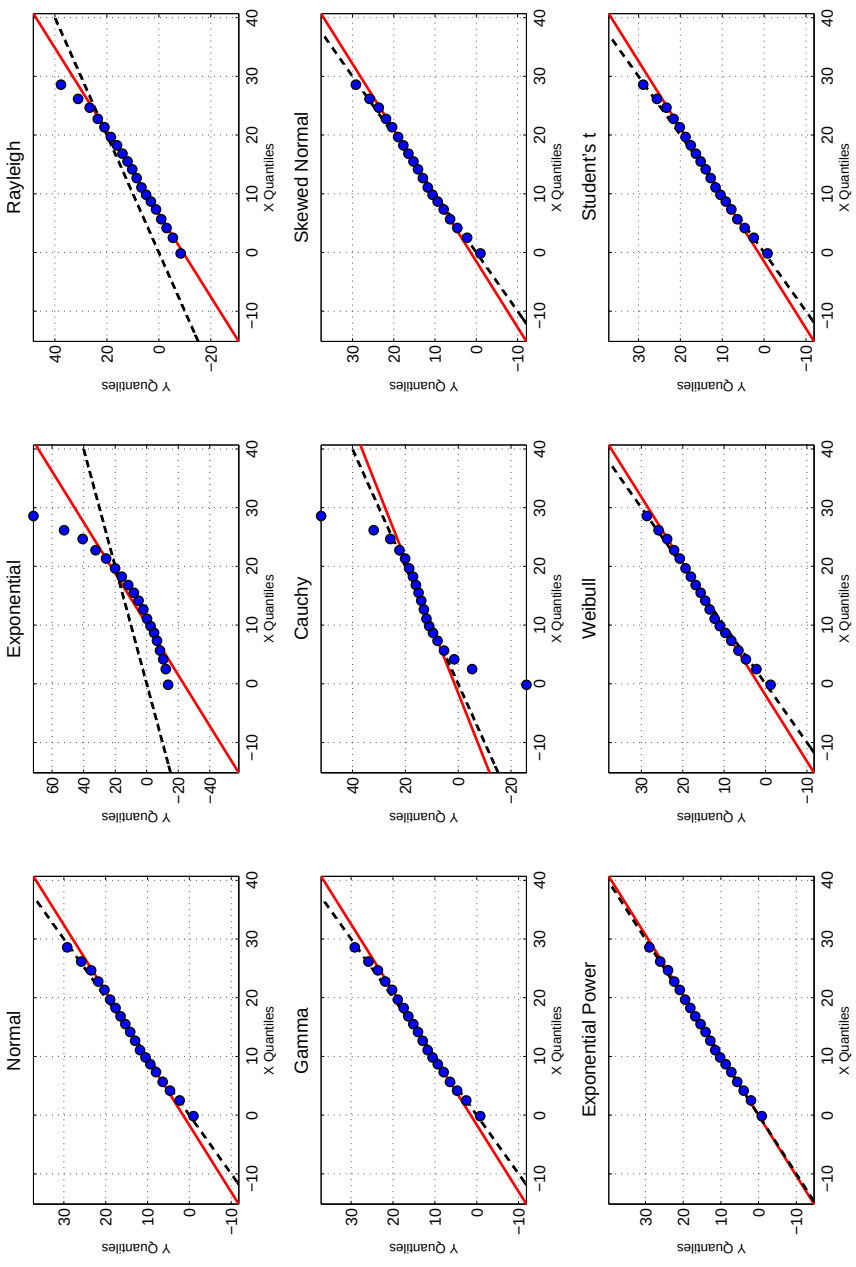

Figure 4.38: QQ plot of the quantiles of the error of all successful ranging operations under the NLOS scenario and in the indoor environment versus the fitted distribution for nine different types of distributions.

	Normal	Exponential	Rayleigh
3 MHz, 10 dB	0.0693	1.4029	0.5787
3 MHz, 15 dB	0.0235	1.1107	0.3418
3 MHz, 20 dB	0.0345	1.4979	0.6301
6 MHz, 10 dB	0.1222	0.9137	0.2524
6 MHz, 15 dB	0.0363	0.8636	0.1815
6 MHz, 20 dB	0.0574	0.9650	0.2499
18 MHz, 10 dB	0.0728	1.0821	0.3303
18 MHz, 15 dB	0.0457	1.0191	0.2862
18 MHz, 20 dB	0.0359	1.1106	0.3344
Mean	0.0553	1.1073	0.3539

	Gamma	Cauchy	Skew Normal
3 MHz, 10 dB	0.0695	0.2174	0.0690
3 MHz, 15 dB	0.0238	0.2472	0.0235
3 MHz, 20 dB	0.0344	0.2992	0.0345
6 MHz, 10 dB	0.1178	0.4119	0.1188
6 MHz, 15 dB	0.0363	0.3425	0.0363
6 MHz, 20 dB	0.0574	0.3938	0.0574
18 MHz, 10 dB	0.0729	0.4103	0.0728
18 MHz, 15 dB	0.0462	0.3622	0.0457
18 MHz, 20 dB	0.0362	0.3703	0.0359
Mean	0.0549	0.3394	0.0549

	Exponential Power	Weibull	Student's t
3 MHz, 10 dB	0.0527	0.0948	0.0554
3 MHz, 15 dB	0.0208	0.0351	0.0188
3 MHz, 20 dB	0.0345	0.0554	0.0326
6 MHz, 10 dB	0.1080	0.1175	0.1231
6 MHz, 15 dB	0.0234	0.0275	0.0372
6 MHz, 20 dB	0.0317	0.0506	0.0586
18 MHz, 10 dB	0.0423	0.0663	0.0741
18 MHz, 15 dB	0.0297	0.0356	0.0466
18 MHz, 20 dB	0.0171	0.0291	0.0370
Mean	0.0400	0.0569	0.0537

Table 4.18: Table of KL-divergence values between the error of all successful ranging operations under the NLOS scenario and in the indoor environment and the fitted distributions for nine different types of distributions for different values of SNR and bandwidth.

4.5 Discussion

In the previous section, we saw that, in general, the Cauchy, exponential power, and Student's t-distributions provide good fits for the error in the LOS and weak LOS scenarios, with the exponential power and Student's t-distributions providing better fits than the Cauchy. This is something that we would expect, given that the exponential power and Student's t-distributions each have three parameters to do the fitting over, whereas the Cauchy distribution only has two. We provide a summary of the fitted parameter values for the LOS scenario in the outdoor environment in Table 4.19.

Looking at Table 4.19, it becomes clear that, although the exponential power and Student's t-distributions provide better fits than the Cauchy distribution, the Cauchy distribution may in practice be better at simulating errors for the LOS and weak LOS scenarios. For a simulation, the parameter values for the Cauchy distribution would be easy to select. The location parameter x_0 is around 0 while the scale parameter γ simply increases as the situation gets worse (i.e. as SNR and bandwidth decrease). The same is true for the location parameter and scale parameters of the exponential power and Student's t-distributions as well - however, for these distributions the shape parameter and the degrees of freedom parameters change erratically with changing conditions. They would be hard to pick and select for a simulation. It is this extra parameter that makes these distributions a better fit, but the flexibility of this parameter also makes it more difficult to use these distributions for simulations. It is also important to not overfit our models to the data. Therefore, for the LOS and weak LOS scenarios, we see that the Cauchy distribution is a good choice for simulating the errors, especially in the outdoor and highway environments.

If we consider the physical situation, we can see an additional reason why the Cauchy distribution is a good fit, at least in the outdoor and highway environments. The PDF of the Cauchy distribution has a high center peak and heavy tails. The high peak makes sense because we are thinking about the LOS and weak LOS scenarios - we expect the first peak identified the majority of the time to correspond to the LOS path. Thus, we expect for much of the probability mass to be concentrated around 0. At the same time, since the RMS delay spread is large in the outdoor and highway environments, if we do miss the peak from the LOS path, the peak that we do detect may have a large delay. The Cauchy distribution models this well because of its heavy tails. In the indoor environment, however, the Cauchy distribution is not such a good fit. It still simulates the high center peak well; however, since the RMS delay spread is much smaller, if we miss the peak from the LOS path, the peak that we do detect will not have a large delay. Thus, the heavy tails of the Cauchy distribution do not model the situation as well.

We run into a similar situation when we consider the NLOS scenarios. In Table 4.20, we summarize the fitted parameter values for the NLOS scenario in the highway environment for the normal, Rayleigh, gamma, and Weibull distributions.

Although the gamma and Weibull distributions provide better fits than the normal and Rayleigh distributions, in practice it may be better to use the normal and Rayleigh distributions to simulate errors in the NLOS scenario for the same reasons as in the LOS and weak LOS scenarios. Once

again it is the extra shape parameters of the gamma and Weibull distributions that help to yield better fits, but it is also the reason that makes them less desirable for simulation purposes. This is especially clear for the gamma distribution.

Another issue in the NLOS scenario is the fact that the location parameter for the Rayleigh, gamma, and Weibull distributions seems to change erratically. This is because, normally, these three distributions cannot take on negative values. By adding the extra location parameter to indicate how far to shift them left along the x-axis, we get around this problem. However, the problem with doing so is that when there is an especially negative error value in our data set, it can have a large effect on the the fitted distribution. The location parameter needs to be large enough so that the negative error value can occur with nonzero probability in the fitted distribution, and that can cause a distribution to be poorly fitted. This is why the Rayleigh distribution is a poor fit for the NLOS scenario in the indoor environment, as shown in Figure **??**. In this scenario, the normal distribution may be a better choice for the NLOS scenario - although it does not typically provide as good a fit to the data, it handles the situation when there is an especially negative error value well. Therefore, we see that for the NLOS scenario, a good choice for simulating errors would either be the Rayleigh distribution or the normal distribution. Both are two parameter distributions, and thus are better choices than the three parameter distributions. The Rayleigh is a good fit for the data, if we consider the chance of especially negative error values occurring small enough to ignore - in this case, we could fix its location parameter x_0 to be some acceptable value and increase the scale parameter σ as conditions worsen. Otherwise, the normal distribution is a good choice - in this case, we would increase both its location parameter μ and its scale parameter σ as conditions worsen.

Cauchy

	x_0	γ
3 MHz, 10 dB	-0.6739	10.8009
3 MHz, 15 dB	-0.5311	9.9777
3 MHz, 20 dB	-1.1935	9.4250
6 MHz, 10 dB	-0.9550	5.4703
6 MHz, 15 dB	-0.9239	5.1367
6 MHz, 20 dB	-0.8415	4.4953
18 MHz, 10 dB	0.5203	1.7973
18 MHz, 15 dB	0.4821	1.6128
18 MHz, 20 dB	0.5816	1.6124

Exponential Power

	μ	α	β
3 MHz, 10 dB	0.1667	7.7549	0.6446
3 MHz, 15 dB	-0.1667	13.9333	0.9323
3 MHz, 20 dB	-1.5000	9.2390	0.7426
6 MHz, 10 dB	-1.1667	3.4432	0.6054
6 MHz, 15 dB	-0.8333	6.0978	0.8328
6 MHz, 20 dB	-1.0000	4.2501	0.7208
18 MHz, 10 dB	0.5000	1.0379	0.5805
18 MHz, 15 dB	0.5000	1.4980	0.7153
18 MHz, 20 dB	0.5000	1.4962	0.7179

Student's t

	μ	σ	ν
3 MHz, 10 dB	-0.3132	14.0999	2.1706
3 MHz, 15 dB	-0.0923	14.1083	2.9465
3 MHz, 20 dB	-0.6422	12.8782	2.3469
6 MHz, 10 dB	-0.6799	6.9044	1.8878
6 MHz, 15 dB	-0.6396	7.1764	2.7043
6 MHz, 20 dB	-0.6332	6.0510	2.1547
18 MHz, 10 dB	0.5882	2.2558	1.8817
18 MHz, 15 dB	0.5408	2.1424	2.1227
18 MHz, 20 dB	0.6731	2.1570	2.1421

Table 4.19: Table of fitted parameter values for the Cauchy (top), exponential power(middle), and Student's t-distributions (bottom) to the data from the LOS scenario in the outdoor environment for different values of SNR and bandwidth.

Normal

	μ	σ
3 MHz, 10 dB	141.0880	83.8597
3 MHz, 15 dB	134.4610	84.8260
3 MHz, 20 dB	127.8426	86.2834
6 MHz, 10 dB	114.7762	78.3736
6 MHz, 15 dB	92.4429	71.9725
6 MHz, 20 dB	79.7302	63.4693
18 MHz, 10 dB	58.9226	50.0572
18 MHz, 15 dB	34.5445	29.4005
18 MHz, 20 dB	27.6532	23.5926

Rayleigh

	σ	x_0
3 MHz, 10 dB	139.0840	36.8341
3 MHz, 15 dB	142.9242	49.0034
3 MHz, 20 dB	154.5571	72.9832
6 MHz, 10 dB	114.5949	27.0744
6 MHz, 15 dB	104.2194	36.1779
6 MHz, 20 dB	93.7506	36.6743
18 MHz, 10 dB	66.0687	19.9724
18 MHz, 15 dB	39.7132	13.3082
18 MHz, 20 dB	33.5354	13.4885

Gamma

	k	θ	x_0
3 MHz, 10 dB	25.9193	16.6235	289.7807
3 MHz, 15 dB	30.2579	15.5454	335.9094
3 MHz, 20 dB	77.7283	9.8156	635.1089
6 MHz, 10 dB	3.0372	47.3603	29.0652
6 MHz, 15 dB	3.1679	41.2453	38.2184
6 MHz, 20 dB	3.7928	33.0159	45.4941
18 MHz, 10 dB	1.7604	36.7692	5.8043
18 MHz, 15 dB	2.1942	19.5453	8.3416
18 MHz, 20 dB	3.1287	13.3052	13.9749

Weibull

	λ	k	x_0
3 MHz, 10 dB	220.9358	2.5396	54.7207
3 MHz, 15 dB	224.7998	2.5596	64.7928
3 MHz, 20 dB	246.6367	2.7969	91.3753
6 MHz, 10 dB	156.2791	1.8450	23.8181
6 MHz, 15 dB	143.6923	1.8621	34.7842
6 MHz, 20 dB	129.4907	1.8947	35.0192
18 MHz, 10 dB	70.6348	1.3564	5.5665
18 MHz, 15 dB	47.1428	1.5148	7.8117
18 MHz, 20 dB	44.7270	1.7677	12.0609

Table 4.20: Table of fitted parameter values for the normal (top left), Rayleigh (top right), gamma (middle), and Weibull distributions (bottom) to the data from the NLOS scenario in the highway environment for different values of SNR and bandwidth.

Chapter 5

Conclusion

In this report we have given motivation for the need for good models of the estimation error in time of flight ranging systems in both the LOS and NLOS scenarios. We see that the models used in prior literature oftentimes do not have robust justifications and that there is also a lack of consistency in the kinds of models used. The work that has been done to develop models based on simulations or real-world measurements also have various shortcomings.

We have provided good models for the estimation error through the simulation of the wireless channel and a time of flight ranging system in software. We have done work on fitting the simulated data to theoretical distributions and have shown that the Cauchy distribution is a good model for the distribution of errors that we see in LOS scenarios. In the NLOS scenario, we have shown that the normal distribution or a shifted version of the Rayleigh distribution are good models for distribution of errors that we see.

Bibliography

[1] K. Baddour and N. Beaulieu, "Autoregressive Modeling for Fading Channel Simulation," *IEEE Transactions on Wireless Communications*, vol. 4, no. 4, pp. 1650-1662, July 2005.

[2] R. Bultitude, S. Mahmoud, and W. Sullivan, "A Comparison of Indoor Radio Propagation Characteristics at 910 MHz and 1.75 GHz," *IEEE Journal on Selected Areas in Communications*, vol. 7, no. 1, January 1989.

[3] Y. Chan, W. Tsui, H. So, and P. Ching, "Time-of-Arrival Based Localization Under NLOS Conditions," *IEEE Transactions on Vehicular Technology*, vol. 55, no. 1, pp. 17-24, January 2006.

[4] A. Chandra, "Comparative study of 900 MHz and 450 MHz radio signals propagation in an indoor environment," *IEEE International Conference on Personal Wireless Communications, 1996*, pp. 247-253, February 1996.

[5] A. Chandra, A. Kumar, and P. Chandra, "Estimation of path loss parameters using propagation measurements at 900 MHz and 1.89 GHz in the corridors of a multifloor building," *Proceedings of the IEEE 5th International Symposium on Spread Spectrum Techniques and Applications, 1998*, vol. 2, pp. 532-535, September 1998.

[6] A. Chandra, A. Kumar, and P. Chandra, "Comparative study of path losses from propagation measurements at 450 MHz, 900 MHz, 1.35 GHz and 1.89 GHz in the corridors of a multifloor laboratory-cum-office building," *IEEE VTS 50th Vehicular Technology Conference, 1999*, vol. 4, pp. 2272-2276, September 1999.

[7] H. Chen, et al., "Non-line-of-sight Node Localization based on Semi-Definite Programming in Wireless Sensor Networks."

[8] L. Cheng, et al., "Multi-Path Propagation Measurements for Vehicular Networks at 5.9 GHz", *Wireless Communications and Networking Conference, 2008*, pp. 1239-1244, April 2008.

[9] C. Cheon, G. Liang, and H. Bertoni, "Simulating radio channel statistics for different building environments," *IEEE Journal on Selected Areas in Communications*, vol. 19, no. 11, pp. 2191-2200, November 2001.

[10] M. Ciurana, F. Barcelo-Arroyo, and F. Izquierdo, "A ranging system with IEEE 802.11 data frames," *IEEE Radio and Wireless Symposium, 2007*, pp. 133-136, December 2006.

[11] M. Ciurana, F. Barcelo-Arroyo, and S. Cugno, "A novel TOA-based indoor tracking system over IEEE 802.11 networks," *16th IST Mobile and Wireless Communications Summit*, pp. 1-5, June 2007.

[12] M. Ciurana, S. Cugno, and F. Barcelo-Arroyo, "WLAN indoor positioning based on TOA with two reference points", *4th Workshop on Positioning, Navigation and Communication*, pp. 23-28, February 2007.

[13] M. Ciurana and F. Barcelo-Arroyo, "Facing the obstructed path problem in indoor TOA-based ranging between IEEE 802.11 nodes, " *IEEE 19th International Symposium on Personal, Indoor and Mobile Radio Communications*, pp. 1-5, August 2008.

[14] C. Comsa, J. Luo, A. Haimovich, and S. Schartz, "Wireless Localization using Time Difference of Arrival in Narrow-Band Multipath Systems," *International Symposium on Signals, Circuits and Systems*, vol. 2, pp. 1-4, July 2007.

[15] J. Davis and J. Linnartz, "Vehicle to Vehicle RF Propagation Measurements," *1994 Conference Record of the Twenty-Eighth Asilomar Conference on Signals, Systems, and Computers, 1994*, pp. 470-474, November 1994.

[16] G. Dimitrakopoulos and C. Capsalis, "Statistical Modeling of RMS-Delay Spread Under Multipath Fading Conditions in Local Areas," *IEEE Transactions on Vehicular Technology*, vol. 49, no. 5, September 2000.

[17] D. Donald, S. Kumar, and B. Daku, "Measurement of the Indoor RF Propagation Channel at Ku Frequency Band," *Conference Proceedings of IEEE WESCANEX 93 - "Communications, Computers and Power in the Modern Environment"*, pp. 66-71, May 1993.

[18] F. Fontan and P. Espineira, *Modeling the Wireless Propagation Channel: A Simulation Approach with MATLAB*, West Sussex, UK: John Wiley and Sons Ltd., 2008.

[19] S. Golden and S. Bateman, "Sensor Measurements for Wi-Fi Location with Emphasis on Time-of-Arrival Ranging," *IEEE Transactions on Mobile Computing*, vol. 6, no. 10, pp. 1185-1198, August 2007.

[20] H. Hashemi and D. Tholl, "Statistical Modeling and Simulation of the RMS Delay Spread of Indoor Radio Propagation Channels", *IEEE Transactions on Vehicular Technology*, vol. 43, no. 1, pp. 110-120, February 1994.

[21] C. Hoene and J. Willmann, "Four-way TOA and software-based trilateration of IEEE 802.11 devices," *IEEE 19th International Symposium on Personal, Indoor and Mobile Radio Communications, 2008*, pp. 1-6, August 2008.

[22] J. Huerta, J. Vidal, A. Giremus, and J. Tourneret, "Joint Particle Filter and UKF Position Tracking in Severe Non-Line-of-Sight Situations", IEEE Journal of Selected Topics in Signal Processing, vol. 3, no. 5, pp. 874 - 888, October 2009.

[23] F. Izquierdo, et al., "Performance evaluation of a TOA-based trilateration method to locate terminals in WLAN," *1st International Symposium on Wireless Pervasive Computing*, pp. 1-6, December 2005.

[24] W. Jakes, *Microwave mobile communications*, Piscataway, NJ: IEEE Press, 1993.

[25] S. Lanzisera, "RF Ranging for Location Awareness," Ph.D. dissertation, UC Berkeley, 2009.

[26] M. Llombart, M. Ciurana, and F. Barcelo-Arroyo, "On the scalability of a novel WLAN positioning system based on time of arrival measurements,", *Proceedings of the 5th Workshop on Positioning, Navigation, and Communication, 2008*, pp.15-21, February 2008.

[27] X. Mao, Y. Lee, and B. Ng, "Wideband Channel Modelling in UHF Band for Urban Area", *IEEE International Symposium on Wireless Communication Systems, 2008*, pp. 240-244, October 2008.

[28] C. Mayorga, et al., "Cooperative Positioning Techniques for Mobile Localization in 4G Cellular Networks," *IEEE International Conference on Pervasive Services*, pp. 39-44, June 2007.

[29] J. Medbo, H. Hallenberg, and J. Berg, "Propagation characteristics at 5 GHz in typical radio-LAN scenarios," *IEEE 49th Vehicular Technology Conference, 1999*, pp. 185-189, July 1999.

[30] J. Molia-Garcia-Pardo, V. Penarrocha, and L. Juan-Lacer, "Wideband Radio Communication Measurements at 450, 900, 1800 and 2400 MHz at Regular and Chaflane Street Corners", *IEEE Antennas and Propagation Society International Symposium, 2003*, vol. 4, pp. 911-914, June 2003.

[31] A. Paier, et al., "Car-to-car radio channel measurements at 5 GHz: Pathloss, power-delay profile, and delay-Doppler spectrum," *4th International Symposium on Wireless Communication Systems, 2007*, pp. 224-228, October 2007.

[32] T. Rappaport, S. Seidel, and R. Singh, "900-MHz Multipath Propagation Measurements for U.S. Digital Cellular Radiotelephone," *IEEE Transactions on Vehicular Technology*, vol. 39, no. 2, pp. 132-139, May 1990.

[33] M. Riback, H. Asplund, J. Medbo, and J. Berg, "Statistical Analysis of Measured Radio Channels for Future Generation Mobile Communication Systems," *IEEE 61st Vehicular Technology Conference, 2005*, pp. 68-72, June 2005.

[34] S. Seidel, et al., "Path Loss, Scattering, and Multipath Delay Statistics in Four European Cities for Digital Cellular and Microcellular Radiotelephone," *IEEE Transactions on Vehicular Technology*, vol. 40, no. 4, pp. 721-730, November 1991.

[35] I. Sen and D. Matolak, "VehicleVehicle Channel Models for the 5-GHz Band," *IEEE Transactions on Intelligent Transportation Systems*, vol. 9, no. 2, pp. 235-245.

[36] J. Smith, "A Computer Generated Multipath Fading Simulation for Mobile Radio," *IEEE Transactions on Vehicular Technology*, vol. 24, no. 3, pp. 39-40, August 1975.

[37] D. Tse and P. Viswanath, *Fundamentals of Wireless Communication*, New York: Cambridge University Press, 2005.

[38] G. Turin, et al., "A Statistical Model of Urban Multipath Propagation," *IEEE Transactions on Vehicular Technology*, vol. 21, no. 1, pp. 1-9, February 1972.

[39] Y. Yang, Z. Zhong, and G. Xu, "Delay Spread Characteristics of Wideband MIMO Channels Based on Outdoor Non-Line-of-Sight Measurements," *IEEE Global Telecommunications Conference, 2007*, pp. 2745-2749, November 2007.

[40] D. Young and N. Beaulieu, "The Generation of Correlated Rayleigh Random Variates by Inverse Discrete Fourier Transform," *IEEE Transactions on Communications*, vol. 48, no. 7, pp. 1114-1127, July 2000.

[41] V. Zhang and A. Wong, "Combined AOA and TOA NLOS Localization Using Nonlinear Programming in Severe Multipath Environments," *IEEE Wireless Communications and Networking Conference, 2009*, pp. 1-6, April 2009.

Appendix A

Fitted Model Parameter Values

In this appendix we give the parameter values for the fitted models to the estimation error data for different scenarios, environments, bandwidths, and values of SNR. In each table we highlight a particular scenario and environment and look at how the model parameter values change with different values of bandwidth and SNR. We group the data in this way because our goal is to find a good model for a particular scenario in a particular environment (i.e., we want a good model for the LOS scenario in the indoor environment). By grouping the data in this way we can see how the parameter values change with different conditions, and we can also use that information to evaluate how

	Normal		Exponential		Rayleigh	
	μ	σ	λ	x_0	σ	x_0
3 MHz, 10 dB	5.8100	51.4251	108.3100	102.5000	84.9055	102.6950
3 MHz, 15 dB	1.7438	22.9537	70.0772	68.3333	52.2146	68.4406
3 MHz, 20 dB	2.4095	26.9571	91.4095	89.0000	67.4685	89.1182
6 MHz, 10 dB	3.3067	30.0269	37.4733	34.1667	34.7659	35.6255
6 MHz, 15 dB	0.6920	13.1845	53.0253	52.3333	38.6800	52.3972
6 MHz, 20 dB	0.6793	14.0371	41.0127	40.3333	30.6924	40.3938
18 MHz, 10 dB	2.1287	11.0712	11.4650	9.3333	12.2854	11.2612
18 MHz, 15 dB	1.1857	5.2118	15.0190	13.8333	11.2561	13.8555
18 MHz, 20 dB	1.3107	4.6860	13.1439	11.8333	9.8804	11.8532

	Gamma			Cauchy		Skew Normal		
	k	θ	x_0	x_0	γ	ϵ	ω	α
3 MHz, 10 dB	11.6607	9.7057	107.3650	-0.6739	10.8009	-33.9646	65.0120	4.8059
3 MHz, 15 dB	24.4796	4.4796	107.9143	-0.5311	9.9777	-20.1206	31.7005	1.9543
3 MHz, 20 dB	18.8160	5.5890	102.7532	-1.1935	9.4250	-23.6087	37.4651	2.5942
6 MHz, 10 dB	5.1712	7.5905	35.9456	-0.9550	5.4703	-18.6020	37.1700	5.8241
6 MHz, 15 dB	29.9788	2.2540	66.8810	-0.9239	5.1367	-11.9281	18.2509	2.2303
6 MHz, 20 dB	16.2656	3.0787	49.3970	-0.8415	4.4953	-12.4628	19.2291	2.4577
18 MHz, 10 dB	3.8501	3.0329	9.5481	0.5203	1.7973	-5.4588	13.4217	8.3140
18 MHz, 15 dB	15.1428	1.1408	16.0885	0.4821	1.6128	-3.7068	7.1484	2.9011
18 MHz, 20 dB	12.9657	1.1696	13.8543	0.5816	1.6124	-3.2753	6.5566	2.7441

	Exponential Power			Weibull			Student's T		
	μ	α	β	λ	k	x_0	μ	σ	ν
3 MHz, 10 dB	0.1667	7.7549	0.6446	120.6270	2.0273	102.7093	-0.3132	14.0999	2.1706
3 MHz, 15 dB	-0.1667	13.9333	0.9323	78.7877	2.9971	69.3000	-0.0923	14.1083	2.9465
3 MHz, 20 dB	-1.5000	9.2390	0.7426	101.3724	2.9946	89.6002	-0.6422	12.8782	2.3469
6 MHz, 10 dB	-1.1667	3.4432	0.6054	41.9029	1.5816	34.2087	-0.6799	6.9044	1.8878
6 MHz, 15 dB	-0.8333	6.0978	0.8328	58.4737	3.4919	52.8448	-0.6396	7.1764	2.7043
6 MHz, 20 dB	-1.0000	4.2501	0.7208	45.7113	2.6523	40.5594	-0.6332	6.0510	2.1547
18 MHz, 10 dB	0.5000	1.0379	0.5805	12.7960	1.4415	9.3494	0.5882	2.2558	1.8817
18 MHz, 15 dB	0.5000	1.4980	0.7153	16.7161	2.5726	13.9044	0.5408	2.1424	2.1227
18 MHz, 20 dB	0.5000	1.4962	0.7179	14.7141	2.6502	11.9093	0.6731	2.1570	2.1421

Table A.1: Table of fitted parameter values to the data for the LOS scenario in the outdoor environment for different values of bandwidth and SNR.

	Normal		Exponential		Rayleigh	
	μ	σ	λ	x_0	σ	x_0
3 MHz, 10 dB	2.9103	26.3781	81.5770	78.6667	60.7006	78.7801
3 MHz, 15 dB	3.4898	28.5958	71.6565	68.1667	54.6395	68.2962
3 MHz, 20 dB	2.8072	25.5830	74.6405	71.8333	55.8688	71.9468
6 MHz, 10 dB	1.6839	18.7862	43.0172	41.3333	33.2434	41.4128
6 MHz, 15 dB	0.6677	13.6312	45.1677	44.5000	33.4021	44.5606
6 MHz, 20 dB	1.3937	13.4813	37.8937	36.5000	28.4807	36.5610
18 MHz, 10 dB	1.9833	12.3877	13.6500	11.6667	13.5187	12.5787
18 MHz, 15 dB	1.1942	4.9415	13.8608	12.6667	10.4192	12.6875
18 MHz, 20 dB	0.9665	4.9253	16.6332	15.6667	12.2807	15.6880

	Gamma			Cauchy		Skew Normal		
	k	θ	x_0	x_0	γ	ϵ	ω	α
3 MHz, 10 dB	15.4680	6.1413	92.0823	-0.2887	11.3774	-23.6483	37.4321	2.6438
3 MHz, 15 dB	11.1416	7.6953	82.2488	-0.5774	11.1493	-24.8047	40.2281	2.7701
3 MHz, 20 dB	14.8436	6.1915	89.0974	-0.7020	11.4511	-23.1819	36.4681	2.5705
6 MHz, 10 dB	9.9019	4.7970	45.8150	-0.5241	5.9000	-15.6876	25.5869	3.2571
6 MHz, 15 dB	20.6267	2.7518	56.0922	-1.3272	5.1387	-12.5941	19.0180	2.4992
6 MHz, 20 dB	15.1498	3.1766	46.7319	-0.2526	5.0621	-11.7061	18.7975	2.4449
18 MHz, 10 dB	5.3257	2.6007	11.8673	0.5262	1.7096	-5.6415	14.5462	7.4282
18 MHz, 15 dB	13.0737	1.2103	14.6292	0.3634	1.6652	-3.5974	6.8832	2.8622
18 MHz, 20 dB	19.7443	0.9504	17.7978	0.3746	1.4814	-3.6144	6.7263	2.8178

	Exponential Power			Weibull			Student's T		
	μ	α	β	λ	k	x_0	μ	σ	ν
3 MHz, 10 dB	0.6667	16.0602	0.9583	90.9269	2.8514	79.2002	0.4006	16.0005	3.3689
3 MHz, 15 dB	-1.5000	12.9539	0.8313	80.5652	2.4393	68.5666	0.2731	15.1641	2.7467
3 MHz, 20 dB	-0.0000	16.9759	0.9950	83.6222	2.7915	72.4281	0.2536	16.2072	3.4717
6 MHz, 10 dB	-0.5000	5.7379	0.7481	48.1817	2.1967	41.4652	-0.2684	7.9314	2.5226
6 MHz, 15 dB	-0.8333	6.0010	0.8192	50.1521	2.9621	44.8235	-1.0917	6.9969	2.4650
6 MHz, 20 dB	-0.1667	5.7597	0.8078	42.4655	2.6698	36.7813	-0.0359	6.8702	2.4545
18 MHz, 10 dB	0.3333	0.8773	0.5646	15.2742	1.5134	11.6776	0.6211	2.1817	2.1116
18 MHz, 15 dB	0.3333	1.5121	0.7125	15.5061	2.6287	12.7419	0.4692	2.2185	2.1632
18 MHz, 20 dB	0.3333	1.0434	0.6383	18.4040	2.8696	15.7558	0.4172	2.0021	2.1476

Table A.2: Table of fitted parameter values to the data for the LOS scenario in the highway environment for different values of bandwidth and SNR.

	Normal		Exponential		Rayleigh	
	μ	σ	λ	x_0	σ	x_0
3 MHz, 10 dB	-2.5830	8.7197	46.0837	48.6667	33.2014	48.7202
3 MHz, 15 dB	-2.8185	6.4696	41.3483	44.1667	29.6249	44.2118
3 MHz, 20 dB	-2.4672	5.7934	50.6995	53.1667	36.1205	53.2197
6 MHz, 10 dB	-1.2959	4.9784	23.7041	25.0000	17.1464	25.0281
6 MHz, 15 dB	-1.7711	4.5572	24.7289	26.5000	17.8008	26.5293
6 MHz, 20 dB	-1.7173	4.5362	32.7827	34.5000	23.4264	34.5352
18 MHz, 10 dB	0.8506	3.6489	12.1840	11.3333	9.0051	11.3505
18 MHz, 15 dB	0.8758	3.4293	11.7092	10.8333	8.6382	10.8493
18 MHz, 20 dB	0.6218	3.4854	14.1218	13.5000	10.2972	13.5173

	Gamma			Cauchy		Skew Normal		
	k	θ	x_0	x_0	γ	ϵ	ω	α
3 MHz, 10 dB	7807.1441	0.0994	778.4696	-1.6601	4.5341	-2.5837	8.7197	0.0001
3 MHz, 15 dB	10403.3862	0.0638	666.5342	-2.0949	3.2101	-2.8187	6.4696	0.0000
3 MHz, 20 dB	16577.2185	0.0456	757.6603	-1.6503	2.2582	-2.4676	5.7934	0.0001
6 MHz, 10 dB	5953.4543	0.0649	387.4971	-1.0142	2.8917	-1.2962	4.9784	0.0001
6 MHz, 15 dB	10814.9708	0.0441	478.4246	-1.1713	2.1830	-1.7715	4.5572	0.0001
6 MHz, 20 dB	13258.9986	0.0397	528.5602	-1.2265	1.9588	-1.7177	4.5362	0.0001
18 MHz, 10 dB	54.7561	0.4870	25.8156	0.8495	1.9470	-2.2058	4.7599	1.4010
18 MHz, 15 dB	40.5213	0.5300	20.6021	0.6779	1.7278	-2.2194	4.6196	1.6358
18 MHz, 20 dB	56.7844	0.4539	25.1545	0.4137	1.6810	-2.4711	4.6599	1.6002

	Exponential Power			Weibull			Student's T		
	μ	α	β	λ	k	x_0	μ	σ	ν
3 MHz, 10 dB	-2.0621	8.2878	1.2379	57.4815	6.7934	56.5625	-2.0709	6.7202	4.8121
3 MHz, 15 dB	-2.3333	5.4733	1.1378	56.9181	9.5999	57.0818	-2.3070	4.6369	4.0050
3 MHz, 20 dB	-1.6667	2.6145	0.8202	89.6711	18.4570	89.8329	-1.7966	3.1352	2.5878
6 MHz, 10 dB	-1.2032	6.1738	1.6245	31.4393	6.7423	30.6949	-1.1840	4.5221	11.4911
6 MHz, 15 dB	-1.3324	3.5862	1.0743	50.0086	12.7035	49.8619	-1.3385	3.2111	3.6824
6 MHz, 20 dB	-1.3333	2.7365	0.9310	52.5044	13.1532	52.3663	-1.2899	2.7605	2.9148
18 MHz, 10 dB	0.8338	3.5785	1.2799	13.6682	3.3230	11.5431	0.7897	2.9243	6.0728
18 MHz, 15 dB	0.7175	2.9818	1.1620	13.1335	3.4091	11.0338	0.7278	2.5200	4.3564
18 MHz, 20 dB	0.4801	2.7560	1.0923	15.6513	3.8053	13.7230	0.4562	2.4221	3.8381

Table A.3: Table of fitted parameter values to the data for the LOS scenario in the indoor environment for different values of bandwidth and SNR.

	Normal		Exponential		Rayleigh	
	μ	σ	λ	x_0	σ	x_0
3 MHz, 10 dB	52.1060	162.4864	142.0358	89.8333	185.2136	153.3359
3 MHz, 15 dB	17.1035	68.6002	131.9368	114.8333	105.3400	115.1352
3 MHz, 20 dB	12.0862	46.6839	82.9195	70.8333	67.6471	71.4176
6 MHz, 10 dB	19.1990	63.0467	56.6990	37.5000	72.1089	60.9540
6 MHz, 15 dB	8.1780	32.2680	59.6780	51.5000	48.0737	51.6629
6 MHz, 20 dB	4.8858	22.2407	57.8858	53.0000	43.9096	53.0923
18 MHz, 10 dB	7.5973	27.9730	21.2785	13.6667	31.0076	26.1733
18 MHz, 15 dB	2.5758	8.7565	18.0758	15.5000	14.2268	15.5384
18 MHz, 20 dB	2.9185	8.4437	17.7565	14.8333	13.9498	14.9112

	Gamma			Cauchy		Skew Normal		
	k	θ	x_0	x_0	γ	ϵ	ω	α
3 MHz, 10 dB	2.0445	69.5701	90.1316	2.2887	17.3639	-52.0851	193.0223	15.8294
3 MHz, 15 dB	6.9452	19.5156	118.4357	0.2432	15.5193	-42.7383	91.0331	5.2625
3 MHz, 20 dB	5.3543	16.6527	77.0774	1.9455	14.3851	-33.0944	64.9667	4.2445
6 MHz, 10 dB	2.0843	27.2682	37.6364	0.3988	8.2340	-23.8990	76.3697	13.8205
6 MHz, 15 dB	5.8575	10.4683	53.1401	-0.0461	7.4123	-20.8819	43.4247	4.9625
6 MHz, 20 dB	10.4268	6.0294	57.9818	0.0351	7.0014	-16.8041	31.0661	3.2771
18 MHz, 10 dB	2.1129	10.0867	13.7148	0.8428	2.7151	-8.4515	32.2499	16.3889
18 MHz, 15 dB	6.8712	2.7175	16.0965	0.6178	2.3847	-5.6862	12.0391	4.4239
18 MHz, 20 dB	7.2617	2.6439	16.2808	0.5865	2.1989	-5.1035	11.6468	4.0463

	Exponential Power			Weibull			Student's T		
	μ	α	β	λ	k	x_0	μ	σ	ν
3 MHz, 10 dB	1.1667	4.2799	0.4248	153.7975	1.2131	89.8747	2.2271	17.0606	0.9638
3 MHz, 15 dB	-0.8333	7.1311	0.5354	148.8276	1.9938	115.1297	0.9107	18.5029	1.4699
3 MHz, 20 dB	0.6667	11.4621	0.6670	93.8889	1.8933	71.1872	2.9767	18.5031	1.9546
6 MHz, 10 dB	1.3333	1.4234	0.4077	61.6740	1.2344	37.5188	0.4499	8.4757	1.0663
6 MHz, 15 dB	-0.6667	3.4614	0.5351	67.5824	1.9620	51.6435	0.1266	8.5799	1.3795
6 MHz, 20 dB	-0.6667	5.4292	0.6550	65.0546	2.5231	53.2897	0.5279	8.9618	1.8538
18 MHz, 10 dB	0.8333	0.3139	0.3800	22.9276	1.1876	13.6719	0.8602	2.8129	1.0818
18 MHz, 15 dB	0.5000	1.5584	0.6071	20.4440	2.1224	15.5542	0.7146	2.9159	1.6556
18 MHz, 20 dB	0.3333	1.0916	0.5489	20.1415	2.1596	14.9566	0.6991	2.6052	1.4258

Table A.4: Table of fitted parameter values to the data for the weak LOS scenario in the outdoor environment for different values of bandwidth and SNR.

	Normal		Exponential		Rayleigh	
	μ	σ	λ	x_0	σ	x_0
3 MHz, 10 dB	19.0067	54.9420	90.6974	71.6667	75.4978	72.5422
3 MHz, 15 dB	10.8780	39.6068	91.5447	80.6667	70.6477	80.8470
3 MHz, 20 dB	9.0385	39.2311	114.7052	105.6667	85.8353	105.8367
6 MHz, 10 dB	10.6004	34.5278	49.2802	38.6667	43.2021	39.8047
6 MHz, 15 dB	6.4852	25.6054	47.9852	41.5000	38.5593	41.6604
6 MHz, 20 dB	4.1755	21.2725	52.6755	48.5000	40.2310	48.5933
18 MHz, 10 dB	7.0203	22.1224	18.6997	11.6667	25.0497	20.6488
18 MHz, 15 dB	3.8340	12.4968	16.3383	12.5000	14.8357	13.0190
18 MHz, 20 dB	2.7085	8.4402	21.0418	18.3333	16.0539	18.3680

	Gamma			Cauchy		Skew Normal		
	k	θ	x_0	x_0	γ	ϵ	ω	α
3 MHz, 10 dB	4.0350	23.2629	74.8599	3.7651	17.8556	-36.2901	77.9510	5.4345
3 MHz, 15 dB	7.6778	12.9889	88.8480	2.3196	16.2099	-30.6348	57.3761	3.4613
3 MHz, 20 dB	13.5506	10.0434	127.0550	2.0404	16.0161	-31.1512	56.1631	2.6647
6 MHz, 10 dB	3.5941	13.9443	39.5169	0.9492	8.5489	-20.3805	46.3895	6.4255
6 MHz, 15 dB	5.3498	9.4532	44.0875	0.4604	8.2390	-18.9095	36.0628	4.1401
6 MHz, 20 dB	10.0899	5.8479	54.8287	0.2729	6.7334	4.1758	21.2725	-0.0000
18 MHz, 10 dB	2.0196	9.2757	11.7130	1.0112	2.8816	-7.5198	26.4729	13.0580
18 MHz, 15 dB	3.8003	4.3506	12.6995	1.0225	2.3856	-6.2623	16.0656	6.6487
18 MHz, 20 dB	9.5461	2.3409	19.6383	0.7389	2.3893	-5.4299	11.7248	3.6665

	Exponential Power			Weibull			Student's T		
	μ	α	β	λ	k	x_0	μ	σ	ν
3 MHz, 10 dB	4.6667	16.2476	0.6957	102.7943	1.7983	71.9266	4.7457	21.8576	1.7577
3 MHz, 15 dB	2.8333	20.6992	0.8718	103.5157	2.3506	81.1350	4.2135	21.9409	2.6311
3 MHz, 20 dB	2.8333	20.8533	0.8709	128.8727	2.8844	106.6715	3.1247	21.8933	2.4683
6 MHz, 10 dB	1.0000	5.0858	0.5805	55.6083	1.6335	38.7397	1.3673	10.0691	1.5073
6 MHz, 15 dB	0.8333	7.6461	0.7062	54.3629	1.9791	41.6478	0.9564	10.3012	1.8473
6 MHz, 20 dB	0.0000	5.4430	0.6709	59.2676	2.4180	48.7635	0.6397	8.6360	1.9289
18 MHz, 10 dB	0.8333	0.6443	0.4312	20.2012	1.2051	11.6720	1.0571	3.0709	1.1716
18 MHz, 15 dB	1.0000	1.1745	0.5389	18.3796	1.5757	12.5180	1.0683	2.7459	1.4015
18 MHz, 20 dB	0.6667	1.4881	0.5953	23.6839	2.4412	18.4271	0.8532	2.9472	1.6055

Table A.5: Table of fitted parameter values to the data for the weak LOS scenario in the highway environment for different values of bandwidth and SNR.

	Normal		Exponential		Rayleigh	
	μ	σ	λ	x_0	σ	x_0
3 MHz, 10 dB	-1.3700	10.7233	42.6300	44.0000	31.1222	44.0571
3 MHz, 15 dB	-1.7406	8.2452	46.7593	48.5000	33.6110	48.5531
3 MHz, 20 dB	-2.2534	8.2195	48.4133	50.6667	34.7669	50.7292
6 MHz, 10 dB	-0.6448	6.7500	26.0219	26.6667	19.0347	26.7039
6 MHz, 15 dB	-0.8059	7.1632	41.0275	41.8333	29.4826	41.8807
6 MHz, 20 dB	-1.1261	6.2160	32.3739	33.5000	23.3371	33.5391
18 MHz, 10 dB	2.3763	5.8287	15.5471	13.1667	11.7552	13.1927
18 MHz, 15 dB	2.0062	5.8257	15.5062	13.5000	11.7302	13.5262
18 MHz, 20 dB	1.9034	5.8879	16.9034	15.0000	12.6748	15.0269

	Gamma			Cauchy		Skew Normal		
	k	θ	x_0	x_0	γ	ϵ	ω	α
3 MHz, 10 dB	2409.6538	0.2186	528.1277	-0.8448	6.0415	-1.3702	10.7233	0.0000
3 MHz, 15 dB	7891.7194	0.0934	738.7319	-1.0700	4.0233	-1.7410	8.2452	0.0001
3 MHz, 20 dB	9774.9341	0.0834	817.7503	-1.4697	3.2702	-2.2538	8.2195	0.0001
6 MHz, 10 dB	5816.6904	0.0889	517.6659	-0.0572	3.7089	-0.6452	6.7500	0.0001
6 MHz, 15 dB	6601.2279	0.0884	584.2357	-0.6011	3.0539	-0.8062	7.1632	0.0001
6 MHz, 20 dB	7506.6287	0.0719	540.9354	-0.5961	2.6557	-1.1264	6.2160	0.0001
18 MHz, 10 dB	10.0221	1.7308	14.9701	1.2278	2.4672	-3.7815	8.4790	2.9883
18 MHz, 15 dB	11.6399	1.6451	17.1421	1.2523	2.6731	-4.0577	8.4089	2.5251
18 MHz, 20 dB	17.4930	1.3579	21.8510	1.2373	2.5253	-3.9230	8.2834	2.1807

	Exponential Power			Weibull			Student's T		
	μ	α	β	λ	k	x_0	μ	σ	ν
3 MHz, 10 dB	-1.2071	12.4832	1.5033	49.2336	4.4996	46.5003	-1.2884	9.3341	8.1690
3 MHz, 15 dB	-1.3326	6.7405	1.1057	55.4946	6.7809	53.9198	-1.2109	5.8612	3.8007
3 MHz, 20 dB	-1.6667	4.2128	0.8718	54.2534	5.3515	53.4344	-1.5283	4.4238	2.5388
6 MHz, 10 dB	-0.3786	7.6464	1.4554	37.0463	5.7940	35.0084	-0.4119	5.7885	7.2568
6 MHz, 15 dB	-0.5000	4.0578	0.8992	45.8421	5.4283	43.8439	-0.6105	4.4484	3.0770
6 MHz, 20 dB	-0.6667	3.7135	0.9232	37.6844	5.4952	36.4210	-0.6837	3.7235	2.7488
18 MHz, 10 dB	1.3333	3.3339	0.8972	17.5423	2.6973	13.2891	1.4394	3.3805	2.5774
18 MHz, 15 dB	1.5000	4.1291	1.0107	17.5333	2.7308	13.6527	1.3166	3.7101	2.9696
18 MHz, 20 dB	1.3333	3.4892	0.9160	19.0683	2.8932	15.2095	1.2960	3.5079	2.6875

Table A.6: Table of fitted parameter values to the data for the weak LOS scenario in the indoor environment for different values of bandwidth and SNR.

	Normal		Exponential		Rayleigh	
	μ	σ	λ	x_0	σ	x_0
3 MHz, 10 dB	364.4013	291.6165	398.3760	34.0000	393.9220	110.2658
3 MHz, 15 dB	214.9217	186.2321	271.2550	56.3333	250.3508	86.1906
3 MHz, 20 dB	165.3758	141.4209	240.7092	75.3333	200.9458	81.1167
6 MHz, 10 dB	186.2845	164.3231	201.9512	15.6667	214.8825	69.3458
6 MHz, 15 dB	97.8087	80.3428	138.1789	37.0000	112.5307	39.5645
6 MHz, 20 dB	88.5297	76.6488	121.1963	32.6667	104.8480	38.4002
18 MHz, 10 dB	65.9942	62.9073	71.3262	5.3333	80.5357	28.9515
18 MHz, 15 dB	36.4768	31.4436	46.4768	10.0000	42.1810	14.2161
18 MHz, 20 dB	31.0005	26.1241	43.5005	12.5000	36.2925	13.1789

	Gamma			Cauchy		Skew Normal		
	k	θ	x_0	x_0	γ	ϵ	ω	α
3 MHz, 10 dB	1.8293	218.5861	35.4635	255.1701	157.2312	7.8047	460.6531	22.0759
3 MHz, 15 dB	2.3059	118.9593	59.3924	149.6727	97.2323	-8.8049	291.0944	13.1034
3 MHz, 20 dB	3.3574	75.2901	87.4027	125.2199	75.4973	-7.8158	223.5961	6.6584
6 MHz, 10 dB	1.6262	124.6714	16.4503	123.1369	76.2961	-2.1984	250.0558	25.8121
6 MHz, 15 dB	3.1079	44.3621	40.0645	73.5079	43.1600	-2.7027	128.6759	9.2918
6 MHz, 20 dB	2.7789	44.3847	34.8117	62.8002	39.7893	-4.2258	120.3271	9.0871
18 MHz, 10 dB	1.5013	47.5735	5.4280	40.0033	25.9687	-0.3029	91.3928	30.7650
18 MHz, 15 dB	2.4336	19.2980	10.4868	25.8598	15.5834	-1.1515	49.0366	11.7313
18 MHz, 20 dB	3.1141	14.2101	13.2506	22.1928	13.4942	-0.6399	41.0315	8.9932

	Exponential Power			Weibull			Student's T		
	μ	α	β	λ	k	x_0	μ	σ	ν
3 MHz, 10 dB	344.6760	377.0263	1.7178	439.5895	1.4121	34.4769	335.9047	256.7938	8.6152
3 MHz, 15 dB	185.0292	194.7289	1.3414	303.6402	1.5494	56.9182	187.9757	147.0928	5.2994
3 MHz, 20 dB	146.2444	148.9072	1.3526	272.8196	1.8079	76.5007	147.7933	113.1546	5.5679
6 MHz, 10 dB	142.1667	127.6808	1.0552	219.4651	1.2950	15.8511	147.7807	110.1232	3.2112
6 MHz, 15 dB	87.6869	87.7433	1.4021	152.6556	1.7883	37.4470	87.7994	64.9495	5.7504
6 MHz, 20 dB	76.1656	78.7187	1.3206	136.7144	1.6877	32.9822	77.9916	60.5710	5.3949
18 MHz, 10 dB	43.0000	33.0533	0.8440	76.5640	1.2220	5.3620	47.6102	36.4628	2.4806
18 MHz, 15 dB	29.9997	28.3169	1.1774	52.1488	1.5819	10.0888	30.5762	22.6813	3.8725
18 MHz, 20 dB	26.8222	27.0094	1.3240	49.2760	1.7827	12.6273	26.9512	20.3434	4.8274

Table A.7: Table of fitted parameter values to the data for the NLOS scenario in the outdoor environment for different values of bandwidth and SNR.

	Normal		Exponential		Rayleigh	
	μ	σ	λ	x_0	σ	x_0
3 MHz, 10 dB	141.0880	83.8597	179.9777	34.5000	139.0840	36.8341
3 MHz, 15 dB	134.4610	84.8260	182.4610	48.0000	142.9242	49.0034
3 MHz, 20 dB	127.8426	86.2834	205.1804	72.3333	154.5571	72.9832
6 MHz, 10 dB	114.7762	78.3736	137.6093	22.8333	114.5949	27.0744
6 MHz, 15 dB	92.4429	71.9725	126.5917	34.1667	104.2194	36.1779
6 MHz, 20 dB	79.7302	63.4693	116.2318	33.6667	93.7506	36.6743
18 MHz, 10 dB	58.9226	50.0572	64.4226	5.5000	66.0687	19.9724
18 MHz, 15 dB	34.5445	29.4005	42.2066	7.6667	39.7132	13.3082
18 MHz, 20 dB	27.6532	23.5926	39.3198	11.6667	33.5354	13.4885

	Gamma			Cauchy		Skew Normal		
	k	θ	x_0	x_0	γ	ϵ	ω	α
3 MHz, 10 dB	25.9192	16.6235	289.7806	135.8982	59.7508	87.4652	99.5382	0.9122
3 MHz, 15 dB	30.2580	15.5454	335.9099	128.9771	59.9544	91.0788	95.2758	0.6941
3 MHz, 20 dB	77.7283	9.8156	635.1089	124.1223	60.7809	96.6458	91.7500	0.4710
6 MHz, 10 dB	3.0372	47.3603	29.0652	93.2533	50.4060	7.3216	132.9996	8.7093
6 MHz, 15 dB	3.1679	41.2453	38.2184	71.9217	42.9682	-2.0551	118.7852	8.1914
6 MHz, 20 dB	3.7928	33.0159	45.4941	62.0974	35.9810	-0.6836	102.4437	5.4622
18 MHz, 10 dB	1.7604	36.7692	5.8043	41.0499	23.6873	-0.0942	77.3867	21.6094
18 MHz, 15 dB	2.1942	19.5453	8.3416	24.1173	14.7741	-1.3592	46.4054	12.2534
18 MHz, 20 dB	3.1287	13.3052	13.9749	20.3542	13.1873	-1.8668	37.7894	7.1208

	Exponential Power			Weibull			Student's T		
	μ	α	β	λ	k	x_0	μ	σ	ν
3 MHz, 10 dB	145.3232	147.6429	5.3846	220.9358	2.5396	54.7207	141.0232	83.6138	169.9999
3 MHz, 15 dB	138.0467	150.5644	6.1648	224.7998	2.5596	64.7928	134.4143	84.5751	170.0000
3 MHz, 20 dB	130.2293	150.6183	4.7859	246.6367	2.7969	91.3753	127.8091	86.0124	170.0000
6 MHz, 10 dB	136.3641	143.1938	9.2901	156.2791	1.8450	23.8181	114.5455	78.0941	170.0000
6 MHz, 15 dB	98.3171	112.5864	2.5320	143.6923	1.8621	34.7842	92.1283	71.5750	169.9999
6 MHz, 20 dB	80.4839	91.2674	2.0672	129.4907	1.8947	35.0192	78.7723	62.1754	49.2731
18 MHz, 10 dB	46.0000	39.3256	1.0623	70.6348	1.3564	5.5665	48.7013	35.0999	3.6403
18 MHz, 15 dB	28.8337	28.9102	1.2600	47.1428	1.5148	7.8117	29.6434	22.5953	4.5742
18 MHz, 20 dB	26.0331	29.7386	1.6586	44.7270	1.7677	12.0609	25.5682	20.6388	8.3930

Table A.8: Table of fitted parameter values to the data for the NLOS scenario in the highway environment for different values of bandwidth and SNR.

	Normal		Exponential		Rayleigh	
	μ	σ	λ	x_0	σ	x_0
3 MHz, 10 dB	15.0614	17.5841	68.9130	53.8333	50.4662	54.1085
3 MHz, 15 dB	14.8301	14.9148	48.1762	33.3333	35.7304	33.4490
3 MHz, 20 dB	15.3218	12.4925	52.5024	37.1667	38.2010	37.2382
6 MHz, 10 dB	14.9851	11.6048	30.8184	15.8333	23.4379	16.0632
6 MHz, 15 dB	15.3690	10.9025	29.5357	14.1667	22.3118	14.2412
6 MHz, 20 dB	15.0311	9.9126	28.3644	13.3333	21.2855	13.3922
18 MHz, 10 dB	14.6546	7.9239	25.1001	9.8333	18.2461	9.9025
18 MHz, 15 dB	14.6575	8.7444	26.3241	11.6667	19.6474	11.7164
18 MHz, 20 dB	14.1168	9.1409	29.2835	15.1667	21.7228	15.2124

	Gamma			Cauchy		Skew Normal		
	k	θ	x_0	x_0	γ	ϵ	ω	α
3 MHz, 10 dB	3167.3856	0.3128	975.7411	14.4656	9.6970	24.5605	19.9858	-0.7424
3 MHz, 15 dB	3086.8748	0.2687	814.6292	15.0318	8.9119	14.8288	14.9148	0.0001
3 MHz, 20 dB	1900.2358	0.2867	529.3782	15.5504	7.8930	15.3203	12.4925	0.0002
6 MHz, 10 dB	99.9831	1.1619	101.1870	13.5266	7.5456	5.9591	14.7017	1.1968
6 MHz, 15 dB	1515.0677	0.2800	408.8910	15.9791	7.1436	15.3684	10.9025	0.0001
6 MHz, 20 dB	1400.1992	0.2651	356.1582	14.9178	6.8409	15.0257	9.9126	0.0007
18 MHz, 10 dB	1892.2512	0.1824	330.4976	14.0830	5.4535	14.6538	7.9239	0.0001
18 MHz, 15 dB	3184.5271	0.1553	479.9051	14.9793	5.9183	14.6567	8.7444	0.0001
18 MHz, 20 dB	2637.2951	0.1780	455.3920	14.0165	6.2028	14.1159	9.1409	0.0001

	Exponential Power			Weibull			Student's T		
	μ	α	β	λ	k	x_0	μ	σ	ν
3 MHz, 10 dB	14.8283	20.5946	1.5096	87.7371	5.0261	65.7481	15.0450	15.9981	11.5032
3 MHz, 15 dB	14.8755	19.6715	1.7735	64.0008	4.3311	43.5554	14.8921	14.0953	18.6285
3 MHz, 20 dB	15.3214	17.7040	2.0081	60.9127	4.8740	40.6748	15.3159	12.1320	35.6030
6 MHz, 10 dB	15.3836	18.9259	2.9577	39.1434	3.3299	20.1296	14.9768	11.5557	170.0000
6 MHz, 15 dB	15.2859	17.7525	2.9319	37.0236	3.3986	17.8599	15.3690	10.8571	169.9914
6 MHz, 20 dB	15.0475	16.3854	3.1845	35.8014	3.6416	17.2165	15.0311	9.8738	170.0000
18 MHz, 10 dB	14.6544	13.2303	3.3533	30.5774	3.9336	13.0024	14.6559	7.8949	170.0000
18 MHz, 15 dB	14.4174	14.3190	3.0190	37.0973	4.4252	19.1233	14.6662	8.7082	170.0000
18 MHz, 20 dB	14.0554	14.8174	2.9053	36.8201	4.1265	19.2919	14.1194	9.1000	169.9908

Table A.9: Table of fitted parameter values to the data for the NLOS scenario in the indoor environment for different values of bandwidth and SNR.